Laminated diatomaceous sediments of the Red Sea, their composition and significance as recorders of abrupt changes in productivity and circulation during the Late Quaternary

Dissertation zur Erlangung des Doktorgrades

am Fachbereich Geowissenschaften

der Universität Bremen

vorgelegt von

Ismene A. Seeberg-Elverfeldt

Bremen, Juni 2004

Tag des Kolloquiums:

26. Juli 2004

Gutachter:

Prof. Dr. Gerold Wefer

Prof. Dr. Andreas Mackensen

Prüfer:

Prof. Dr. Gerhard Bohrmann

Dr. Jürgen Pätzold

Danksagung

Für die Vergabe dieses Themas bedanke ich mich bei Prof. Dr. Gerold Wefer, v. a. für die Möglichkeiten, die mir hier in dieser großen Arbeitsgruppe geboten wurden. Prof. Dr. Andreas Mackensen danke ich für die Übernahme des Zweitgutachtens.

Mein besonderer Dank gilt Prof. Dr. Carina Lange und Dr. Jürgen Pätzold, die mich durch ihre unermüdliche Diskussionsbereitschaft und hilfreiche Anregungen im Verlauf der Arbeit sehr unterstützt haben und von deren Fachkenntnissen ich viel lernen konnte.

Für die hervorragende Zusammenarbeit und die Einführung in die Geheimnisse der Präparation laminierter Sedimente danke ich Dr. Jennifer Pike von der Universität in Cardiff.

Des Weiteren möchte ich mich bei meinen Kolleginnen und Kollegen aus dem Fachbereich Geowissenschaften bedanken: für die Diskussionen, Problembewältigungen und das gute Arbeitsklima. Im Besonderen gilt dies für Helge Arz, Barbara Donner, Oscar Romero, Sabine Kasten, Thomas Felis, Henning Kuhnert, Bob Davenport, Martin Čepek, Söhnke Rathmann (ohne Dein Computerverständnis wäre ich verloren gewesen) und André Bahr. Und v. a. Snježana Žarić, die mir als Zimmergenossin und Freundin immer zur Seite stand.

Für die Unterstützung bei der Analytik des Probenmaterials danke ich: Marco Klann, Dr. Monika Segl, Hella Buschoff, Volker Diekamp, Heike Pfletschinger und Christina Fink; Ute Bock, Friedel Hinz und Dr. Richard Crawford vom Alfred-Wegener-Institut; den Technikern der Universität Cardiff und des GeoForschungsZentrums Potsdam.

Bei meiner Familie und meinen Freunden möchte ich mich für die Unterstützung während der letzten drei Jahre ganz besonders bedanken. Bei meinen Eltern für die Möglichkeit, das zu studieren, was ich wollte und damit meine Träume zu verwirklichen.
Den wichtigsten Beistand leistete mein liebster Ehemann: Dein Glaube an mich hat mir durch manch schwere Stunde geholfen.

Die Deutsche Forschungsgemeinschaft hat diese Arbeit im Rahmen des Forschungszentrums Ozeanränder finanziell unterstützt.

Table of Contents

Abstract

Marine laminated sediments from different areas around the world have been studied during the last few decades and their importance in understanding climatic changes became more and more apparent. The signals they carry can be seasonal and hence allow for high resolution climate reconstructions.

In the northern Red Sea laminated sediments are only preserved in a very special environment. Brine-filled deeps are located along the central axis of the Red Sea and are free of oxygen as well as sulphide. No evidence for benthic life has been found in these deeps, although a rich prokaryotic community has been described to thrive at the seawater-brine interface. One of these deeps, the Shaban Deep, was selected as the focus of this work. It consists of four basins (southern, eastern, northern and western basin). Laminated sediments from within the eastern and southern brine basins were investigated with special emphasis on the major biogenic components within the sediments. In particular, diatom assemblages within the sedimentary record were used as tracers of surface water conditions in which they were produced.

As an essential first step to understand the effects of preservation in the sediments and in order to assess the accuracy with which the sedimentary record reproduces the original living assemblage, diatom assemblages from plankton tows distributed in the northern Red Sea were compared with an array of surface sediment samples from brine and non-brine locations. Our results show that the plankton and surface sediments of the northern Red Sea are characterized by a diatom flora that is typical of tropical/subtropical environments. Fragile forms (e.g. *Nitzschia bicapitata* group) that dominate the plankton assemblage are subject to strong dissolution either during their descent through the water column or at the sediment/water interface leaving the sedimentary record enriched in heavily silicified species (e.g. *Alveus marinus*, *Azpeitia neocrenulata*, *A. nodulifera*, *Roperia tesselata*). However, surface brine sediments have higher biogenic opal contents and concentrations of siliceous microplankton remains, higher diatom species diversity and fragile forms are better preserved than in non-brine sediments. These sediments hold therefore a great potential for palaeoenvironmental studies.

Once the preservational aspect was understood, the second step involved the detailed study of the sedimentary record. For this, two cores were used: Gravity core GeoB 5836-2 from the southern basin of the Shaban Deep and Multicore GeoB 7805-1 from the eastern basin. The former covers the time interval between 4 and 22 ka (mid-Holocene to Last Glacial

Maximum, LGM) while the latter encompasses the last ~2000 years of the late Holocene. Backscattered electron imagery was used in order to determine laminae composition and genesis with emphasis on the diatomaceous component. Overall, sediment fabric includes six types: a) a laminated structure with alternating light (mainly coccoliths) and dark (diatom frustules) layers, where the diatom component is indicative of the intra-annual variability between stratification and mixing events; b) a pocket-like structure attributed to the sinking of particles within fecal pellets and aggregates; c) a matrix of tightly packed diatoms that relates to extended stratification/mixing periods of the water column; d) homogenous intervals that result from turbidity deposition; e) silt accumulations which origin may lie in agglutinated foraminifers; and f) pyrite layers with pyrite formation possibly initiated at the seawater-brine interface. We produced sedimentation models for the Holocene through LGM records that take into account the importance of different diatom assemblages as tracers of changes in stratification/mixing in the northern Red Sea. The models include: 1) An annual sedimentation cycle for the last 15 kyr with coccolithophorids reflecting the summer season while diatoms represent fall-winter conditions. 2) A LGM-Deglaciation model that concentrates on the shift from mixed water column conditions of the LGM to stratified conditions of the Deglaciation. No annual cycle could be established for this time frame due to high carbonate dissolution and thus the lack of the summer signal in the sediments. These results were discussed against the background of already existing paleoceanographic data from an oxic core from the northernmost Red Sea.

The results of this thesis show that laminated sediments from the Shaban Deep in the northern Red Sea can be used for reconstructing paleoceanographic and paleoclimatic changes in the region at high resolution.

Chapter 1: Introduction

1.1 Motivation and scientific objectives

Laminated sediments spanning the last 50,000 years (though not continuously) have recently been described in the Shaban Deep, a brine-filled basin in the northern Red Sea (Hemleben et al., 1996b).

In 1981 a cruise took place to the northern Red Sea onboard *RV Valdivia* where a brine filled basin was discovered at about 25°15'N and 35°22'E (Cruise Reports Menor 1 and Menor 2, 1984) and named Shaban Deep since it was discovered during the Arabian month of Shaban (Stoffers et al., 1990). The same deep was described in more detail by Pautot et al. (1984) and named Jean Charcot deep after the ship's name *RV Jean Charcot* disregarding that it already had a name.

In 1995 a cruise onboard *RV Meteor* (M 31/2) set out to study the sediments of the northern Red Sea with emphasis on the southern basin of the Shaban Deep. Several cores were retrieved and sediments were described as consisting of "very fine layering of diatom oozes and calcareous oozes" (Hemleben et al., 1996b). It was further suggested that these sediments would "allow detailed investigations of the sedimentation and climate history of the northern Red Sea" (Hemleben et al., 1996b). However, no action was taken to investigate these laminated sediments from a paleoceanographic viewpoint until 1999, when another cruise onboard *RV Meteor* (M 44/3) visited the Shaban Deep region for the second time. Again, a core from the southern basin was retrieved and was described as "partly laminated olive gray to black brine sediments that have a very high content of hypersaline pore waters" (Pätzold et al., 2000a). Sediment analysis revealed the dominance of diatoms within the biogenic silica components and it was suggested that these diatoms could be used to resolve climatic changes within this region.

Extensive work on sediments of the Red Sea has since been carried out in order to understand the impact of glacial to interglacial paleoenvironmental changes in planktic and benthic ecosystems including planktic and benthic foraminifera and thecosomatous pteropods (e.g. Winter et al., 1983; Almogi-Labin et al., 1991; Almogi-Labin et al., 1998). These studies revealed that: a) the lowered glacial sea level accompanied by a drastic reduction in the Red Sea – Indian Ocean water exchange and an increased aridity in the area was responsible for anomalous high salinities in the Red Sea which exceeded the tolerance level of many planktic organisms (e.g. Hemleben et al., 1996a; Fenton et al., 2000); and b) that the extension of the

oxygen-minimum-zone and changes in water column stratification are reflected by changes in pteropod assemblages during the last termination (Almogi-Labin et al., 1991; 1998).

Most recently Arz et al. (2003a; 2003b) combined alkenone paleothermometry with stable isotope measurements on multiple planktic and benthic foraminifers and sediment compositional data from two cores encompassing together the last 22 kyr in the northern Red Sea. They reported that major shifts in sea surface temperature in the northern Red Sea are strongly connected to the general temperature development of the northern hemisphere since the Last Glacial Maximum while sea surface salinity and vertical isotope gradients are indirectly linked to the course of the postglacial sea level rise.

Despite the numerous studies mentioned above, none to the best of my knowledge, has been published in the literature on the laminated sediments of the Shaban Deep. Most importantly, no previous studies exist on one of the main biogenic components of these sediments, diatoms, and the clues they may hold for unraveling changes in productivity and circulation during the Late Quaternary.

Therefore, this dissertation started in 2001 addressing the following scientific questions:

- Which diatom species are the main components within the laminated sediments?
- Do the laminations carry an annual signal?
- How does the diatom assemblage change over time?
- Which processes may be involved in the formation of laminations?
- Which climatic signals are reflected by diatoms in the northern Red Sea?

In addition the question should be addressed if the climatic signal could be destroyed/disrupted by hydrothermal activity within the brine basin.

With these questions in mind I define the overall objective of this thesis as

To assess the significance of diatoms in laminated sediments of the Shaban Deep (northern Red Sea) as recorders of abrupt changes in productivity and circulation during the Late Quaternary.

1.2 Study area

a) Geographical setting and oceanography

The Red Sea is an enclosed water body which is 1932 km long and about 280 km wide (Morcos, 1970). It is a very unique environment. There are no permanent river inflows, rainfall is sparse, evaporation largely exceeds precipitation, and seawater exchange with the Arabian Sea in the south is limited due to the very shallow sill (137 m) of the Strait of Bab el

Mandab. Due to high evaporation, sea surface salinity values are high and increase from south to north up to 40 psu in the northern Red Sea (Edwards, 1987).

The circulation is mostly driven by thermohaline forcing while wind forcing is only of minor importance. Surface waters flow to the north in Eastern and Western Boundary Currents, getting denser on their way due to evaporation. Details on the anti-estuarine circulation pattern of the Red Sea can be found in Eshel et al. (1994), Eshel and Naik (1997) and in publications and manuscripts in Chapter 3.

The Red Sea itself can be divided into three distinct sections (Fig. 1.1): (1) the southern Red Sea (15°-20°N) where active seafloor spreading still occurs; (2) the central Red Sea, a transition zone between 20°-23°N; and (3) the northern Red Sea without a spreading center (Cochran et al., 1986). Within the northern and central area many small isolated deeps can be found which contain hot brines and metalliferous sediments which suggests hydrothermal activity within these brines (Cochran et al., 1986).

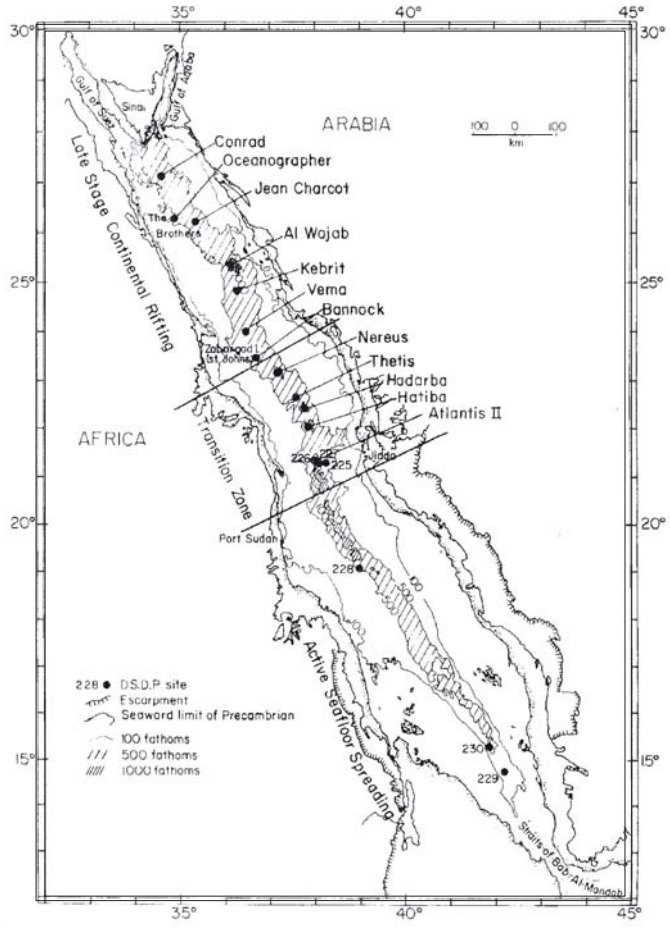

Fig. 1.1: Map of the Red Sea with the three sections defined by Cochran et al. (1986) representing different stages in the development of the margin. Various brine-filled deeps are indicated in the central and northern section. Note that the Shaban Deep is still named Jean Charcot.

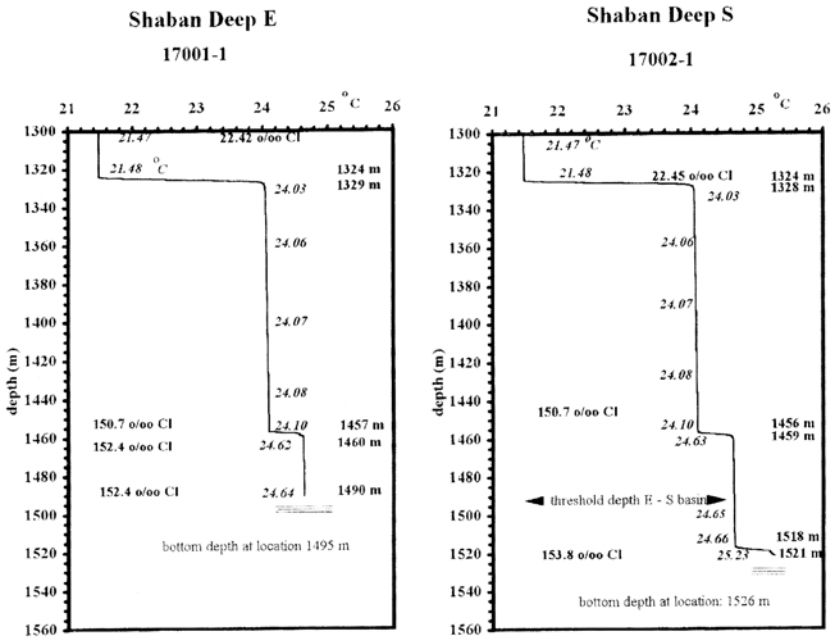

Fig. 1.2: Temperature profiles for two Shaban Deep sub-basins (after Hartmann et al., 1998). Chlorinity values are noted at the respective water depths.

The Shaban Deep, located in the northern Red Sea consists of four basins: southern, eastern, northern and western basin, with near equal brine levels at about 1325 m where the temperature increases about 1-2.5°C (Hartmann et al., 1998) (Fig. 1.2). The southern and eastern basins which are closely connected (while the northern and western basins are separated; Fig. 1.3) have a second temperature interface at about 1465.5 m where temperature again increases by about 0.5°C (Hartmann et al., 1998). The temperature within the northern and western basins is about 2°C lower than in the other two basins. Hartmann et al. (1998) suggested a sub-bottom connection between all four basin.

The brine body has a salinity of about 260 psu, it is almost depleted in dissolved oxygen and is up to 200 m thick within the southern basin (Hartmann et al., 1998). The top of Miocene evaporites (so called s-reflector) crops out within the brine basin at the modern level of the brine-seawater interface (Pautot et al., 1984; Pätzold et al., 2003). There is only minimal exchange (diffusion and convection) at the brine-seawater interface (Hartmann et al., 1998). The Shaban Deep was often described as being hydrothermally active (e.g. Pautot et al., 1984), and Stoffers et al. (1990) found additionally diagenetically formed dolomite and rhodochrosite within organic rich layers of these sediments. Hemleben et al. (1996b) detected hydrothermal activity in two cores from the northern and western basins and found limonitic layers (northern basin) and red staining of the sediment (western basin).

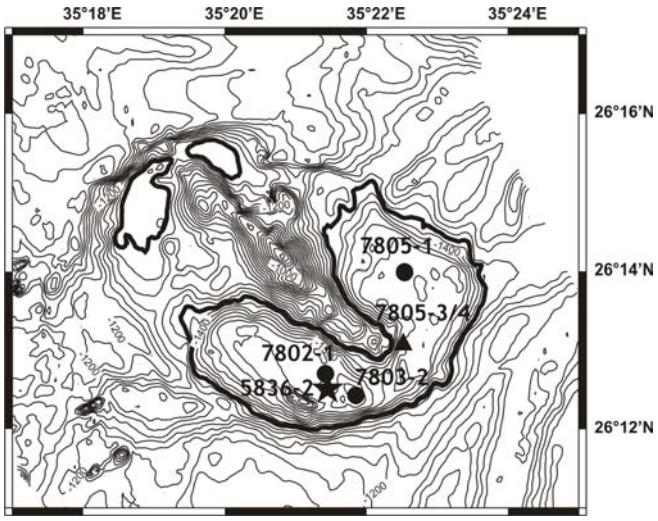

Fig. 1.3: Bathymetry map of the Shaban Deep, located in the northern Red Sea. The Deep is divided into four sub-basins: northern, western, southern and eastern. Sample locations refer to: gravity core (✱), multicore-samples (●) and plankton tow (▲).

b) Phytoplankton and diatoms

The northern Red Sea is an oligotrophic environment and is stratified for most of the year. Dissolved nitrate and phosphate are depleted; silicate is low but still detectable. Thus, the phytoplankton living here is mainly based on nutrient recycling (regenerated production) (Pätzold et al., 2000b). In winter, the depth of the thermocline exceeds 200 m north of 25°N. A shallow thermocline is observed at 30-60 m during spring and summer (Edwards, 1987).

The Red Sea plankton is characterized by the dominance of autotrophic picoplankton while cells of 5 to several 100 µm are scarce in this region (Shaikh et al., 1986; Lindell and Post, 1995). Shaikh et al. (1986) describes four different groups of phytoplankton that are important in the annual cycle of the Red Sea: diatoms are present most of the year and are the predominant group in winter; blue-green algae (*Trichodesmium* spp.) and nanoplankton dominate in late spring and summer, and dinoflagellates in the fall. In general, phytoplankton abundances decrease from the southern Red Sea to the Gulf of Suez (Halim, 1969).

Maximal phytoplankton growth takes place between November and March. Primary production off Jiddah (21°30'N) has a clear bimodal pattern (Shaikh et al., 1986): a) the major seasonal peak of Chlorophyll (Chl) *a* starts in December at 75 m water depth and is clearly dominated by diatoms (e.g. genera *Bacteriastrum*, *Chaetoceros*, *Nitzschia* and *Rhizosolenia*) (Shaikh et al., 1986) when nutrient concentrations are highest; and b) just after the decline of the major pulse of primary production, sub-surface nutrient regeneration takes place and during the early summer nanoplankton dominates.

A second minor sub-surface Chl *a* maximum (75-100 m depth) occurs in September, when blue-green algae are the main contributors, but diatoms of the genera *Leptocylindrus*, *Nitzschia* and *Rhizosolenia* are also present.

1.3 Diatoms

Diatoms are unicellular, eukaryotic microorganisms belonging to the class Bacillariophyceae. They are pigmented (Chlorophyll a and c, betacarotene, fucoxanthin, diatoxanthin and diadinoxanthin) and photosynthetic. They live in the marine and freshwater environment either free in the water column as plankton, attached to other organisms, plants or stones or even within sea ice or e.g. corals or foraminifera as symbionts (Hasle and Syvertsen, 1996). Their cell wall is highly differentiated and impregnated with biogenic silica (SiO_2 * nH_2O), covered with an organic layer (Round et al., 1990). The first geological appearance of diatoms was in the Early Cretaceous with a few species appearing even during the Jurassic (Hasle and Syvertsen, 1996).

The cells are composed of two valves, a hypovalve and a slightly larger epivalve that are connected via girdle bands. These girdle bands protect the cell during vegetative cell division when two new valves are produced. Both mother valves become epivalves during this process and new hypovalves are produced. One of the two daughter cells is therefore smaller than the mother cell while the other stays the same size. This diminishing process can continue up to a certain size when the cell becomes fertile to produce a so-called auxospore. The auxospore forms a large sphere surrounded by an organic membrane while the silica valves get discarded. Within the auxospore a new diatom cell with the original size is restored that starts the whole cycle again (Round et al., 1990; Hasle and Syvertsen, 1996).

Some diatom species (like species of the genus *Chaetoceros*) are known to form resting spores (Hasle and Syvertsen, 1996). These are heavily silicified cells which can greatly differ morphologically from the vegetative form. Usually they are formed during unfavorable environmental conditions. As soon as these conditions improve, vegetative division starts again and new valves are formed or the spore valves are simply discarded.

Marine diatoms are the dominant primary producers in regions with high nutrient levels and turbulent surface waters like e.g. coastal upwelling regions, equatorial divergences and sea ice margins (Ragueneau et al., 2000). Therefore siliceous sediments are limited mainly to the circumpolar belt region and the eastern equatorial Pacific. In addition, diatoms are known to grow under low light conditions where they generate considerable production at depth (Kemp

et al., 2000) and some species are able to vertically migrate in the water column by regulation of their buoyancy (e.g. Villareal, 1988).

Most of the silica produced in the euphotic zone by diatoms and other organisms is dissolved within the upper 500 m of the water column and only 1% remains at 1000 m water depth (Tréguer et al., 1995). Fragile diatom species are more susceptible to dissolution within the water column and the sediment which leaves heavily silicified species overrepresented in the sediment (e.g. Sancetta, 1989). However, the diatom assemblage within the sedimentary record can be used as tracers of the conditions of surface waters in which they were produced. For example, *Chaetoceros* spp. vegetative cells are linked to upwelling conditions with high nutrient concentrations and a mixed surface water column and this genus is often referred to spring bloom conditions (e.g. Rines and Hargraves, 1988). Resting spores of *Chaetoceros* spp. on the other hand, mark the end of favorable conditions in the euphotic zone when nutrients become depleted. Other species like e.g. *Coscinodiscus* spp. or *Rhizosolenia* spp. are more linked to a stratified water column and oligotrophic conditions like in summer/fall when nutrients are consumed (e.g. Kemp et al., 2000).

Diatoms can therefore be used for paleoceanographic reconstructions in those areas of the world ocean where they get preserved in the sediment record.

1.4 Marine laminated sediments

Laminated sediments from different areas around the world have been studied during the last few decades and their importance in understanding climatic changes has become more and more apparent. They are common in freshwater lakes where they have been thoroughly studied (e.g. Lake Holzmaar, Germany by Zolitschka, 1996; Lake Steisslingen, Germany by Kerig and Lechterbeck, 2004; some lakes in Sweden, reviewed by Petterson, 1996; or Artic lakes in the Eastern Canadian Artic studied by Hughen et al., 1996). Laminated sediments can also be found in marine environments. Table 1.1 summarizes most of the studies that have been carried out so far and Fig. 1.4 shows their distribution in the world ocean.

Kemp (1996) summarized the two basic requirements for the development of laminated sediments: "(1) variation in input/chemical conditions/biological activity that will result in compositional changes in the sediment; and (2) environmental conditions (i.e. low oxygen in bottom waters or physical suppression of burrowing activity) that will preserve the laminated sediment fabric from bioturbation".

Table 1.1: Summary of marine laminated sediment sites and examples of studies carried out. Numbers and symbols refer to Fig. 1.4.

Area of Laminated Sediments		Example for Reference
Atlantic Ocean		
North Atlantic	**1** ○	Bodén and Backman, 1996
Orca Basin, Gulf of Mexico	**2** ▲	Leventer et al., 1982
Cariaco Basin, Venezuela	**3** ●	Hughen et al., 1996
the Gotland Deep in the Baltic Sea	**4** ●	Burke et al., 2002
Mediterranean Sea	**5** ●	Thunell et al., 1984;
Urania Basin, eastern Mediterranean	**6** ▲	Corselli et al., 2002
Bannock Basin, eastern Mediterranean	**7** ▲	Erba et al., 1987; Erba 1991
Napoli mud volcano, Mediterranean Ridge	**8** ▲	Pearce et al., 1998
Black Sea	**9** ●	Pilskaln and Pike, 2001
Pacific Ocean		
Saanich Inlet, Canada	**10** ●	Dean et al., 2001; McQuoid and Hobson, 2001
Effingham Inlet, Canada	**11** ●	Chang et al., 2003
Santa Barbara Basin off California	**12** ●	Schimmelmann and Lange, 1996 and references therein
Santa Monica Basin off California	**13** ●	Hagadorn, 1996
Soledad Basin off California	**14** ●	van Geen et al., 2003
Guaymas Basin, Gulf of California	**15** ●	Baumgartner et al., 1985; Pike and Kemp, 1996
Eastern Equatorial Pacific	**16** ○	Kemp et al., 1996
Peruvian coastal upwelling zone	**17** ●	Brodie and Kemp, 1994
Mejillones Bay off northern Chile	**18** ●	Ortlieb et al., 2000
Japan Sea	**19** ●	Grimm, 1992
Indian Ocean		
Arabian Sea, Pakistan margin	**20** ●	von Rad et al., 1999; Staubwasser and Sirocko, 2001
Shaban Deep, northern Red Sea	**21** ▲	Seeberg-Elverfeldt et al., accepted
Southern Ocean		
Palmer Deep off western Antarctica	**22** ●	Leventer et al., 2002
Vega Drift, eastern Antarctic Peninsula	**23** ●	ongoing research, Pike et al., in prep.
Polar Front, Antarctica	**24** ○	Grigorov et al., 2002
Nielsen Shelf Valley, East Antarctic Shelf	**25** ●	Harris 2000
Iceberg Alley, East Antarctic Margin	**26** ●	ongoing research, Stickley et al., in prep.

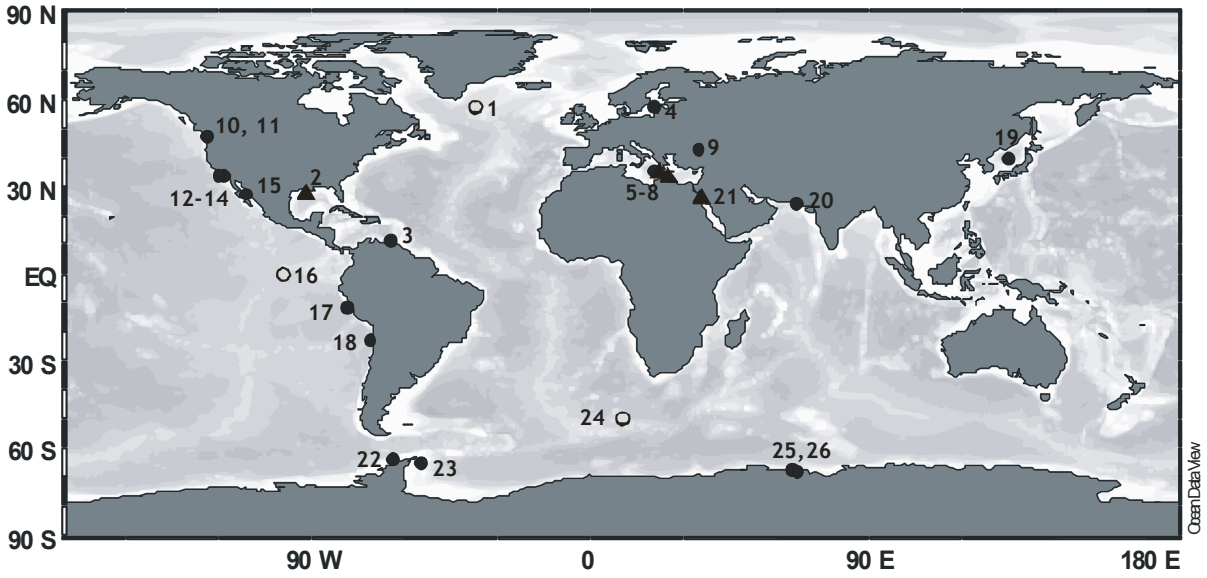

Fig. 1.4: Global map showing the location of marine laminated sediments that have been studied so far (for references see Table 1.1). Laminated sediments resulting from high productivity are indicated by filled circles (●); Laminated sediments from frontal systems are indicated by circles (○); and brine-filled basins are indicated by triangles (▲).

Most marine laminated sediments are generated in areas where anoxia in bottom waters is caused by high productivity in surface waters and strong density gradients prevent vertical mixing (fjords and marginal seas) or because of the oxygen minimum zone impinges on the ocean floor (silled basins, continental shelf and slope). These examples are shown in Fig. 1.4 as filled circles (**3-5**, **9-15**, **17-20; 22-23; 25-26**). Most of them are located close to continental margins or within marginal seas. Some of them are true varves depositional systems that preserve the seasonal input signal. Microorganisms (e.g. diatoms) get preserved in laminae and reflect a seasonal cycle which can be established with the help of e.g. trap data from the water column. In addition to the biogenic component, a second type of lamina (e.g. composed of terrigenous material) is needed to establish annual sedimentation. Changes in assemblages or in productivity correspond to changes in surface waters and therefore climate, and can be recognized by investigations of laminae and/or varve thickness. Laminated sediments from the Santa Barbara Basin off California (**12**) are varves and each varve is composed of a biogenic lamina (produced during spring-early fall) and a winter layer consisting of mainly terrigenous material. Extensive work has been carried out so far on these sediments; this has been summarized by Schimmelmann and Lange (1996). Varve thickness for example is linked to precipitation changes and reveals differences in the Holocene sediment flux into the basin. Other paleoclimatic proxies are geochemical parameters (used for reconstruction of sea surface temperature), marine biogenic components (which reflect changes in productivity) and land-derived components (like pollen to reconstruct wind direction and aridity among others).

The second group of laminated sediments is formed at frontal systems in open waters (Fig. 1.4, circles; **1**, **16**, **24**), where diatom mats that sink to the seafloor can preserve laminae even in the presence of oxygenated bottom waters by suppressing all benthic life. Diatom mats are produced in oligotrophic waters where they grow under low light conditions above the nutricline (e.g. Kemp et al., 2000). They are also known to live at frontal systems like the northern North Atlantic (Bodén and Backman, 1996) or the eastern equatorial Pacific (Kemp et al., 1996). In the latter, episodes of massive flux of *Thalassiothrix longissima* can be linked to La Niña events when strong frontal zones develop in this area. Diatom mats get concentrated at these oceanic fronts and then sink in numbers of up to 200 mats (Kemp et al., 1996). No annual varves can be established for these regions but massive deposition can still be linked to climate events.

Anoxia within single enclosed basins can also result from salt-rich bottom waters like in the Mediterranean Sea (**6-8**), the Gulf of Mexico (**2**) or various brine-filled deeps in the Red Sea (Fig. 1.1). Here, laminated sediments are generated under oligotrophic conditions and the brine interface always acts as a barrier (due to the density gradient) where sinking particles are first accumulated before they sink through the brine itself (e.g. Erba, 1991). The temperature of the brine that preserves laminated sediments is only slightly higher than the surrounding seawater and they could thus be termed “cold seeps”. In the Red Sea many brine-filled basins are present but within the hot brines, like e.g. Atlantis II Deep, laminated sediments are not preserved due to hydrothermal activity. Studies so far have revealed that paleoclimate reconstructions on brine-laminated sediments are possible which gives further investigators an important tool to study climate changes in oligotrophic regions at high resolution.

I will show, based on detailed X-radiography and microscopy analyses that laminations in the Shaban Deep consist of terrigenous and biogenic material. Light layers are mainly composed of coccoliths, terrigenous material and diatom fragments, while dark layers consist of almost exclusively diatom frustules. I further propose that the different diatom assemblages can be used as tracers of changing conditions in stratification/mixing in the northern Red Sea.

References

Almogi-Labin, A., Hemleben, C. and Meischner, D., 1998. Carbonate preservation and climatic changes in the central Red Sea during the last 380 kyr as recorded by pteropods. Marine Micropaleontology, 33: 87-107.

Almogi-Labin, A., Hemleben, C., Meischner, D. and Erlenkeuser, H., 1991. Paleoenvironmental events during the last 13,000 years in the central Red Sea as recorded in Pteropoda. Paleoceanography, 6(1): 83-98.

Arz, H.W., Lamy, F., Pätzold, J., Müller, P.J. and Prins, M., 2003a. Mediterranean moisture source for an early-Holocene humid period in the northern Red Sea. Science, 300: 118-121.

Arz, H.W., Pätzold, J., Müller, P.J. and Moammar, M.O., 2003b. Influence of Northern Hemisphere climate and global sea level rise on the restricted Red Sea marine environment during Termination I. Paleoceanography, 18(2): 1053, doi:10.1029/2002PA000864.

Baumgartner, T., Ferreira-Bartrina, V., Schrader, H. and Soutar, A., 1985. A 20-year varve record of siliceous phytoplankton variability in the central Gulf of California. Marine Geology, 64: 113-129.

Bodén, P. and Backman, J., 1996. A laminated sediment sequence from the northern North Altantic Ocean and its climatic record. Geology, 24(6): 507-510.

Brodie, I. and Kemp, A.E.S., 1994. Variation in biogenic and detrital fluxes and formation of laminae in late Quaternary sediments from the Peruvian coastal upwelling zone. Marine Geology(116): 385-398.

Burke, I.T., Grigorov, I. and Kemp, A.E.S., 2002. Microfabric study of diatomaceous and lithogenic deposition in laminated sediments from the Gotland Deep, Baltic Sea. Marine Geology, 183: 89-105.

Chang, A.S., Patterson, R.T. and McNeely, R., 2003. Seasonal Sediment and Diatom Record from Late Holocene Laminated Sediments, Effingham Inlet, British Columbia, Canada. Palaios, 18(6): 477-494.

Cochran, J.R., Martinez, F., Steckler, M.S. and Hobart, M.A., 1986. Conrad Deep: a new northern Red Sea deep. Origin and implications for continental rifting. Earth and Planetary Science Letters, 78: 18-32.

Corselli, C., Principato, M.S., Maffioli, P. and Crudeli, D., 2002. Changes in planktonic assemblages during sapropel S5 deposition: Evidence from Urania Basin area, eastern Mediterranean. Paleoceanography, 17(3): 10.1029/2000PA000536.

Cruise Reports Menor 1 and Menor 2, 1984. Preussag Meerestechnik. Confidential Reports PREE-CR-03-4 and PREE-CR-05-4, Ministry of Petroleum and Mineral Resources, Deputy Ministry for Mineral Resources, Jeddah, Kingdom of Saudi Arabia.

Dean, J.M., Kemp, A.E.S. and Pearce, R.B., 2001. Palaeo-flux records from electron microscope studies of Holocene laminated sediments, Saanich Inlet, British Columbia. Marine Geology, 174: 139-158.

Edwards, F.J., 1987. Climate and Oceanography. In: S.M. Head (Editor), Key Environments: Red Sea. Pergamon Press, Oxford, pp. 45-70.

Erba, E., 1991. Deep mid-water bacterial mats from anoxic basins of the Eastern Mediterranean. Marine Geology, 100: 83-101.

Erba, E., Rodondi, G., Parisi, E., Ten Haven, H.L., Nip, M. and de Leeuw, J.W., 1987. Gelatinous pellicles in deep anoxic hypersaline basins from the eastern Mediterranean. Marine Geology, 75: 165-183.

Eshel, G., Cane, M.A. and Blumenthal, M.B., 1994. Modes of subsurface, intermediate, and deep water renewal in the Red Sea. Journal of Geophysical Research, 99(C8): 15,941-15,952.

Eshel, G. and Naik, N.H., 1997. Climatological Coastal Jet Collision, Intermediate Water Formation, and the General Circulation of the Red Sea. Journal of Physical Oceanography, 27: 1233-1257.

Fenton, M., Geiselhart, S., Rohling, E.J. and Hemleben, C., 2000. Aplanktic zones in the Red Sea. Marine Micropaleontology, 40: 277-294.

Grigorov, I., Pearce, R.B. and Kemp, A.E.S., 2002. Southern Ocean laminated diatom ooze: mat deposits and potential for palaeo-flux studies, ODP Leg 177, Site 1093. Deep-Sea Research, 49(16): 3391-3407.

Grimm, K.A., 1992. High-resolution imaging of laminated biosiliceous sediments and their paleoceanographic significance (Quaternary, Site 798, Oki Ridge, Japan Sea). In: et.al. (Editor), Proceedings of the Ocean Drilling Program, Scientific Results. College Station, TX, pp. 547-557.

Hagadorn, J.W., 1996. Laminated sediments of Santa Monica Basin, California continental borderland. In: A.E.S. Kemp (Editor), Palaeoclimatology and Palaeoceanography from laminated sediments. Geological Society, Special Publication, pp. 111-120.

Halim, Y., 1969. Plankton of the Red Sea. Oceanography and marine biology: an annual review, 7: 231-275.

Harris, P.T., 2000. Ripple cross-laminted sediments on the East Antarctic Shelf: evidence for episodic bottom water production during the Holocene? Marine Geology, 170: 317-330.

Hartmann, M., Scholten, J.C., Stoffers, P. and Wehner, F., 1998. Hydrographic structure of brine-filled deeps in the Red Sea - new results from the Shaban, Kebrit, Atlantis II, and Discovery Deep. Marine Geology, 144: 311-330.

Hasle, G.R. and Syvertsen, E.E., 1996. Marine Diatoms. In: C.R. Tomas (Editor), Identifying marine diatoms and dinoflagellates. Academic Press, Inc., pp. 5-386.

Hemleben, C., Meischner, D., Zahn, R., Almogi-Labin, A., Erlenkeuser, H. and Hiller, B., 1996a. Three hundred eighty thousand year long stable isotope and faunal records from the Red Sea: Influence of global sea level change on hydrography. Paleoceanography, 11(2): 147-156.

Hemleben, C., Roether, W. and Stoffers, P., 1996b. Östliches Mittelmeer, Rotes Meer, Arabisches Meer; Cruise No. 31, 30 December 1994 - 22 March 1995, Leitstelle METEOR, Institut für Meereskunde der Universität Hamburg, Hamburg.

Hughen, K., 1996. The potential for palaeoclimate records from varved Arctic lake sediments: Baffin Island, Eastern Canadian Artic. In: A.E.S. Kemp (Editor), Palaeoclimatology and Palaeoceanography from laminated sediments. Geological Society, Special Publication, pp. 57-72.

Hughen, K.A., Overpeck, J.T., Peterson, L.C. and Anderson, R.F., 1996. The nature of varved sedimentation in the Cariaco Basin, Venezuela, and its palaeoclimatic significance. In: A.E.S. Kemp (Editor), Palaeoclimatology and Palaeoceanography from laminated sediments. Geological Society, Special Publication, pp. 171-184.

Kemp, A.E.S., 1996. Laminated sediments as palaeo-indicators. In: A.E.S. Kemp (Editor), Palaeoclimatology and Palaeoceanography from laminated sediments. Geological Society, Special Publication.

Kemp, A.E.S., Baldauf, J.G. and Pearce, R.B., 1996. Origins and paleoceanographic significance of laminated diatom ooze from the Eastern Equatorial Pacific Ocean. In: A.E.S. Kemp (Editor), Paleoclimatology and Paleoceanography from laminated sediments. Geological Society, Special Publication, pp. 243-252.

Kemp, A.E.S., Pike, J., Pearce, R.B. and Lange, C.B., 2000. The "Fall dump"-a new perspective on the role of a "shade flora" in the annual cycle of diatom production and export flux. Deep-Sea Research II, 47: 2129-2154.

Kerig, T. and Lechterbeck, J., 2004. Laminated sediments, human impact, and a multivariate approach: a case study in linking palynology and archaeology (Steisslingen, Southwest Germany). Quaternary International, 113: 19-39.

Leventer, A., Domack, E., Barkoukis, A., McAndrews, B. and Murray, J., 2002. Laminations from the Palmer Deep: A diatom-based interpretation. Paleoceanography, 17(2): 10.1029/2001PA000624.

Leventer, A., Williams, D.F. and Kennett, J.P., 1982. Dynamics of the Laurentide ice sheet during the last deglaciation: evidence from the Gulf of Mexico. Earth and Planetary Science Letters, 59: 11-17.

Lindell, D. and Post, A.F., 1995. Ultraphytoplankton succession is triggered by deep winter mixing in the Gulf of Aqaba (Eilat), Red Sea. Limnology and Oceanography, 40(6): 1130-1141.

McQuoid, M.R. and Hobson, L.A., 2001. A Holocene record of diatom and silicoflagellate microfossils in sediments of Saanich Inlet, ODP Leg 169S. Marine Geology, 174: 111-123.

Morcos, S.A., 1970. Physical and chemical oceanography of the Red Sea. Oceanography and marine biology: an annual review, 8: 73-202.

Ortlieb, L., Escribano, R., Follegati, R., Zuniga, O., Kong, I., Rodriguez, L., Valdés, J., Guzman, N. and Iratchet, P., 2000. Recording of ocean-climate changes during the last 2,000 years in a hypoxic marine environment off northern Chile (23°S). Revista Chilena de Historia Natural, 73: 221-242.

Pätzold, J., Abd El-Wahab Farha, O., Abu-Ouf, M., Al Hazmi, Y.M.M., Al-Rousan, S., Arz, H.W., Bagabas, K.A.A., Bassek, D., Blaschek, H., Böke, W., Donner, B., Eder, W., Felis, T., Gayed, H.Y.K., Gutowski, M., Hemleben, C., Hübner, H., Hübscher, C., Kadi, K.A., Kästner, R., Klauke, S., Körner, S.O., Kuhlmann, H., Lützeler, T., Meier, S., Melegy, M.M., Moammar, M.O., Mohamuda, A.Z., Mokhtar, T.A., Moos, C., Omar, O.M., Rasheed, M., Rosiak, U., Salem, M., Schmidt, M., Schmitt, M., Stoffers, P., Shata, A.M., Themann, S. and Weldeab, S., 2000a. Report and preliminary results of *Meteor* cruise M 44/3 Aqaba (Jordan) - Safaga (Egypt) - Dubá (Saudia Arabia) - Suez (Egypt) - Haifa (Israel). Berichte aus dem Fachbereich Geowissenschaften der Universität Bremen, 149: 135.

Pätzold, J., Halbach, P.E., Hempel, G. and Weikert, H., 2000b. Meteor-Berichte: Östliches Mittelmeer - Nördliches Rotes Meer 1999 Cruise No. 44. 00-3, Leitstelle METEOR: Institut für Meereskunde der Universität Hamburg, Hamburg.

Pätzold, J., Moammar, M.O., Al Farawati, R., Al Hazmi, Y.M.M., Al Otibi, A., Antunes, A., Arz, H.W., Berger, J., Botz, R., Donner, B., Erhardt, A., Garbe-Schönberg, C.-D., Ghandourah, M., Hübscher, C., Kahl, G., Klann, M., Klauke, S., Klitzke, U., Legge, H.L., Lichowski, F., Schewe, F., Schmidt, M., Schmitt, M., Seeberg-Elverfeldt, I.A. and Truscheit, T., 2003. Black Sea - Mediterranean - Red Sea, Part 3, Cruise No. 52, Leg 3, March 10 - March 27, 2002, Limassol-Limassol. In: C. Hübscher (Editor), METEOR-Berichte, Black Sea - Mediterranean - Red Sea, Cruise No. 52, January 2 - March 27, 2002. Universität Hamburg, Hamburg, pp. 62; available under http://www.marum.de/M52_-_Schwarzes_Meer_-_Mittelmeer_-_Rotes_Meer.html.

Pautot, G., Guennoc, P., Coutelle, A. and Lyberis, N., 1984. Discovery of a large brine deep in the northern Red Sea. Nature, 310: 133-136.

Pearce, R.B., Kemp, A.E.S., Koizumi, I., Pike, J., Cramp, A. and Rowland, S.J., 1998. A lamina-scale, SEM-based study of late quaternary diatom-ooze sapropel from the mediterranean ridge, site 971. In: A. Camerlenghi (Editor), Proceedings of the Ocean Drilling Program, Scientific results. College Station, TX, pp. 349-363.

Petterson, G., 1996. Varved sediments in Sweden: a brief review. In: A.E.S. Kemp (Editor), Palaeoclimatology and Palaeoceanography from laminated sediments. Geological Society, Special Publication, pp. 73-78.

Pike, J. and Kemp, A.E.S., 1996. Records of seasonal flux in Holocene laminated sediments, Gulf of California. In: A.E.S. Kemp (Editor), Palaeoclimatology and Palaeoceanography from laminated sediments. Geological Society, Special Publication, pp. 157-170.

Pilskaln, C.H. and Pike, J., 2001. Formation of Holocene sedimentary laminae in the Black Sea and the role of the benthic flocculent layer. Paleoceanography, 16(1): 1-19.

Ragueneau, O., Tréguer, P., Leynaert, A., Anderson, R.F., Brzezinski, M.A., DeMaster, D.J., Dugdale, R.C., Dymond, J., Fischer, G., Francois, R., Heinze, C., Maier-Reimer, E., Martin-Jezequel, V., Nelson, D.M. and Queguiner, B., 2000. A review of the Si cycle in the modern ocean: recent progress and missing gaps in the application of biogenic opal as a paleoproductivity proxy. Global and Planetary Change, 26: 317-365.

Rines, J.E.B. and Hargraves, P.E., 1988. The *Chaetoceros* Ehrenberg (Bacillariophyceae) flora of Narragansett Bay, Rhode Island, U.S.A. Bibliotheca Phycologica. J. Cramer, 196 pp.

Round, F.E., Crawford, R.M. and Mann, D.G., 1990. The diatoms: biology & morphology of the genera. Cambridge University Press, Cambridge, 747 pp.

Sancetta, C., 1989. Processes controlling the accumulation of diatoms in sediments: a model derived from British Columbian Fjords. Paleoceanography, 4(3): 235-251.

Schimmelmann, A. and Lange, C.B., 1996. Tales of 1001 varves: a review of Santa Barbara Basin sediment studies. In: A.E.S. Kemp (Editor), Palaeoclimatology and Palaeoceanography from laminated sediments. Geological Society, Special Publication, pp. 121-142.

Seeberg-Elverfeldt, I.A., Lange, C.B., Arz, H.W., Pätzold, J. and Pike, J., accepted. The significance of diatoms in the formation of laminated sediments in the Shaban Deep, Northern Red Sea. Marine Geology.

Shaikh, E.A., Roff, J.C. and Dowidar, N.M., 1986. Phytoplankton ecology and production in the Red Sea off Jiddah, Saudi Arabia. Marine Biology, 92: 405-416.

Staubwasser, M. and Sirocko, F., 2001. On the formation of laminated sediments on the continental margin off Pakistan: the effects of sediment provenance and sediment redistribution. Marine Geology, 172: 43-56.

Stoffers, P., Botz, R. and Scholten, J., 1990. Isotope Geochemistry of Primary and Secondary Carbonate Minerals in the Shaban-Deep (Red Sea). In: P. Stoffers (Editor), Sediments and Environmental Geochemistry. Springer, Berlin, pp. 83-94.

Thunell, R.C., Williams, D.F. and Belyea, P.R., 1984. Anoxic events in the mediterranean sea in relation to the evolution of late neogene climates. Marine Geology, 59: 105-134.

Tréguer, P., Nelson, D.M., van Bennekom, A.J., DeMaster, D.J., Leynaert, A. and Queguiner, B., 1995. The silica balance in the world ocean: a reestimate. Science, 268: 375-379.

van Geen, A., Zheng, Y., Bernhard, J.M., Cannariato, K.G., Carriquiry, J., Dean, W.E., Eakins, B.W., Ortiz, J.D. and Pike, J., 2003. On the preservation of laminated sediments along the western margin of North America. Paleoceanography, 18(4): 1098, doi:10.1029/2003PA000911.

Villareal, T.A., 1988. Positive buoyancy in the oceanic diatom *Rhizosolenia debyana* H. Peragallo. Deep-Sea Research, 35(6): 1037-1045.

von Rad, U., Schaaf, M., Michels, K.H., Schulz, H., Berger, W.H. and Sirocko, F., 1999. A 5000-yr record of climate change in varved sediments from the oxygen minimum zone off Pakistan, northeastern Arabian Sea. Quaternary Research, 51: 39-53.

Winter, A., Almogi-Labin, A., Erez, Y., Halicz, E., Luz, B. and Reiss, Z., 1983. Salinity tolerance or marine organisms deduced from Red Sea quaternary record. Marine Geology, 53: M17-M22.

Zolitschka, B., 1996. Image analysis and microscopic investigation of annually laminated lake sediments from Fayetteville Green Lake (NY, USA), Lake C2 (NWT, Canada) and Holzmaar (Germany): a comparison. In: A.E.S. Kemp (Editor), Palaeoclimatology and Palaeoceanography from laminated sediments. Geological Society, Special Publication, pp. 49-56.

Chapter 2: Methodology

2.1 Material used in this study

The samples used in this thesis were collected during RV Meteor cruises M 44/3 in 1999 and M 52/3 in 2002 (Table 2.1; Figs 1.3 and 2.1). Plankton samples were collected in 2002 with a multiple closing plankton net (HYDROBIOS) with 20 µm mesh size which was towed at five stations with 0.3 m s^{-1}, and from two different water depth intervals, 200–120 m and 120–20 m. Samples were preserved with 37 % formaldehyde (stabilized with 10 % methanol) directly after retrieval.

Table 2.1: Location of all sampling sites in the northern Red Sea used in this thesis from two RV Meteor cruises M 44/3 (GeoB 58xx; 28°-26°N, March/April 1999) and M 52/3 (GeoB 78xx; 27°-21°N; March/April 2002). Sample locations are shown in Figs 1.3 and 2.1.

Core GeoB	Lat. N	Long. E	Water depth [m]	Type of sample
5823-1	26°25.26'	35°40.19'	789	MUC ●
5825-1	26°30.47'	35°56.94'	1031	MUC ●
5827-1	26°19.11'	35°31.20'	959	MUC ●
5831-1	27°05.30'	35°33.98'	884	MUC ●
5837-1	27°36.69'	34°51.85'	771	MUC ●
5836-2	26°12.61'	35°21.56'	1475	gravity core ★
5838-1	27°34.54'	34°44.16'	832	MUC ●
5843-2	27°52.69'	34°58.16'	529	MUC ●
7802-1	26°12.7'	35°21.4'	1464	MUC ●
7803-2	26°12.4'	35°21.8'	1474	MUC ●
7805-1	26°13.9'	25°22.6'	1447	MUC ●
7805-3	26°13.2'	35°22.5'	1445	Plankton ▲
7805-4	26°13.2'	35°22.5'	1438	Plankton ▲
7813-1	24°44.9'	36°15.6'	1137	Plankton ▲
7813-2	24°45.0'	36°15.6'	1137	Plankton ▲
7813-3	24°44.9'	36°15.6'	1137	MUC ●
7818-1	23°16.1'	37°25.1'	895	Plankton ▲
7818-2	23°16.2'	37°25.1'	895	Plankton ▲
7818-3	23°16.1'	37°25.1'	895	MUC ●
7819-2	22°31.0'	38°06.2'	852	MUC ●
7819-3	22°31.6'	38°06.1'	823	Plankton ▲
7819-4	22°31.6'	38°06.1'	823	Plankton ▲
7824-3	21°27.2'	38°50.6'	684	MUC ●
7825-3	21°24.4'	38°32.6'	841	Plankton ▲
7825-4	21°24.3'	38°32.5'	841	Plankton ▲

Surface sediments were collected using a multicorer (MUC). A total of 13 surface sediment sites (11 non-brine, 2 brine) were selected for this study which yield good geographical coverage of the northern Red Sea.

Downcore studies included one gravity core (GeoB 5836-2; 26°12.61'N, 35°21.56'E; water depth 1475 m; 790 cm long) which was retrieved from the southern basin and one multicore (GeoB 7805-1; 26°13.9'N, 25°22.6'E; water depth 1447 m; 60 cm long) from the eastern basin (Fig. 1.3) of the Shaban Deep in 1999 and 2002, respectively. All samples were stored at 4°C prior to sampling.

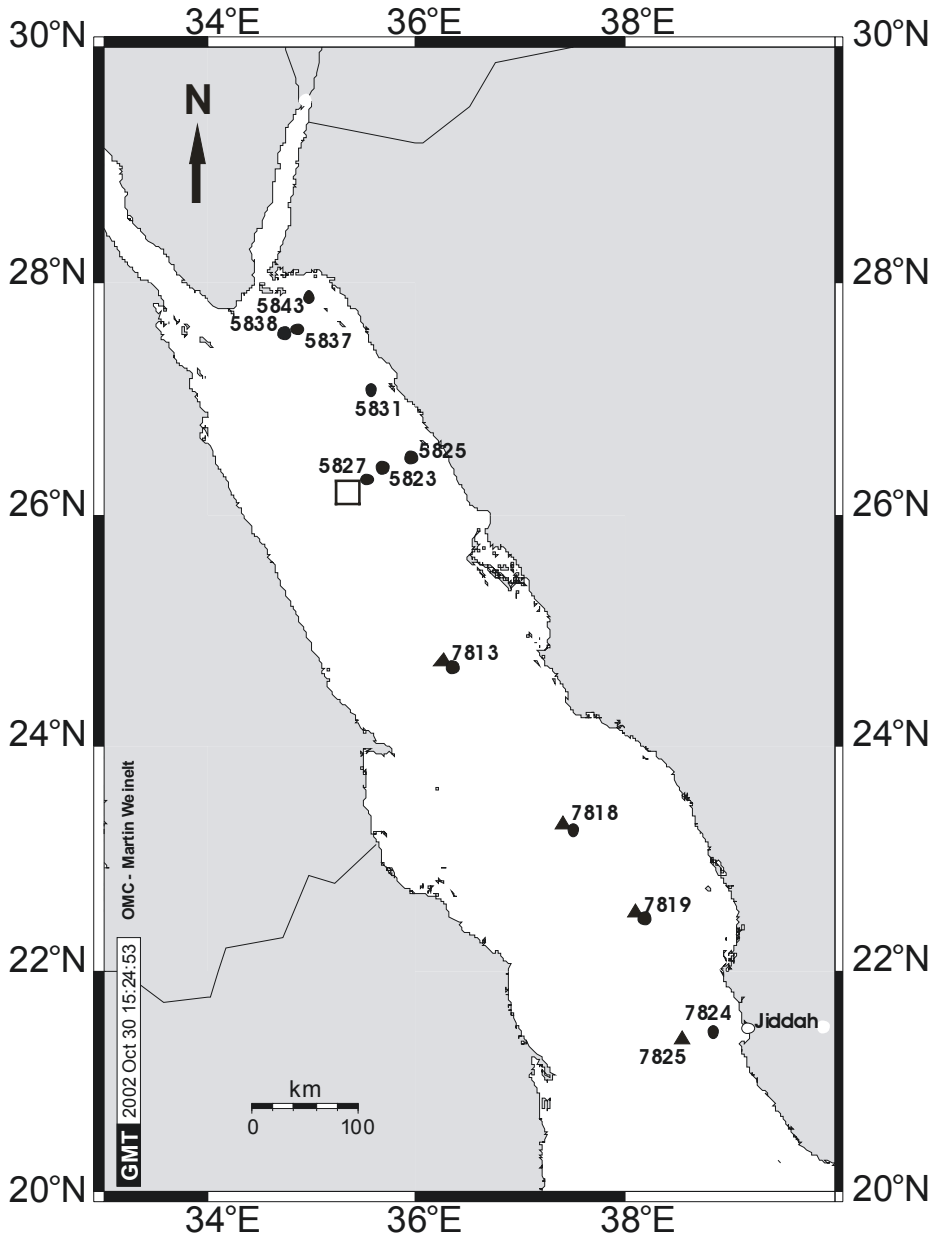

Fig. 2.1: Location of sampling sites in the northern Red Sea. Square marks the position of the Shaban Deep. Symbols refer to Table 2.1: ● = Multicore sample; ▲ = plankton sample. Details of sampling sites within the Shaban Deep are given in Fig. 1.3.

2.2 X-radiography

Cookie cutter slabs (15 cm (L) x 1 cm (W) x 5 cm (D)) were taken within the laminated intervals of gravity core GeoB 5836-2 and multicore GeoB 7805-1, following the method described by Schimmelmann et al. (1990) and Dean et al. (1999). X-radiographs of slabs were done to record differences in sediment density and structure. A Faxitron 43855A was used (45 kV; 3.5 min exposure time) to produce X-radiographs which were then developed in the darkroom. The X-radiograph negatives were scanned to establish a direct relationship with the thin sections that are described below. In the scanned negatives, light bands represent layers of very dense material and dark bands indicate layers of lower density.

2.3 XRF and opal analysis

An X-ray fluorescence (XRF) core scanner was used for the determination of bulk sediment chemistry of multicore GeoB 7805-1. Measurements were done at high-resolution every 0.2 cm for the following elements: Al, Si, P, S, Cl, K, Ca, Ti, Mn and Fe.

Selected discrete samples of core GeoB 5836-2 were freeze-dried and ground in an agate mortar. Biogenic opal content was determined by the basic leaching method of DeMaster (1981), modified by Müller and Schneider (1993). The results are given in wt% SiO_2.

2.4 Preparation of diatom slides and smear slides

Permanent diatom slides were prepared for plankton and surface sediment samples following the methods described in Simonsen (1974) and Lange et al. (1994), respectively. Samples from within the brine were washed with distilled water prior to freeze-drying for the removal of the salt. Details about the counting procedure are described in "Preservation of siliceous microplankton in surface sediments of the northern Red Sea" (Seeberg-Elverfeldt et al., 2004; Chapter 3).

Smear slide preparation and analysis for both gravity core GeoB 5836-2 and multicore 7805-1 followed ODP standard procedure.

2.5 Embedding of laminated sediments

For the study of laminated sediments the preparation of polished thin sections has become accepted in the scientific community as the best methodology. For this purpose the sediments need to be resin-embedded first. During this study two different embedding methods were used, as follows:

The 15 cm long sediment slabs of Core GeoB 5836-2 used for X-radiography were taken to the University of Cardiff for resin-embedding after the methodology of Pike and Kemp (1996). There, a ca. 1 cm thick strip of the sediment was cut off and, wrapped in aluminium foil, put into small plastic containers. Since the sediment contains very salty pore water (brine salinity ~ 260 psu), we had to adapt the method to accommodate our sediments. The sediment blocks were therefore first soaked in distilled water for removal of the salt. This was done five times over a period of two days. After the sediments were salt-free, the drying process started with technical grade acetone. After six replacements (with 3 replacements on one day), analytical grade acetone (which has a much lower water content than the technical grade) was used for the next four replacements. The sediments were then "dry" enough to start with the resin-embedding procedure.

The resin itself consists of four different chemicals that were mixed together just before usage:

- Vinylcyclohexene dioxide (VCD) 10 parts
- Diglycidol ether of polypropyleneglycol (DER 736) 6 parts
- Nonenyl succinic anhydride (NSA) 26.6 parts
- Dimethylaminoethanol (DMAE) 0.2 parts

The embedding was done over a period of five days with two replacements per day. The replacements shouldn't be more than 14 hours apart to avoid curing. For the first 3 ½ days the resin was still mixed with an increasing amount of acetone to lower the viscosity of the resin. This ensures that the resin reaches right into the centre of the samples. This was done with the following proportions:

- First three additions: 3:2 resin:analytical grade acetone
- Fourth and fifth addition: 11:4 resin:acetone
- Sixth and seventh: 13:2 resin:acetone

The final pure resin was then added on the fourth day and again replaced two more times before the sediments were left soaking for the following four weeks. Thereafter, the resin was cured in an oven:

- For 24 hours at 30°C
- For 24 hours at 45°C
- For 24 hours at 60°C

The samples were left to cool for 12 hours between every step.

Polished thin sections of ~50 µm thickness were then prepared (Fig. 2.2).

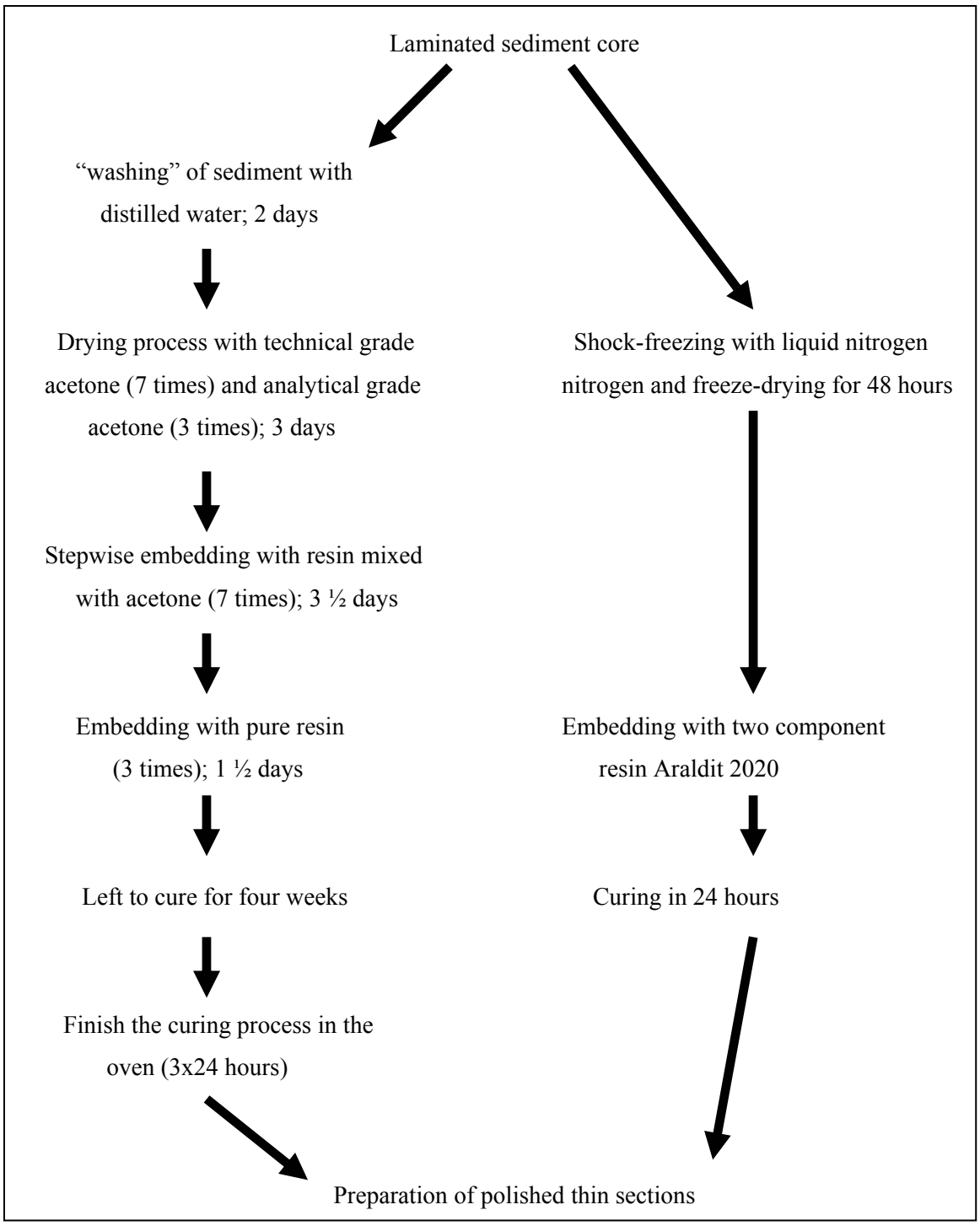

Fig. 2.2: Comparison of the methods used during this study to produce resin-embedded polished thin sections.

The preparation of polished thin sections from multicore GeoB 7805-1 was carried out at the GeoForschungsZentrum Potsdam and followed the procedure of Köhler and Berger (pers. comm.). Seven-cm long sediment blocks were taken with a 3 cm overlap to adjacent samples. The sediment blocks were put into aluminium foil to keep them from falling apart and then shock-frozen in liquid nitrogen and freeze-dried for 48 hours. After the sediments were dry

they were impregnated with Araldit 2020, a two-component epoxy-resin. This embedding was done stepwise under vacuum to ensure the thorough soaking process. This resin cures at room temperature within 24 hours. Thereafter, polished thin sections were prepared. The 7 cm long embedded blocks were cut up into 3 sub-samples with an overlap to the adjacent sections to ensure a continuous record. Polished thin sections of 80-100 µm thickness were then prepared (Fig. 2.2).

The main differences between these two methods refer to the process by which water is removed from within the sediment and the two different resin-types used. The Cardiff-method involves a mixing of the resin from different components which are toxic and in one case carcinogenic. They should be handled with special care and a special laboratory should be used to prevent endangering others. Furthermore the usage of these chemicals is not allowed in Germany which was the main reason to use a different method for the second core. Araldit 2020, on the other hand is not toxic but should be handled with care and used in the fume cupboard as well. It is composed of two components which are mixed together just before usage: the resin itself and a curing agent. It is a very fast method since the resin does not need to be replaced many times and the resin cures within a much shorter time period.

The drying-processes are also completely different. The freeze-drying used in Potsdam is a very fast method and excludes the working with acetone which again should be handled with care. But, on the other hand, the soaking in acetone used in Cardiff is a very gentle method which does not disturb the sediment fabric. For example, thin sections that were prepared in Potsdam had several cracks which were caused by the freeze-drying process.

For future preparation of thin sections it might be useful to run some tests on combining the two methods: it might be possible to use Araldit 2020 in the same way as the resin in Cardiff and first mix it with acetone or some other chemical to keep it viscous. (Acetone can be used to clean equipment that is contaminated with Araldit 2020 that is not cured yet [http://www.kremer-pigmente.de/97920.htm]). If this is possible, the drying process could also be changed to the gentler way of slowly drying with acetone. The quality of the thin sections could be improved.

In case of the preparation of sediments from a high-saline environment I furthermore recommend to first remove the salt from the sediments. Although this was not the case with the Red Sea samples prepared in Potsdam, salt crystals can crack the microscope slide on which the sediment is sitting and thereby destroy the thin section completely (Berger and Arnold, pers. comm.). In our case the salt was actually visible on the thin section in the Scanning Electron Microscope (SEM).

2.6 Investigation of polished thin sections in the SEM (scanning electron microscope)

Polished thin sections were prepared for the investigation of sediments in the scanning electron microscope (SEM) under high magnification to analyse the fine structure of laminated sediments. For this purpose, the thin sections were coated with carbon and an SEM with back scattered electron detector was used. The backscatter coefficient η is defined through the proportion between the backscattered electron beam and the incident electron beam (Reimer and Pfefferkorn, 1973). It is recorded on a photograph or a digital image as image brightness (Pike and Kemp, 1996). Backscattered electrons have the further advantage of entering the sample (in our case the thin section) and providing information about its composition. Secondary electrons on the other hand, are produced at the sample surface and provide information about the topography of the sample. Backscattered Electron Imagery (BSEI) photo mosaics can be used to produce a compositional as well as a porosity map. Mineral grains (pyrite, quartz) and also carbonate have high atomic numbers (higher backscatter coefficients) and produce bright images. Organic matter and the resin used for embedding on the other hand, have low atomic numbers (low backscatter coefficients) and appear therefore dark (Pike and Kemp, 1996). In addition, lithogenic laminae comprised of terrigenous material, have a low porosity and appear therefore as brighter layers than biogenic laminae. Diatom frustules on the other hand are filled with resin which is carbon-based and generate dark layers due to their high porosity (Pike and Kemp, 1996).

First, low magnification images were produced to create a basemap for further high magnification work (Pike and Kemp, 1996). Our basemaps were done with 30x or 80x magnification depending on microscope settings. They consist of a series of digital pictures that were taken from the top of the slide to the bottom and later joined at the computer to form one long image of the thin section. Secondly, light and dark layers on the BSEI photomosaic were investigated with higher magnification (our study: up to 3500x) to determine the composition of single laminae.

2.7 Preparation of stubs

In addition to the thin sections, raw sediment blocks were cracked open along lamina boundaries and coated with Au/Pd. They were studied to get topographic images of single laminae using Secondary Electron Imagery (SEI). Results were used to help with the identification of single diatom species that can otherwise only be observed in cross-section in thin sections.

References

Dean, J.M., Kemp, A.E.S., Bull, D., Pike, J., Patterson, G. and Zolitschka, B., 1999. Taking varves to bits: Scanning electron microscopy in the study of laminated sediments and varves. Journal of Paleolimnology, 22: 121-136.

DeMaster, D.J., 1981. The supply and accumulation of silica in the marine environment. Geochimica et Cosmochimica Acta, 45(2): 1715-1732.

Lange, C.B., Treppke, U.F. and Fischer, G., 1994. Seasonal diatom fluxes in the Guinea Basin and their relationship to trade winds, hydrography and upwelling events. Deep-Sea Research I, 41: 859-878.

Müller, P.J. and Schneider, R., 1993. An automated leaching method for determination of opal in sediments and particulate matter. Deep-Sea Research I, 40(3): 425-444.

Pike, J. and Kemp, A.E.S., 1996. Preparation and analysis techniques for studies of laminated sediments. In: A.E.S. Kemp (Editor), Palaeoclimatology and Palaeoceanography from laminated sediments. Geological Society, Special Publication, pp. 37-48.

Reimer, L. and Pfefferkorn, G., 1973. Rasterelektronenmikroskopie. Springer Verlag, Berlin, 263 pp.

Schimmelmann, A., Lange, C.B. and Berger, W.H., 1990. Climatically controlled marker layers in Santa Barbara Basin sediments and fine-scale core-to-core correlation. Limnology and Oceanography, 35(1): 165-173.

Simonsen, R., 1974. The diatom plankton of the Indian Ocean Expedition of R/V "Meteor". "Meteor" Forschungs-Ergebnisse, 19. Institut für Meeresforschung Bremerhaven, Bremerhaven, 66 pp.

Chapter 3: Results

During the three years of the course of my dissertation, three manuscripts covering various aspects of diatoms in the northern Red Sea were prepared. In all manuscripts, I am the first author.

Here I include a short summary of the topics covered by each manuscript, followed by the full text.

Manuscript 1

Preservation of siliceous microplankton in surface sediments of the northern Red Sea

Seeberg-Elverfeldt, I. A., C. B. Lange, J. Pätzold (*Marine Micropaleontology*, 51 (3/4), 193-211. 2004)

We studied the siliceous microplankton assemblages (mainly diatoms) from plankton tows and surface sediments along a N-S transect in the northern Red Sea between 28° and 21°N, as an essential first step of understanding the effects of preservation in the sediments in order to assess the accuracy with which the sedimentary record reproduces the original living assemblage. Sediment samples included two different types of sediment: oxic, non-brine sediments and anoxic, brine sediment from the Shaban Deep. We report on differences/similarities between plankton and sediment assemblages with special attention on the comparison between brine and non-brine sediments. We show that surface brine sediments have higher biogenic opal contents and concentrations of siliceous microplankton, higher diatom species diversity and that fragile forms are better preserved than in non-brine sediments.

Manuscript 2

The significance of diatoms in the formation of laminated sediments of the Shaban Deep, Northern Red Sea

Seeberg-Elverfeldt, I. A., C. B. Lange, H. W. Arz, J. Pätzold, J. Pike (accepted for publication in *Marine Geology*)

Laminated sediments in the Shaban Deep (northern Red Sea) were analyzed with backscatter electron imagery in order to determine laminae composition with emphasis on the diatomaceous component, from different time intervals: mid-Holocene, early Holocene,

deglaciation and Last Glacial Maximum (LGM). Special emphasis was given to the question of whether these sediments would contain a seasonal signal and therefore present annual varves. Sedimentation models for every time interval were produced. The different assemblages are discussed against the background of already existing paleoceanographic data from an oxic core of the northern Red Sea.

Manuscript 3

Laminae type and possible mechanisms for the formation of laminated sediments in the Shaban Deep, Northern Red Sea

Seeberg-Elverfeldt, I. A., C. B. Lange and J. Pätzold (Manuscript in preparation)

Laminated sediments (Late Holocene to Last Glacial Maximum) from the Shaban Deep were analyzed to present possible mechanisms involved in the formation of laminae of various types and homogenous intervals. Our rationale behind the suggested scenarios includes several assumptions: 1) particulate matter sinks relatively fast through the water column as fecal pellets, aggregates and/or diatom mats; 2) particulate matter then concentrates at the seawater-brine interface due to density differences – until they are dense enough to break the interface - before sinking through the brine; 3) all particles that have accumulated at this interface might be subject to bacterial decomposition; 4) sorting may occur during accumulation at the seawater-brine interface and during transport to the seafloor; 5) BSEI light layers are generated by the disintegration of fecal pellets carrying mainly coccoliths (and sometimes coccospheres); and 6) the paleoflux scenarios presented earlier are correct.

3.1 Preservation of siliceous microplankton in surface sediments of the northern Red Sea

Ismene A. Seeberg-Elverfeldt[a], Carina B. Lange[b] and Jürgen Pätzold[a]

[a]Research Center Ocean Margins, University of Bremen, P.O. Box 330440, 28334 Bremen, Germany
[b]Departamento Oceanografía, Universidad de Concepción, Centro FONDAP-COPAS, Casilla 160-C, Concepción, Chile

Marine Micropaleontology, 51 (3/4), 193-211, 2004

Abstract

We studied the siliceous microplankton assemblages (mainly diatoms) from plankton tows (mesh size 20 µm) and surface sediment samples collected along a N-S transect in the northern Red Sea (28° to 21°N). In addition, we analyzed differences/similarities between plankton and sediment assemblages within a brine-filled basin (the southern basin) of the Shaban Deep, and compared these assemblages with those from outside the brine. Plankton samples revealed the overwhelming dominance of diatoms over other siliceous groups. Diatoms accounted for ca. 97 % of all biosiliceous particles at 120-20 m (vs. 2.9 % silicoflagellates and 0.4 % radiolarians), and ca. 94 % at 200-120 m (vs. 4.5 % silicoflagellates and 1.6 % radiolarians). In general, a marine, warm-water (tropical/ subtropical) diatom assemblage characterizes the plankton samples. Representatives of the *Nitzschia bicapitata* group are by far the most abundant contributors at both depth intervals (average = 43 %), ranging from ca. 30 % in the North to ca. 60 % in the South. Biogenic opal content in non-brine surface sediments is very low, (below 0.2 wt % SiO_2); and concentration of siliceous microorganisms is also low and of the order of 5 x 10^3- 10^4 microorganisms g^{-1} dry sediment. Diatoms are the main contributors to the opal signal in the 20-40 µm fraction while they share dominance with radiolarians in the > 40 µm fraction. Total diatom concentrations average 1.2 x 10^4 valves g^{-1} in the 20-40 µm fraction, and 4 x 10^3 valves g^{-1} in the > 40 µm fraction. Robust taxa of warm water affinity (*Alveus marinus*, *Azpeitia neocrenulata*, *Azpeitia nodulifera* and *Roperia tesselata*) characterize the surface sediments. In contrast, biogenic opal content in brine surface sediment samples is much higher than in the non-brine samples, ranging from 2.8 wt % to 3.8 wt % SiO_2, and concentration of siliceous microorganisms is 3-4 orders of magnitude higher. In addition here, diatoms dominate the opal signal. The taxa found in these samples are a mixture of non-brine and plankton samples, and fragile forms (e.g. *N. bicapitata*

group, *Neodelphineis indica*) are well preserved in these sediments. Thus, brine sediments in this region seem to offer a great potential for palaeoenvironmental studies.

***Keywords**: Red Sea; diatoms; plankton; sediments; brine basin; biogenic silica; preservation*

Introduction

The Red Sea is an oligotrophic water body (Fig. 1) characterized by special features due to its enclosed position. There is almost no rainfall as no permanent rivers flow into the Red Sea, and evaporation is high especially during winter (Edwards, 1987). Salinity values increase from south to north with decreasing surface temperatures (Edwards, 1987), away from the only large inflow of water from the Indian Ocean. Sinking and formation of intermediate and bottom waters occurs in the north (Edwards, 1987; Eshel et al., 1994; Eshel and Naik, 1997). During the SW Monsoon (June to September), surface currents flow to the south; this flow is reversed during the NE Monsoon (December to March).

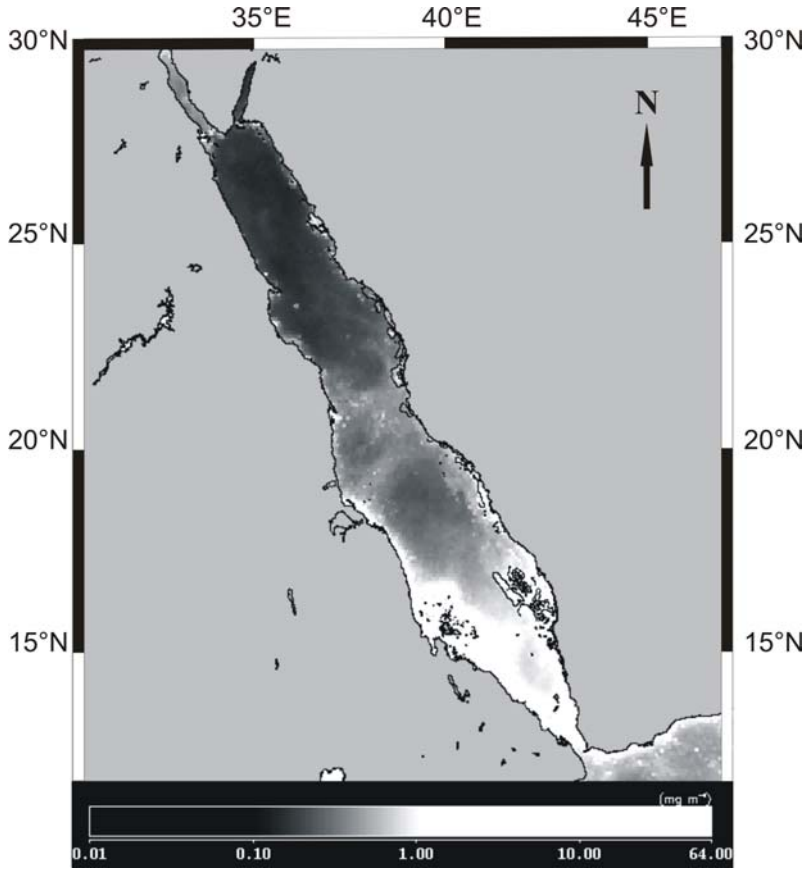

Figure 1: Average chlorophyll *a* distribution in the Red Sea for 2002. Note the contrast between north and south, and the very low Chl *a* values year-round in the northern part. Data provided by the SeaWiFS Project and the Distributed Active Archive Center, Goddard Space Flight Center, Greenbelt, MD, USA.

Brine-filled basins are found along the Red Sea central axis (Hartmann et al., 1998) where salinity values reach up to 250 ‰ (e.g. in the Shaban Deep; Pätzold et al., 2000a). The high salinities are due to leaching of subbottom Miocene evaporites (Manheim, 1974).

The northern Red Sea is permanently stratified throughout the year, mixing depth is < 100 m, a deep chlorophyll maximum (DCM) is present year-round at about 80-100 m depth (Fig. 2), and the euphotic depth is well beyond 100 m (Pätzold et al., 2000b). A secondary, albeit minor, chlorophyll peak at 120-160 m is also evident (Fig. 2). Phytoplankton is scarce in the oligotrophic Red Sea (Sommer, 2000; Sommer et al., 2002) and dominated by small cells. Autotrophic picoplankton contributes more than 95 % of the chlorophyll (Chl) *a* biomass (Pätzold et al., 2000b).

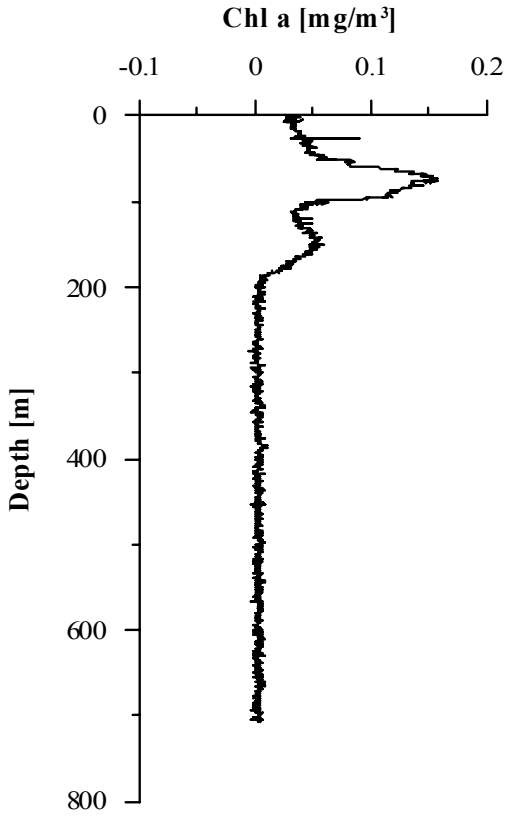

Figure 2: Chlorophyll *a* depth profile at 24°59.0'N and 36°5.1'E in the same region as sample GeoB 7813 (16.03.2002, Meteor cruise M 52/3). Note a deep chlorophyll maximum (DCM) at about 80-100 m depth and a secondary minor chlorophyll peak at 120-160 m.

Very little is known about the microplankton of the Red Sea. Halim (1969) studied the plankton and Kimor and Golandsky (1977) recorded the distribution patterns of four major groups of microplankton (Cyanophyta, Bacillariophyta, Pyrrhophyta and Tintinnida) in the Gulf of Elat in 1974. Kimor and Golandsky (1977) report decreasing numbers of organisms with depth and a peak in diatom abundance at the end of February/March. However, no in-

formation on species composition is given. Shaikh et al. (1986) describe a bimodal pattern with one maximum in December-February and a smaller one in June-August. The authors found diatom species of the genera *Bacteriastrum*, *Chaetoceros*, *Nitzschia* and *Rhizosolenia* as the major contributors to the diatom assemblage in the winter plankton off Jiddah, Saudia Arabia. Lenz et al. (1988) studied the diatom assemblage in the Sudanese open waters but no information about species succession and/or dominance is reported. The work of Veldhuis et al. (1997), on seasonal and spatial variability in phytoplankton biomass of the southern Red Sea, and that of Sommer (2000) in the northern area do not include information on species composition. Recently, Taha et al. (2002) investigated the phytoplankton in the Gulf of Aqaba; only a short list of 8 dominant diatom species is given in their report. To the best of our knowledge, there is no information on siliceous microorganisms preserved in the sediments of the Red Sea.

Here we report on siliceous microplankton assemblages (mainly diatoms) from plankton tows and surface sediment samples collected along a N-S transect in the northern Red Sea (28° to 21°N). Our study addresses (a) N-S distribution patterns of assemblage abundance and composition, and (b) the effects of preservation in the sediments along this N-S transect in order to assess the accuracy with which the sedimentary record reproduces the original living assemblage. This is an essential first step if we are to use the fossil record to interpret past oceanographic/climatic conditions. In addition, we analyze differences/similarities between plankton and sediment assemblages within a brine-filled basin (the southern basin) of the Shaban Deep, and compare these assemblages with those from outside the brine.

Material and Methods

Surface sediments

Sediments were collected with a Multicorer (MUC, GeoB) equipped with six large (10 cm diameter) and four small (6 cm diameter) acrylic tubes of 60 cm length, during two *RV Meteor* cruises in the Red Sea: M 44/3 (28°-26°N; March/April 1999) and M 52/3 (27°-21°N; March/April 2002). A total of 11 surface sediment sites were selected for this study which yield good geographical coverage to allow for interpretation of distribution patterns (Table 1; Fig. 3).

For the analysis of siliceous microorganisms the topmost cm (0-1 cm) of each multicorer station was freeze-dried. About 5 g (non-brine samples) and 0.6-2 g (brine samples) of dry sediment of each sample was treated with hydrogen peroxide and hydrochloric acid to dissolve organic matter and carbonates, following the method of Schrader and Gersonde (1978).

Table 1: Location of sampling sites in the northern Red Sea visited during two *RV Meteor* cruises: M 44/3 (28°-26°N; March/April 1999) and M 52/3 (27°-21°N; March/April 2002). Net-plankton hauls (▲), non-brine surface sediment samples (●), brine surface sediment samples (◆).

Core GeoB	Lat. N	Long. E	Water depth [m]	Type of sample
5823-1	26°25.26'	35°40.19'	789	MUC ●
5825-1	26°30.47'	35°56.94'	1031	MUC ●
5827-1	26°19.11'	35°31.20'	959	MUC ●
5831-1	27°05.30'	35°33.98'	884	MUC ●
5837-1	27°36.69'	34°51.85'	771	MUC ●
5838-1	27°34.54'	34°44.16'	832	MUC ●
5843-2	27°52.69'	34°58.16'	529	MUC ●
7802-1	26°12.7'	35°21.4'	1464	MUC ◆
7803-2	26°12.4'	35°21.8'	1474	MUC ◆
7805-3	26°13.2'	35°22.5'	1445	Plankton ▲
7805-4	26°13.2'	35°22.5'	1438	Plankton ▲
7813-1	24°44.9'	36°15.6'	1137	Plankton ▲
7813-2	24°45.0'	36°15.6'	1137	Plankton ▲
7813-3	24°44.9'	36°15.6'	1137	MUC ●
7818-1	23°16.1'	37°25.1'	895	Plankton ▲
7818-2	23°16.2'	37°25.1'	895	Plankton ▲
7818-3	23°16.1'	37°25.1'	895	MUC ●
7819-2	22°31.0'	38°06.2'	852	MUC ●
7819-3	22°31.6'	38°06.1'	823	Plankton ▲
7819-4	22°31.6'	38°06.1'	823	Plankton ▲
7824-3	21°27.2'	38°50.6'	684	MUC ●
7825-3	21°24.4'	38°32.6'	841	Plankton ▲
7825-4	21°24.3'	38°32.5'	841	Plankton ▲

Acid remains were removed by repeated steps of rinsing with distilled water and settling. Because of the large amount of silt and clay in the non-brine samples and to make the counting procedure easier, these samples were sieved and split into two fractions, 20-40 µm and > 40 µm. We found no microorganism remains in the < 20 µm fraction.

Preparation of permanent slides (mounted with Mountex) of acid-cleaned material for qualitative and quantitative analyses was performed according to Lange et al. (1994). Samples from the brine were washed with distilled water prior to freeze-drying for removal of salt, and then prepared as described above. Brine samples presented no “clay problem” and were therefore not sieved.

Analysis of permanent slides was performed using a Zeiss-Axioscope with phase-contrast illumination at magnifications of 400X; when necessary, a magnification of 1000X was used. Several traverses across an entire coverglass or part of it were examined, depending on mi-

croorganism abundance. In general, more than 400 diatom valves, silicoflagellate skeletons and radiolarians altogether were counted in each slide. For each sample, two replicate slides were counted and the average of both calculated; analytical error between replicate slides is < 15 %.

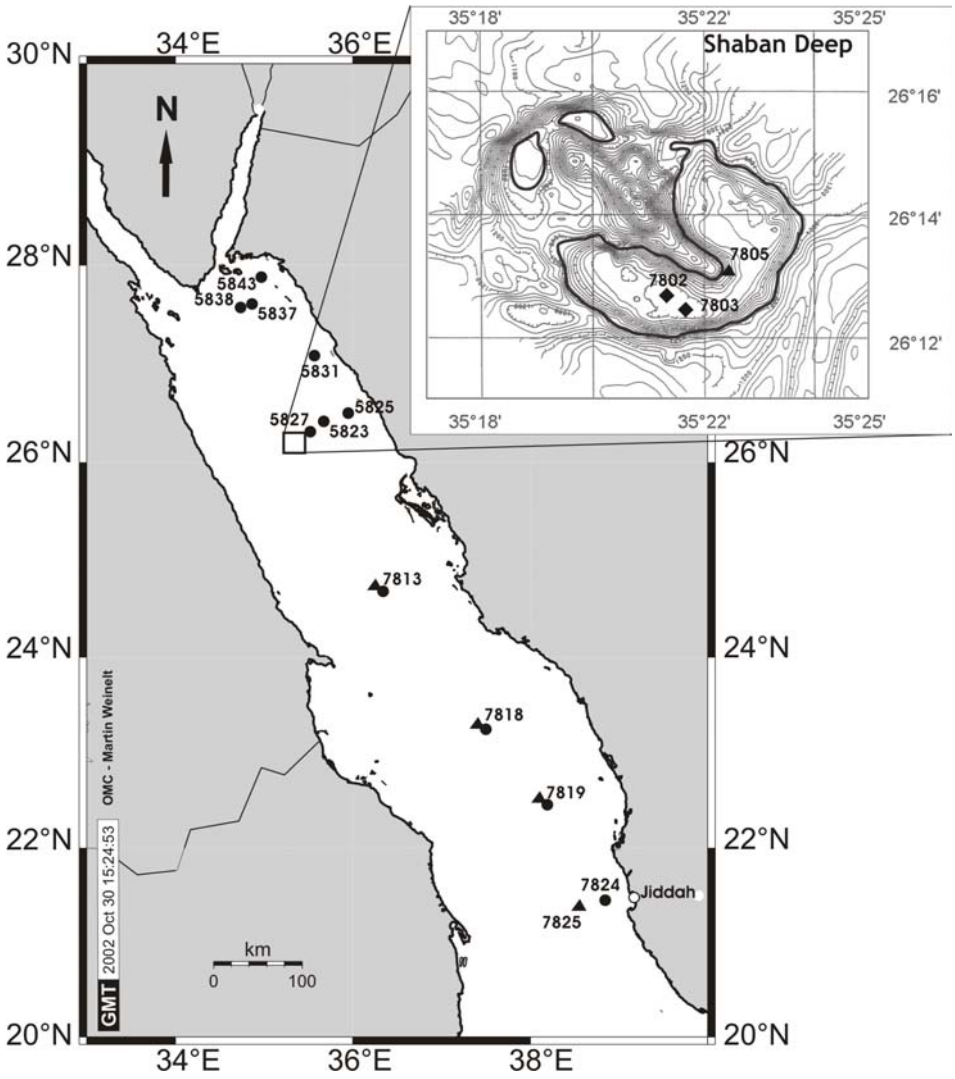

Figure 3: Location of sampling sites in the northern Red Sea. The square marks the position of the Shaban Deep (upper right corner). Right panel, modified from Hartmann et al. (1998). Dark contour line marks the depth of the modern brine surface. ▲ = plankton samples; ● = non-brine surface sediment samples; ◆ = brine surface sediment samples.
(Map after http://www.aquarius.geomar.de/omc_intro.html)

Diatoms and silicoflagellates were identified to the lowest taxonomic level possible, whereas radiolarians were only separated into the two major groups Spumellaria and Nassellaria. Definition of counting units followed Schrader and Gersonde (1978). Abundances of taxa and/or microorganism groups were calculated as concentration per gram of dry sediment. For diatoms, counts refer to valves g^{-1}; resting spores were considered as each spore being

constituted by two valves. Silicoflagellates and radiolarians are expressed as individuals/skeletons g^{-1}. Relative abundances of individual species or group of species were calculated as percent of total assemblage.

Biogenic opal content was determined by the basic leaching method of Müller and Schneider (1993).

Plankton samples

Plankton samples were collected during the Meteor cruise M 52/3 along the same N-S transect as the multicorer samples (Table 1; Fig. 3). A multiple closing plankton net (HYDRO-BIOS) with 20 µm mesh size was used and towed at 0.3 m/s at two different water depth intervals, 200-120 m and 120-20 m. This allowed for sampling of the major and minor chlorophyll peaks separately (Fig. 2). Samples were preserved with 37 %-formaldehyde (stabilized with 10 % methanol) directly after retrieval. In the laboratory, samples were rinsed with distilled water and acid-cleaned following the method described by Simonsen (1974). Permanent slides (Naphrax mounting medium) were prepared following the same methodology as described above for sediment samples. Prior to acid-cleaning, a small aliquot of the original plankton materials was screened in water mount under 400X and 1000X magnification, and the occurrence of aggregates, zooplankton, dinoflagellates, lithic materials, etc. was noted as a guidance for sample reconnaissance.

Because we lack information about the volume of water filtered through the net, plankton samples were used for qualitative analysis only. Diatoms, silicoflagellates and radiolarians were identified as explained above. Estimates of relative abundances of species and groups were based on counting traverses across the cover slip until a number of ~400 valves of diatoms were reached.

For each sample, diatom diversity (H') was calculated according to Shannon and Weaver (1949).

$$H' = - \sum p_i \ln(p_i)$$

where p_i is the number of individuals of species i divided by the total number of individuals in the sample.

All samples and microscope slides are deposited in the repository of the Geology Department at Bremen University, Germany. All data are available under the name of the corresponding author through the PANGAEA server (www.pangaea.de/PangaVista).

Results

Siliceous phytoplankton from net tows

When looking at aliquots of the original plankton material, it becomes evident that diatoms, silicoflagellates and some radiolarians are mostly packed in aggregates sometimes entangled in *Chaetoceros* setae, antennules and/or leg spines of copepods (Fig. 4A). This is especially noticeable in the shallow hauls (120-20 m).

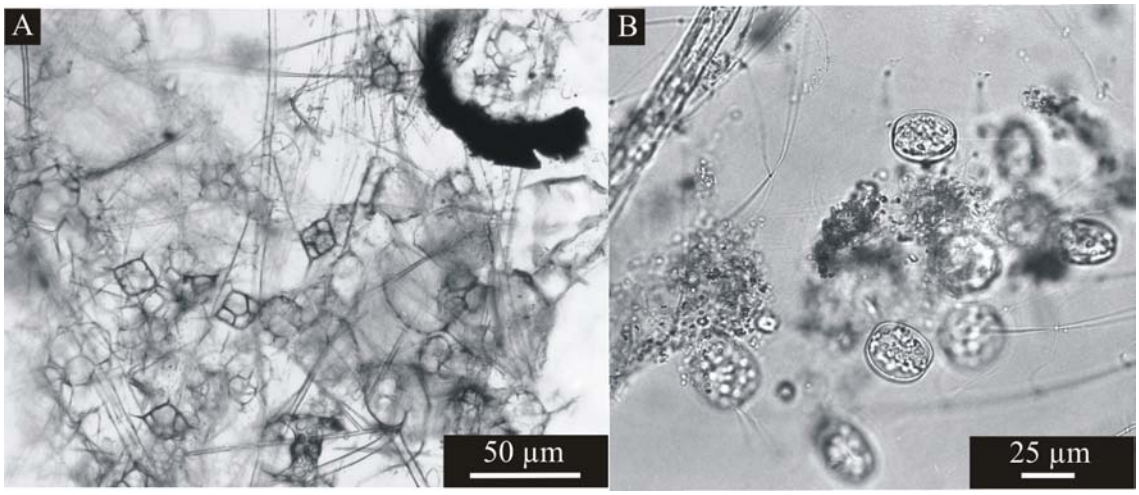

Figure 4: Light microscopy photographs of raw plankton material. (A) Aggregate composed of radiolaria, silicoflagellates and diatoms, entangled in *Chaetoceros* setae from GeoB 7813. (B) Cluster of *Thalassiosira subtilis* from the southernmost station of the investigated transect.

Comparison of water mounts with the acid-cleaned samples indicates that the weakly silicified frustules of *Thalassiosira subtilis,* which are usually found in small clusters in the raw material (Fig. 4B), were partially destroyed during processing and *T. subtilis* was a minor contributor to the assemblage in permanent mounts (1.4 % at 120-20 m and 1.9 % at 200-120 m). However, this taxon was not a dominant component of any sample, so that the bias introduced by the loss is minor.

Permanent mounts revealed the overwhelming dominance of diatoms over the other siliceous groups. Diatoms accounted for ca. 97 % at 120-20 m (*vs*. 2.9 % silicoflagellates and 0.4 % radiolarians), and ca. 94 % at 200-120 m (vs. 4.5 % silicoflagellates and 1.6 % radiolarians).

The whole diatom assemblage was divided into three ecological groups: marine planktonic, non-planktonic and freshwater (see Appendix A): The marine planktonic group represents > 80 % of the entire diatom assemblage at both depth intervals (Fig. 5). Non-planktonic diatoms (including benthic, epiphytic and epilithic species) are also present but in low numbers

and are especially scarce in the southernmost samples. Freshwater species are very rare occurring only at the northernmost and southernmost stations of the N-S transect (Fig. 5).

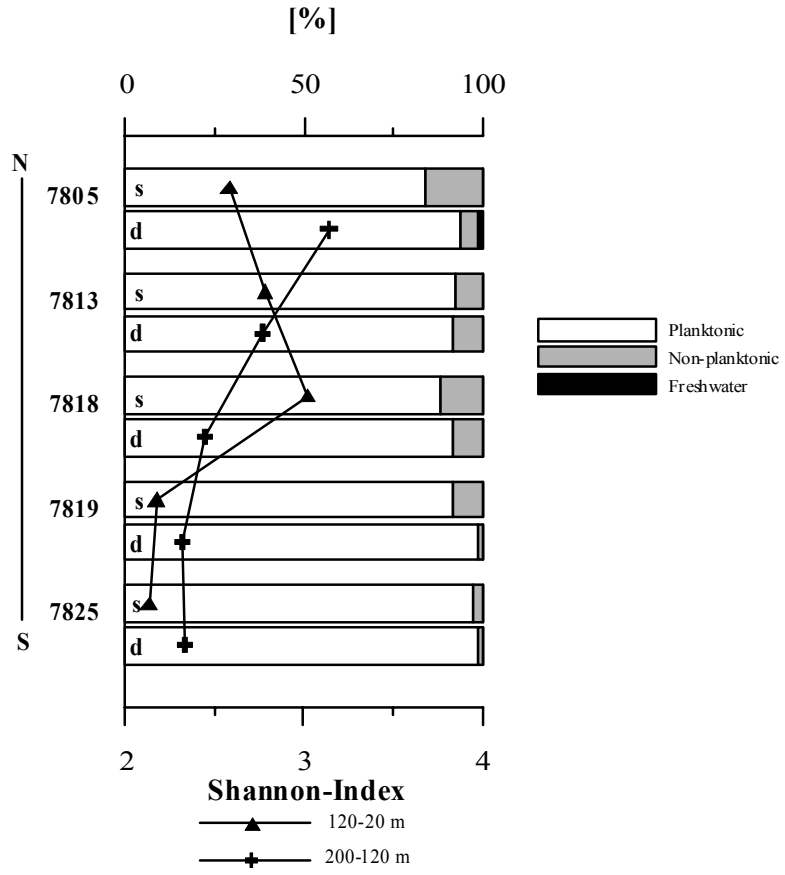

Figure 5: Relative abundance of planktonic, non-planktonic and freshwater diatoms in plankton samples collected at two water depths (120-20 m and 200-120 m) (bars), and the Shannon-Index of diversity (120-20 m: ▲; 200-120 m: +). Sampling sites are arranged from N to S. s = shallow samples (120-20 m); d = deep samples (200-120 m).

In general, a marine, warm-water (tropical/ subtropical) diatom assemblage characterizes the plankton samples. It is composed of 87 taxa in the 120-20 m hauls, and 108 in the 200-120 m haul.

Species diversity (as measured by the Shannon index) shows some dissimilarities between shallow and deep hauls: Diversity is highest at the middle station (7818-1) for the 120-20 m interval, while diversity decreases steadily from North to South for the 200-120 m interval. At both depths, the lowest values are found in the south (Fig. 5).

Nitzschia bicapitata (and associated species within the "*bicapitata*" group; Kaczmarska and Fryxell, 1994) is by far the most abundant species at both depth intervals (average = 43 %; Table 2), ranging from ca. 30 % in the north to ca. 60 % at the southern site. It is accompanied by a non-planktonic assemblage dominated by *Navicula perminuta* at both depths, by *Neodel-*

phineis indica and *Nitzschia* cf. *dissipata* (among others) in the shallow haul, and by *Azpeitia neocrenulata* (among others) in the deeper haul (Table 2).

A small, but net decrease with depth is observed in the contribution of some fragile species (e.g. *N. indica, N.* cf. *dissipata*, *Pseudo-nitzschia delicatissima*, *N. perminuta*). Conversely, the 200-120 m depth interval shows an enrichment in robust taxa (e.g. *Azpeitia neocrenulata*, *Azpeitia nodulifera*, *Nitzschia interruptestriata*) (Table 2). However, our limited database does not allow us to detect: (a) loss of material through the water column for the fragile forms, (b) enrichment of robust forms due to some means of midwater lateral transportation that adds material at depth, or (c) differences in species' habitats (shallow *vs.* deep species).

Table 2: Plankton: Average contribution (as percent of total diatom assemblage) of taxa with > 1 % at both depths.

Species	**120-20 m**	**200-120 m**
Azpeitia neocrenulata	1.0	6.8
A. nodulifera	0.6	1.5
Chaetoceros		
Subgenus Phaeoceros	1.3	1.0
Subgenus Hyalochaete	3.0	2.1
resting spores	0.0	0.1
Leptocylindrus mediterraneus	1.5	1.2
Neodelphineis indica	5.4	4.5
Nitzschia bicapitata group	42.9	42.6
N. braarudii	3.0	3.1
N. interruptestriata	1.4	3.7
N. cf. *dissipata*	4.9	1.0
Pseudo-nitzschia delicatissima	3.2	1.3
P. prolongatoides	1.8	2.0
Skeletonema sp.	1.6	1.8
Thalassionema bacillare	1.9	2.6
T. nitzschioides var. *parva*	1.3	1.1
Thalassiosira lineata	0.3	1.4
T. mala	2.0	0.1
T. subtilis	1.4	1.9
Non-planktonic species	9.1	4.8

Surface sediments

Non-brine samples

In order to characterize the surface sediments of the Red Sea and determine variations in opal content and siliceous microorganism concentrations, a set of 11 non-brine surface sediment samples were analyzed. These samples lie in the N-S transect along the main axis of the Red Sea (Table 1; Fig. 3). Smear-slide analysis reveals high carbonate content in all surface sediment samples, and the major lithological unit is foraminifer-bearing nannofossil ooze with moderate bioturbation (Pätzold et al., 2000a). Available sedimentation rates for the northern section (cores 5823, 5837, 5838) vary between 2.5 and 4.8 cm/kyr (Pätzold et al., 2000a).

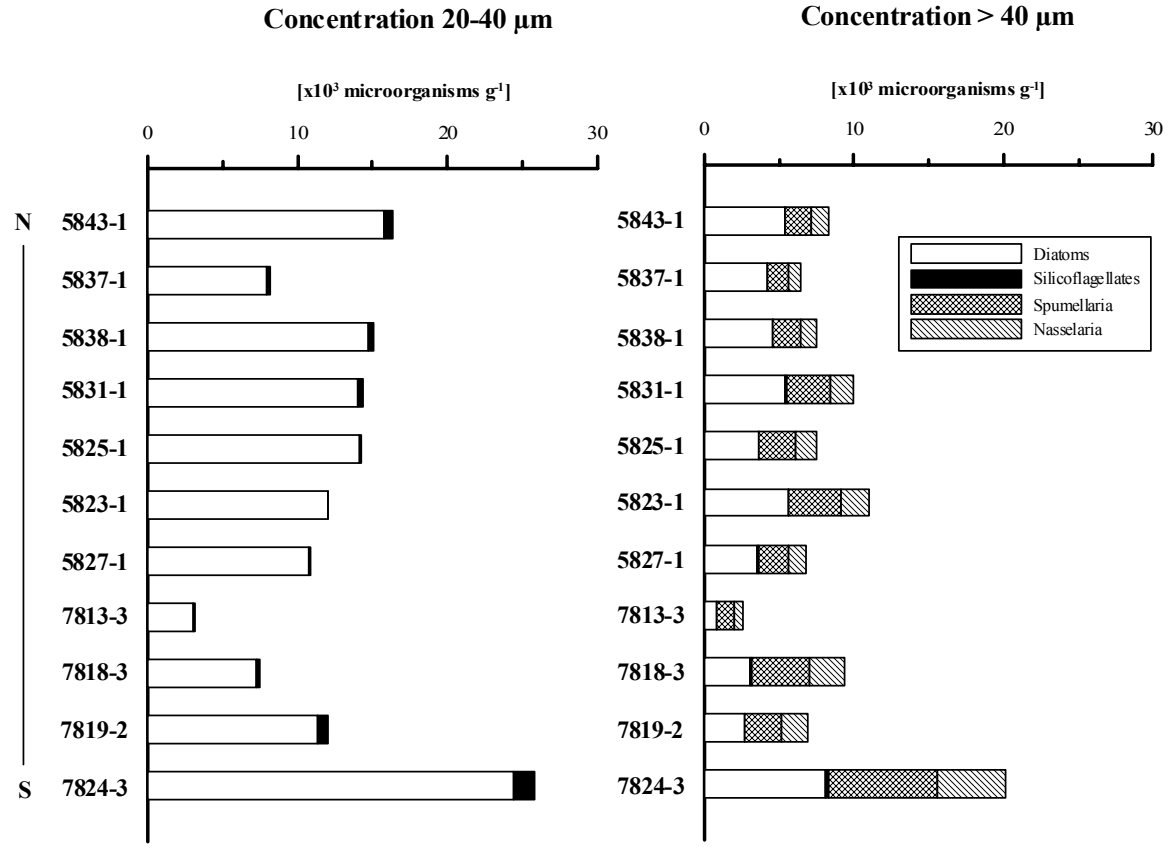

Figure 6: Concentration of siliceous microorganisms per gram of dry sediment in non-brine surface sediment samples from the northern Red Sea, for size fractions 20-40 µm and > 40 µm. Sampling sites are arranged from N to S and from the coast to offshore. Diatoms are the main contributors to the opal signal in the 20-40 µm fraction while they share dominance with Radiolaria in the > 40 µm fraction. The contribution of Radiolaria is insignificant in the 20-40 µm fraction and is therefore not shown.

Biogenic opal content in surface sediments is very low, below 0.2 wt % SiO_2. Hence, concentration of siliceous microorganisms is also low and of the order of 5×10^3-10^4 microorganisms g^{-1} dry sediment, except in the south where concentrations are somewhat higher (ca. 3×10^4 microorganisms g^{-1}) (Fig. 6). Diatoms are the main contributors to the opal

signal in the 20-40 µm fraction while they share dominance with radiolarians in the > 40 µm fraction (Fig. 6). Total diatom concentrations average 1.2 x 10^4 in the 20-40 µm fraction and 4 x 10^3 in the > 40 µm fraction. Highest values in both fractions are found at the southernmost site (7824-3) and lowest values at the central station 7813-3 (Figs. 6 and 7).

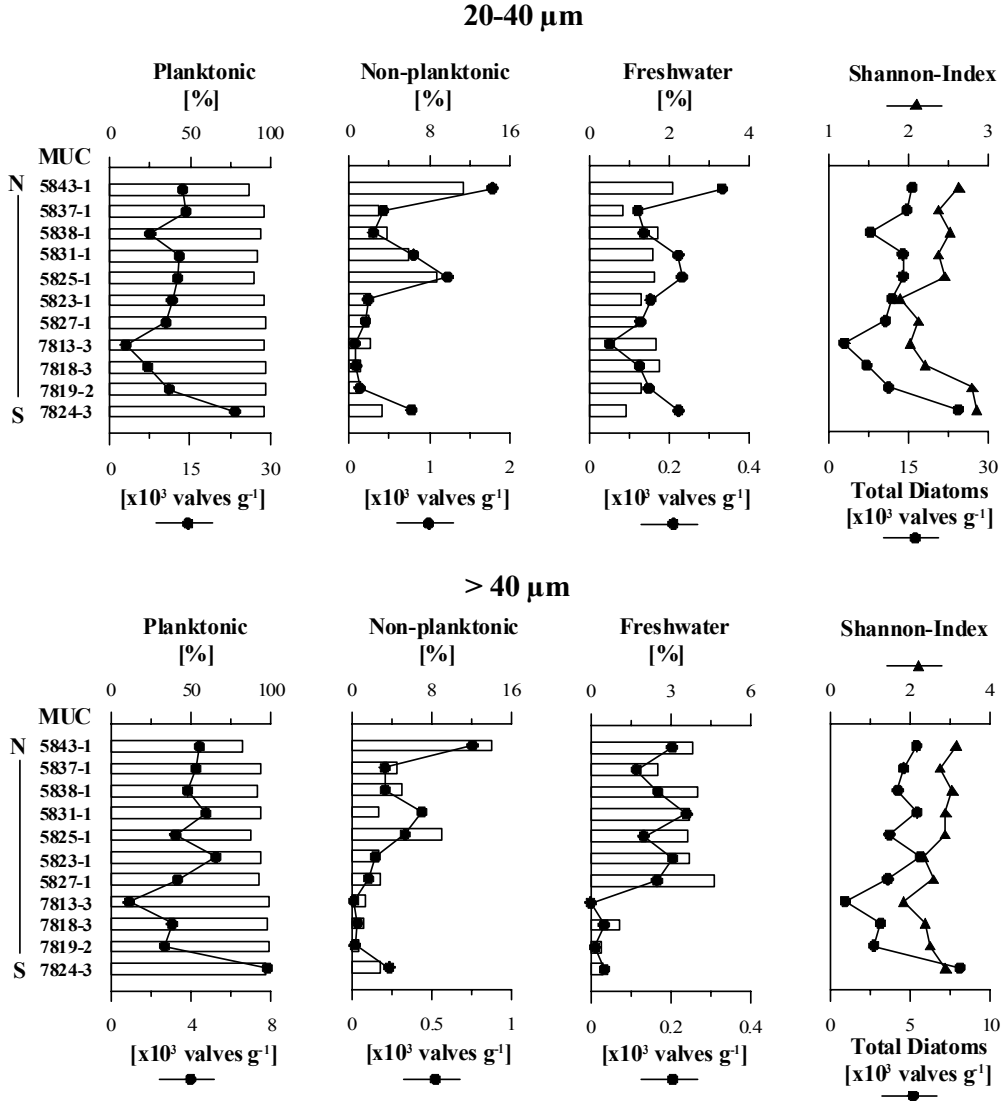

Figure 7: Concentration of planktonic, non-planktonic and freshwater diatoms per gram of dry sediment (lines) and their relative abundances (bars) in non-brine surface samples, for size fractions 20-40 µm and > 40 µm. Diversity and total diatom concentration are plotted to the far right within each size fraction. Note that concentrations are an order of magnitude higher in the 20-40 µm fraction than in the > 40 µm.

Over 100 diatom taxa are found in the surface sediments of the Red Sea. Species diversity (as measured by the Shannon index) shows a similar pattern in both fractions being highest in the south, in contrast to the plankton (compare Figs. 5 and 7). Diatom taxa were assigned to ecological groups (see Appendix A) in the same fashion as was done for plankton samples.

Table 3: Non-brine surface sediments: Average contribution of taxa with > 1 % in both size fractions (20-40 µm and > 40 µm).

	20-40 µm		> 40 µm	
Species	**Average [%]**	**Average [valves g^{-1}]**	**Average [%]**	**Average [valves g^{-1}]**
Actinocyclus subtilis	0.2	23.8	1.0	39.9
Alveus marinus	5.7	739.6	14.7	640.9
Asteromphalus flabellatus	2.8	320.8	1.0	42.4
A. heptactis	0.8	151.8	1.1	66.6
Azpeitia africana	1.8	221.9	1.4	60.8
A. barronii	2.0	226.4	1.3	48.6
A. neocrenulata	22.9	2850.6	8.3	380.9
A. nodulifera	35.3	4091.1	35.6	1401.8
Hemidiscus cuneiformis	1.1	119.6	4.6	172.0
Nitzschia interruptestriata	1.3	163.2	2.0	98.6
Planktoniella sol	0.8	106.5	2.0	88.3
Roperia tesselata	6.9	846.1	3.3	148.2
Thalassionema nitzschioides var. *inflata*	0.8	133.3	1.3	72.9
Thalassiosira eccentrica	0.6	93.1	1.4	56.1
T. leptopus	0.1	5.3	2.1	57.0
T. lineata	1.9	218.7	0.6	28.6
Non-planktonic species	4.0	546.9	4.3	226.4
Freshwater species	1.5	171.0	2.5	119.0

A marine, planktonic, warm-water (tropical/ subtropical) diatom assemblage characterizes the surface sediments. It represents > 82 % of the entire diatom assemblage in both fractions. Non-planktonic diatoms are present in low numbers and become more important at sites closer to the coast (cores 5843-1, 5831-1, 5825-1 and 7824-3). Freshwater species are scarce in both fractions (and almost completely absent from the southern stations in the > 40 µm fraction) which is not surprising since there are no permanent rivers flowing into the Red Sea.

Robust taxa dominate the assemblage found in the surface sediments: *Alveus marinus*, *Azpeitia neocrenulata*, *Azpeitia nodulifera* and *Roperia tesselata* (Table 3). These four species contribute 60-80 % in the 20-40 µm and 55-68 % in the > 40 µm fraction in each station. Their individual concentrations mirror the pattern of the whole marine planktonic group (Fig. 8). Main contributors to the non-planktonic group are species of the genera *Campylodiscus*, *Diploneis*, *Nitzschia* and *Surirella*. The almost complete absence of *Navicula perminuta* in both fractions (and from smear slides performed prior to acid-cleaning) is noteworthy. This species is the main representative of the non-planktonic group in the net samples. Thus, when comparing non-brine surface sediments with plankton it is apparent that these two datasets are

very different from each other: fragile forms in the plankton *vs*. heavily silicified species in the sediments.

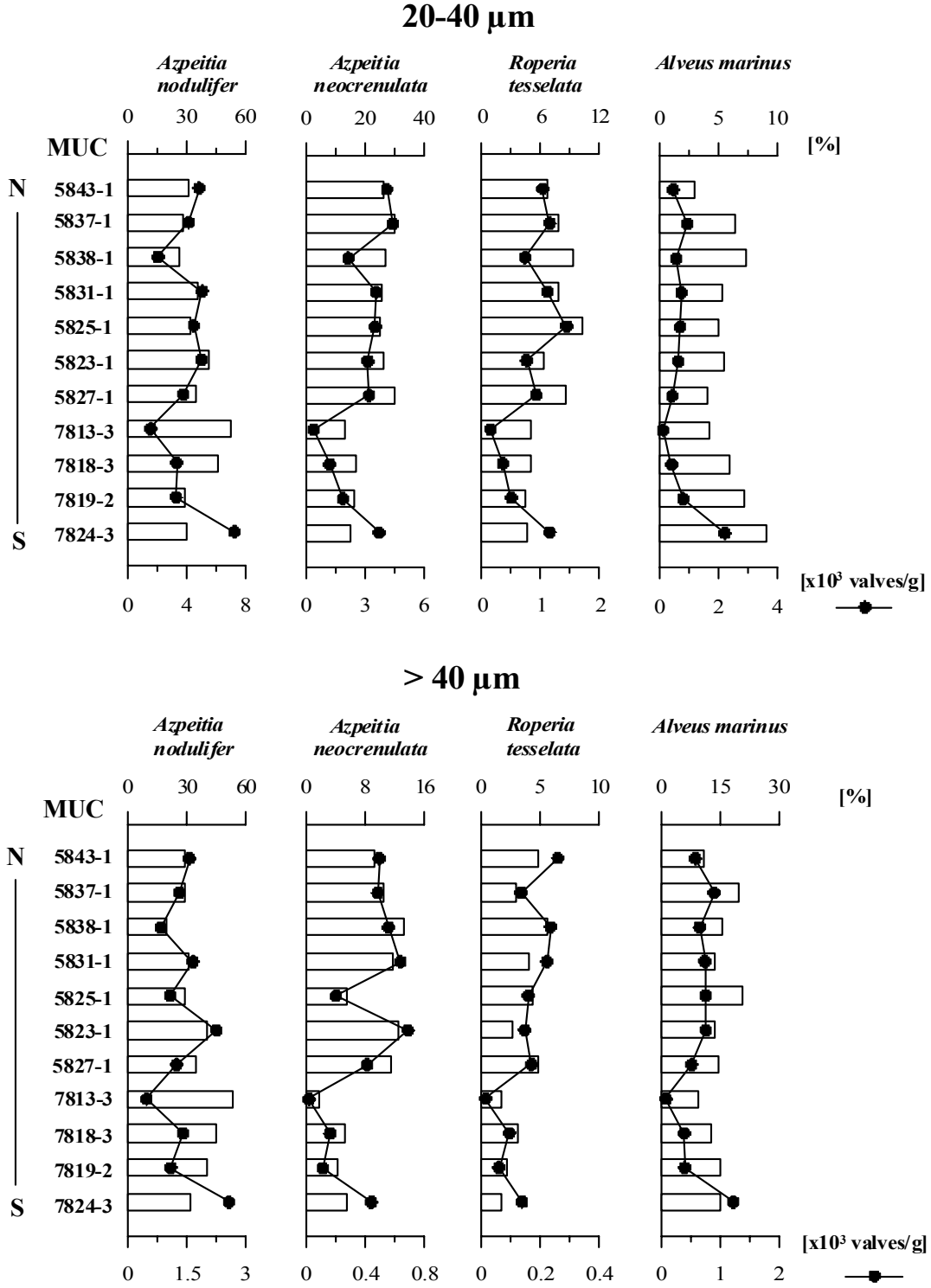

Figure 8: Concentration of the dominant (> 5 % of total assemblage) diatom taxa per gram of dry sediment (lines) and their relative abundances (bars) in non-brine surface sediments for size fractions 20-40 µm and > 40 µm.

Shaban Deep (brine samples)

Surface sediments from the Shaban Deep have a high water content, and are described as diatom-bearing nannofossil ooze (Pätzold et al., 2000a). Biogenic opal content is much higher than in the non-brine samples, ranging from 2.8 % (core 7802-1) to 3.8 wt % SiO_2 (core 7803-2). Concomitantly, concentration of siliceous microorganisms (Fig. 9) is 3-4 orders of magnitude higher than in non-brine sediments (Fig. 6) and even somewhat higher in core 7803-2.

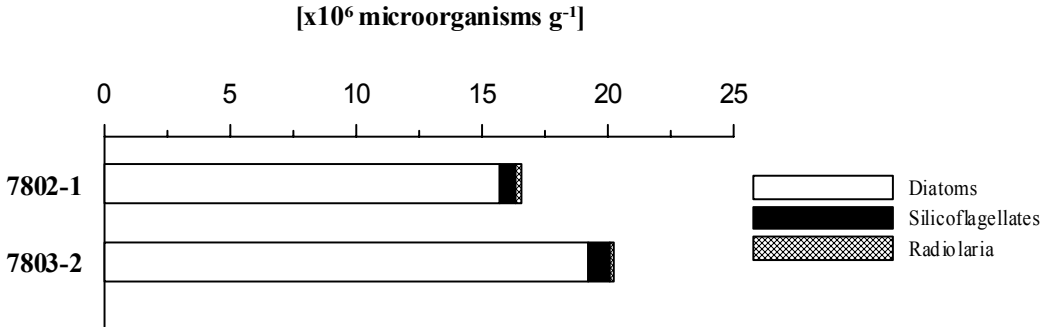

Figure 9: Concentration of siliceous microorganisms per gram of dry sediment in brine surface sediments of the Shaban Deep (26°12.5'N; 35°21.5'E). Note that values are 3-4 orders of magnitude higher than in non-brine sediments (compare with Fig. 6).

Diatoms dominate the opal signal. Species diversity (as measured by the Shannon index) is high, between 3 and 3.5. In addition to the marine planktonic, warm-water species *N. bicapitata* and *Thalassionema nitzschioides* var. *parva*, these surface sediments contain many resting spores of *Chaetoceros* spp. (mainly of *C. affinis* and unidentified species) (Fig. 10) which is rather surprising given the fact that *Chaetoceros* is not abundant in our plankton samples (see Table 2).

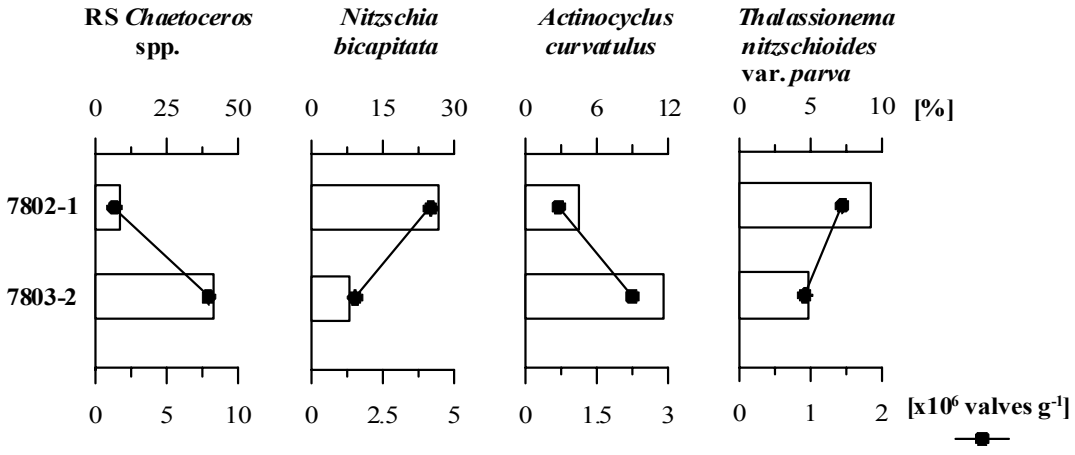

Figure 10: Concentration of dominant (> 5 % of total assemblage) diatom taxa per gram of dry sediment (lines) and their relative abundances (bars) in brine surface samples of the Shaban Deep.

Discussion

Plankton

The Red Sea plankton is characterized by the dominance of autotrophic pico-organisms; cells of 5 to several 100 µm in size are extremely scarce in this region (Pätzold et al., 2000b). The northern Red Sea is permanently stratified throughout the year and while dissolved N and P are depleted, Si is low but still detectable. Thus, the phytoplankton living here is mainly based on nutrient recycling (regenerated production) (Pätzold et al., 2000b). A deep chlorophyll maximum (DCM) is present all year round (Pätzold et al., 2000b). In the winter the depth of the thermocline exceeds 200 m north of 25°N (Edwards, 1987).

The plankton samples used in this study can only give a very small insight into the diatom assemblage living in the northern Red Sea since they are merely a snapshot representing one month (March) of one year (2002). Nevertheless, our results represent a detailed species inventory which can be used to compare with previous studies. For example, our species list differs greatly from that of Halim (1969), especially for the month of March (compare Table X of Halim, op. cit. with Table 2 of this work), when he found *Chaetoceros coarctatum*, *Hemidiscus cuneiformis*, *Rhizosolenia schrubsolei* and *Rhizosolenia semispina*. However, interannual differences in the composition of diatom assemblages should not be a surprise. Seasonal inflow of surface waters from the Gulf of Aden seems to play an important role in the recruitment of pelagic organisms in the Red Sea (Halim, 1969), as well as an exchange of diatom species through the Gulf of Suez (Dowidar, 1976). About six species were found to have crossed the Suez Canal from the Mediterranean Sea in 1969 and 1970 (Dowidar, 1976). Thus, the phytoplankton assemblage encountered in the Red Sea seems to be a mixture of species known to live both in the Indian Ocean and in the Mediterranean Sea.

According to Shaikh et al. (1986), our sampling period (March) does not lie within the maximum distribution of diatoms in the northern Red Sea. Shaikh et al. (1986) describe a bimodal seasonal pattern with one marked primary peak of diatoms in December and January and a secondary peak in July which is dominated by blue-green algae of the genus *Trichodesmium*. Furthermore, they name *Bacteriastrum*, *Chaetoceros*, *Nitzschia* and *Rhizosolenia* as the major contributors within the diatom assemblage of the primary peak. We collected two plankton samples per station: the 120-20 m tows included the main chlorophyll maximum at 80 m depth while the 200-120 m tows sampled the minor, secondary peak (Fig. 2). In both tows, the genus *Nitzschia* dominated the assemblage (> 40 %), although the other three genera named by Shaikh et al. (op. cit.) were also present (Tables 2 and 4) but never dominant. The

comparison with Shaikh et al.´s (1986) database is further limited by the fact that they lack relative abundance data.

Table 4: Average contribution (as percent of total diatom assemblage) of dominant taxa in selected plankton (7805-3 and 7805-4), non-brine (5823-1 and 5827-1) and brine surface sediment samples (7802-1 and 7803-2). All samples are from the area of the Shaban Deep. Gray shading refers to those species with an average contribution > 5 %.

			PERCENT CONTRIBUTION					
Species	**7805-3**	**7805-4**	**5823-1**		**5827-1**		**7802-1**	**7803-2**
	120-20 m	**200-120 m**	**20-40 µm**	**> 40 µm**	**20-40 µm**	**> 40 µm**		
Actinocyclus curvatulus	0	1.0	0.4	1.3	0.5	0.6	4.4	11.6
Alveus marinus	0.2	0.4	5.5	13.7	4.1	14.7	1.0	1.3
Azpeitia neocrenulata	0.5	7.8	26.4	12.4	29.8	11.5	0.5	1.5
A. nodulifera	0.8	4.2	41.5	40.3	35.3	34.5	0.8	0.7
RS *Chaetoceros* spp.	0	0	0	0	0.4	0.8	8.5	41.2
Neodelphineis indica	5.9	4.0	0	0	0	0	2.6	0.9
Nitzschia bicapitata	41.0	31.5	0	0	0.1	0.1	26.8	8.1
Pseudo-nitzschia prolongatoides	1.2	5.0	0	0	0	0	0.4	0.5
Roperia tesselata	0.2	1.4	6.3	2.6	8.5	4.8	0.9	0.6
Thalassionema nitzschioides var. *parva*	1.3	0.5	0	0	0.1	0.3	9.2	4.8
Thalassiosira lineata	0.1	5.2	0.9	0.4	2.2	0.8	0.8	0.7
nonplanktonic species	15.9	4.9	2.0	3.7	1.8	4.7	3.7	2.1

No major differences in species composition were found between our tows, only a higher contribution of *Navicula perminuta* in the shallow tow and a slight enrichment of solution-resistant diatoms (e.g. *Azpeitia neocrenulata*) with water depth (Table 2).

Surprisingly, the contribution of *Rhizosolenia* to the plankton diatom assemblage was negligible. We expected the contrary since *Rhizosolenia* species play an important role in Holocene laminated sediments of the Shaban Deep (Seeberg-Elverfeldt et al., 2003). In these sediments, monogeneric *Rhizosolenia* layers alternate with layers containing coccoliths and terrigenous material, and are interpreted as the result of an annual cycle with diatoms representing the winter signal, and coccoliths with terrigenous debris corresponding to the summer signal (Seeberg-Elverfeldt et al., 2003).

There is evidence that the diatom genus *Rhizosolenia* is capable of building large mats that sink to the bottom and get preserved in the sediments. Kemp et al. (2000) describe several species including *Rhizosolenia* as being part of a “fall dump” group. These are deep living

species (DCM) that sink as soon as autumn or winter mixing starts and stratification of the water column breaks down. Alldredge and Silver (1982) point out that within these mats in the eastern Pacific, *Rhizosolenia* comprises all of the phytoplankton biomass while they are very scarce in the seawater between the mats. Whether *Rhizosolenia* was actually concentrated in mats in the northern Red Sea and also growing at the time of our sampling, or not, is uncertain. Our sampling design and timing of sampling may have missed them altogether.

Surface sediments

Of the biogenic silica produced in the euphotic zone, only 5 % remains at a water depth of 500 m and only 1 % remains at 1000 m (Tréguer et al., 1995). Below 1000 m, silica dissolution has been reported as minimal (e.g. Berger, 1976; Takahashi, 1986). Investigations by Bishop et al. (1977) in the eastern equatorial Atlantic reveal that diatom abundance decreases by about 86 % from 50 to 400 m. The fraction of biogenic silica that escapes dissolution (see Ragueneau et al., 2000, for factors governing the dissolution of biogenic opal formed in surface waters), sinks through the water column as phytoplankton particulate silicon (biogenic Si) or $Si(OH)_4$-rich fecal pellets (e.g. Dugdale et al., 1995; Tréguer et al., 1995), and reaches the seafloor where dissolution continues. Furthermore, cell size, silicification of the diatom frustule and the species composition of the diatom assemblage play an important role in determining whether the siliceous material of a given species will reach the seafloor and be preserved in the sediments (e.g. Nelson et al., 1995). Strong dissolution at the sediment/water interface drastically changes the relative abundances of heavily and weakly silicified diatom taxa. In several areas of the ocean, dissolution is so strong that the assemblage preserved in the sediments has no resemblance with the one produced in surface waters (see review in Romero et al., 1999). For example, in the equatorial Atlantic, robust taxa (*Aulacoseira granulata*, *Azpeitia barronii*, *Azpeitia nodulifera, Roperia tesselata* and *Rhizosolenia bergonii*) are preferentially concentrated in the sediments while small, lightly silicified forms (e.g. the *Nitzschia bicapitata* group) dominate the water column (Romero et al., 1999) but are not preserved in the surface sediments.

This also seems to be the case for the northern Red Sea. Here, non-brine sediments are enriched in robust taxa (*Azpeitia neocrenulata*, *Azpeitia nodulifera*, *Alveus marinus* and *R. tesselata*; Fig. 8) while the plankton in this region is dominated by fragile forms of the *Nitzschia bicapitata* group (Table 4) which are almost completely removed from the sedimentary record.

Brine sediments (Shaban Deep), on the other hand, differ considerably from the non-brine sediments. At present, a 200-m-thick brine body exists within the Shaban Deep that is almost depleted in dissolved oxygen (Hartmann et al., 1998). The mechanisms to accumulate brine within a deep are various and not fully understood to this day. However, changes in deep and bottom circulation as well as stagnation of water circulation may play a major role (Rossignol-Strick, 1987). Oxygen is a major key-player in the preservation of organic matter (e.g. Rullkötter, 2000). In addition, it seems as if the brine solution combined with anoxic conditions provides a better medium for siliceous microplankton preservation; not only are concentrations of skeletons 3-4 orders of magnitude higher than in non-brine sediments but also fragile forms are preserved in greater abundances (8-26 % vs. < 1 %; Table 4). Within brine sediments, more than 0.15 % of the biogenic opal produced in the water column is clearly preserved. Thus, brine sediments in this region seem to offer a great potential for palaeoenvironmental studies. This agrees well with studies regarding preservation of siliceous microfossils in brine-filled basins of the Mediterranean. For example, diatom preservation is excellent in one core from the deepest part of the Napoli mud volcano region which is filled with saline bottom waters (Kemp et al., 2000). Only sediments from Eemian age (ca. 120-125 kyr BP) were studied but it became apparent that the anoxic, saline depressions in the Mediterranean Sea permit very good opal preservation (Erba, 1991).

At this time, it is impossible for us to define if the high salinity is responsible for the good opal preservation in the Shaban Deep sediments or if it is just the anoxic conditions. However, the study of an oxic sediment core in the northern Red Sea (GeoB 5844-2 at 27°42.81'N, 34°40.90'E; 963 m water depth) by Arz et al. (2003a; 2003b) reveals the presence of two distinct sapropels (Red Sea sapropel RS1a and RS1b, defined after Arz et al., 2003b) at around 14.5 ka and 11.4 ka. According to the authors, these were formed under anoxic conditions due to stagnation of deep water formation (Arz et al., 2003b). The opal preservation in these core sections does not change considerably compared to regular oxic sediments (Arz and Legge, pers. comm.). We therefore believe that the existence of the brine body within the Shaban Deep plays a major role in the preservation of siliceous microfossils.

Surprisingly, we recorded abundant resting spores of various *Chaetoceros* species in the brine sediments (Table 4). First, the genus *Chaetoceros* is not abundant in the plankton (see Table 2), and thus addition of spores due to some midwater lateral transportation should be taken into consideration. Second, because resting spores are heavily silicified and thus resistant to dissolution, we would have expected to find them in abundance in all surface sediments and not only within the brine. Furthermore, even within the brine sediments, the contri-

bution of these resting spores differs when comparing both brine samples used in this study (Fig. 10). The brine solution in the Shaban Deep has a very high salinity (~ 250 ‰) (Pätzold et al., 2000b) and a very sharp seawater/brine interface. We may assume that sinking particles (as aggregates, marine snow, single cells or even mats) first accumulate at this particular interface and then sink through the brine to the seafloor in one event. Sinking could be initiated by a small disturbance at the seawater/brine interface, dragging with it all material that has accumulated. Since accumulation, disturbance and sinking processes may act differentially even within a reduced area, the "output" (= sediment composition) may be patchy.

Although the relative abundances of resistant diatoms in the sediments are significantly higher than those in the water column, we believe that the preserved assemblage does reflect general hydrographic conditions in the surface water. An increase of diatom concentrations at the southernmost site may indicate higher nutrient levels, resulting in an increase of primary production as well as phytoplankton abundances (Weikert, 1987). Highest values of Chl *a* are reached in the southern part of the Red Sea (Fig. 1) due to inflow of water from the Indian Ocean, and decrease northward (Edwards, 1987). It is possible that our southernmost sample is reached by these more productive waters, and therefore the concentration in the sediment record is higher than in the other samples of our transect.

In general, the diatom assemblage recorded in all surface sediments can be characterized as typical of tropical/subtropical regions. Large differences in species distribution along the N-S-transect could not be observed. As expected, non-planktonic species are somewhat more abundant at sites closer to the coast. Freshwater species are rare, and because there are no permanent rivers leading into the Red Sea, we assume an eolian pathway as a possible mechanism of deposition; however, our database does not allow identification of their source areas.

Conclusions

- The plankton and surface sediments of the Red Sea are characterized by a diatom flora that is typical of tropical/subtropical environments. Non-planktonic species are of minor importance in the plankton samples but become slightly more abundant in surface sediments closer to the coast. Freshwater species are rare and their presence in both settings may be related to eolian transport since there is no major river input to the Red Sea.
- Dissolution of diatom frustules is evident when comparing non-brine surface sediments with plankton samples. Fragile forms (e.g. *Nitzschia bicapitata* group) that dominate the plankton assemblage are removed from the sediment/water interface leaving the sedi-

mentary record enriched in heavily silicified species (e.g. *Alveus marinus*, *Azpeitia. neocrenulata*, *Azpeitia nodulifera*, *Roperia tesselata*).

- Surface sediments within the Shaban Deep differ greatly from non-brine sediments: (a) Biogenic opal contents and concentrations of siliceous microplankton are higher; (b) diatom species diversity is higher; and (c) fragile forms are better preserved. These sediments hold a great potential for palaeoenvironmental studies.

Acknowledgements

We thank the captain and crew of *R/V Meteor* for their efforts and support at sea. We also acknowledge the generous grant of permission for conducting research in the territorial waters of the Kingdom of Saudi Arabia. Bob Davenport was of great assistance with the satellite chlorophyll data. Special thanks go to Marco Klann for opal analysis, Friedel Hinz at the Alfred-Wegener-Institut for her help with preparation of plankton samples and Helge Arz for encouragement during this project. We also appreciate comments and suggestions by Richard Crawford, as well as critical reviews by Juliane Fenner and Kozo Takahashi. We are very grateful to the Hanse Institute of Advanced Study, Delmenhorst, Germany, for the Fellowship awarded to C. B. Lange. This work was supported by the Deutsche Forschungsgemeinschaft as part of the DFG-Research Center "Ocean Margins" of the University of Bremen, Germany, No. RCOM0104.

Appendix A

Marine planktonic species

Actinocyclus curvatulus Janisch in A. Schmidt 1878 ▲●◆
Actinocyclus elongatus Grunow in Van Heuck 1883 ▲●◆
Actinocyclus exiguus Fryxell & Semina 1981 ●◆
Actinocyclus octonarius Ehrenberg 1838 ▲●◆
Actinocyclus subtilis (Gregory) Ralfs in Pritchard 1861 ▲●◆
Actinocyclus sp. Ehrenberg 1837 ●
Alveus marinus (Grunow) Kaczmarska & Fryxell 1996 ▲●◆
Asterolampra marylandica Ehrenberg 1844 ◆
Asteromphalus arachne (Brébisson) Ralfs in Pritchard 1861 ●◆
Asteromphalus cleveanus Grunow 1876 in Schmidt et al. 1874 ▲●◆
Asteromphalus flabellatus (Brebisson) Greville 1859 ▲●◆
Asteromphalus heptactis (Brebisson) Ralfs in Pritchard 861 ▲●◆
Azpeitia africana (Janisch ex Schmidt) G.Fryxell & T.P.Watkins in Fryxell et al. 1986 ▲●◆
Azpeitia barronii G.Fryxell & T.P.Watkins in Fryxell et al. 1986 ▲●
Azpeitia neocrenulata (Van Landingham) G.Fryxell & T.P.Watkins in Fryxell et al. 1986 ▲●◆
Azpeitia nodulifera (A. Schmidt) G.Fryxell & P.A. Sims in Fryxell et al. 1986 ▲●◆
Azpeitia spp. M. Peragallo in Tempère & Pergallo 1912 ▲●
Bacteriastrum delicatulum Cleve 1897 ▲●◆
Bacteriastrum elongatum Cleve 1897 ▲●◆
Bacteriastrum furcatum Shadbolt 1854 ▲●◆
Bacteriastrum hyalinum Lauder 1864 ▲●◆
Subgenus Phaeoceros
Chaetoceros aequatorialis Cleve 1873 ▲
Chaetoceros atlanticus Cleve 1873 ▲●◆
Chaetoceros concavicornis Mangin 1917 ▲●◆
Chaetoceros dichaeta Ehrenberg 1844 ●
Chaetoceros peruvianus Brightwell 1856 ▲●◆
Subgenus Hyalochaete
Chaetoceros affinis Lauder 1864 ●◆
Chaetoceros compressus Lauder 1864 ◆
Chaetoceros decipiens Cleve 1873 ▲
Chaetoceros didymus Ehrenberg 1845 ◆
Chaetoceros laciniosus Schütt 1895 ▲
Chaetoceros lorenzianus Grunow 1863 ▲●◆
Chaetoceros messanensis Castracane 1875 ▲●◆
Chaetoceros pseudocurvisetus Mangin 1910 ▲
Chaetoceros spp. Ehrenberg 1844 ▲●◆
Coscinodiscus janischii Schmidt 1878 in Schmidt et al. 1874 ●◆
Coscinodiscus marginatus Ehrenberg 1843 ●
Coscinodiscus radiatus Ehrenberg 1844 ▲●◆
Coscinodiscus reniformis Castracane 1886 ▲●◆
Coscinodiscus thorii Pavillard 1925 ▲●◆
Coscinodiscus spp. Ehrenberg 1839 emend. Hasle & Sims 1986 ▲●◆
Cyclotella litoralis Lange & Syvertsen 1989 ▲●◆
Cyclotella meneghiniana Kützing 1844 ▲●
Dactyliosolen sp. Castracane 1886 ◆
Detonula sp. Schütt ex De Toni 1894 ▲◆
Eucampia sp. Ehrenberg 1839 ▲
Fragilariopsis doliolus (Wallich) Medlin & Sims 1993 ▲●◆
Fragilariopsis spp. Hustedt in Schmidt emend. Hasle 1993 ●◆
Guinardia sp. H. Pergallo 1892 ▲
Haslea spp. Simonsen 1974 ▲◆
Hemiaulus hauckii Grunow in van Heurck 1882 ▲●◆
Hemiaulus sinensis Greville 1865 ▲●◆
Hemiaulus spp. Heiberg 1863 ▲
Hemidiscus cuneiformis Wallich 1860 ▲●◆
Leptocylindrus mediterraneus (H. Peragallo) Hasle 1975 ▲◆
Lioloma spp. Hasle 1996 ▲●◆
Mastogloia rostrata (Wallich) Hustedt 1933 ◆
Neodelphineis indica (F.J.R. Taylor) Tanimura 1992 ▲●◆
Neodelphineis spp. Takano 1982 ▲◆
Nitzschia bicapitata Cleve 1901 ▲●◆
Nitzschia braarudii Hasle 1960 ▲●◆
Nitzschia capuluspalae Simonsen 1974 ▲●◆
Nitzschia cf. *dissipata* (Kützing) Grunow 1862 ▲
Nitzschia interruptestriata (Heiden) Simonsen 1974 ▲●◆
Nitzschia longissima (Brébisson, in Kützing) Ralfs in Pritchard 1861 ▲●◆
Nitzschia sicula (Castracane) Hustedt 1875 ▲●◆
Nitzschia spp. Hassall 1845 ▲●
Odontella spp. C.A. Agardh 1832 ●◆
Orthoseira sp. Thwaites 1848 ●
Paralia sp. Heiberg 1863 ▲●◆
Planktoniella sol (Wallich) Schütt 1892 ▲●◆
Pleurosigma directum Grunow in Cleve & Grunow 1880 ▲●◆
Pleurosigma spp. W.Smith 1852 ▲●◆
Proboscia sp. Sundström 1986 ▲●◆
Pseudo-nitzschia australis Fringuelli 1939 ▲●
Pseudo-nitzschia delicatissima (Cleve) Heiden in Heiden & Kolbe 1928 ▲◆
Pseudo-nitzschia fraudulenta (Cleve) Hasle 1965 ▲●◆
Pseudo-nitzschia granii Hasle 1964 ▲●◆
Pseudo-nitzschia prolongatoides (Hasle) Hasle 1993 ▲●◆
Pseudo-nitzschia pungens (Grunow ex Cleve) Hasle 1965 ▲●
Pseudo-nitzschia subcurvata (Hasle) Fryxell in Fryxell et al. 1991 ▲●
Pseudo-nitzschia fraudolenta (Cleve) Hasle 1993 ▲◆
Pseudo-nitzschia spp. Peragallo in Peragallo 1897-1908 ▲●

Pseudosolenia calvar-avis (Schultze) Sundström 1986 ▲●◆
Pseudotriceratium punctatum (Wallich) Simonsen 1974 ▲●◆
Rhizosolenia acicularis Sundström 1986 ▲●◆
Rhizosolenia bergonii H. Peragallo 1892 ▲●◆
Rhizosolenia castracanei H. Per gallo var. *castracanei* 1888 ▲◆
Rhizosolenia hebetata Bailey *hebetata* 1856 ▲●◆
Rhizosolenia "imbricata" Brightwell 1858 ▲◆
Rhizosolenia pungens Cleve-Euler 1937 ▲●◆
Rhizosolenia setigera Brightwell 1858 ▲◆
Rhizosolenia styliformis Brightwell 1858 ▲
Rhizosolenia temperei H. Peragallo 1888 ▲
Rhizosolenia spp. Brightwell 1858 ▲●◆
Roperia tesselata (Roper) Grunow in Van Heurck 1880-1885 ▲●◆
Skeletonema sp. Greville 1865 ▲
Thalassionema bacillare (Heiden) Kolbe 1955 ▲●◆
Thalassionema nitzschioides var.*capitulata* (Castrane) Moreno-Ruiz 1996 ●◆
Thalassionema nitzschioides var. *claviformis* (Schrader) Moreno-Ruiz in Moreno-Ruiz & Carreño 1993 ●◆
Thalassionema nitzschioides var. *incurvata* Heiden in Heiden & Kolbe 1928 ●◆
Thalassionema nitzschioides var. *inflata* Heiden in Heiden & Kolbe 1928 ▲●◆
Thalassionema nitzschioides var. *nitzschioides* (Grunow) Van Heurck 1896 ●
Thalassionema nitzschioides var. *parva* (Heiden) Moreno-Ruiz emend. 1996 ▲●◆
Thalassionema spp. Grunow ex Mereschkowsky 1902 ▲●◆
Thalassiosira aestivalis Gran & Angst 1931 ▲●
Thalassiosira delicatula Ostenfeld in Borgert 1908 ◆
Thalassiosira diporocyclus Hasle 1972 ●
Thalassiosira eccentrica (Ehrenberg) Cleve 1904 ▲●◆
Thalassioria endoseriata Hasle and G.Fryxell 1977 ▲●
Thalassiosira ferelineata Hasle & G.Fryxell 1977 ▲●◆
Thalassiosira leptopus (Grunow) Hasle & G.Fryxell 1977 ▲●◆
Thalassiosira lineata Jousé 1968 ▲●◆
Thalassiosira mala Takano 1965 ▲
Thalassiosira mendiolana Hasle & Heimdal 1970 ●
Thalassiosira minima Gaarder 1951 ▲
Thalassiosira oceanica Hasle 1983 ▲●◆
Thalassiosira oestrupii var. *oestrupii* (Ostenfeld) Hasle 1972 ▲●◆
Thalassiosira oestrupii var. *venrickae* Fryxell & Hasle 1980 ▲●◆
Thalassiosira pacifica Gran & Angst 1931 ▲◆
Thalassiosira poro-irregulata Hasle & Heimdal 1970 ◆
Thalassiosira sacketii f. *sacketii* G. Fryxell 1977 ▲●◆
Thalassiosira sacketii f. *plana* G.Fryxell 1977 ▲●
Thalassiosira subtilis (Ostenfeld) Gran 1900 ▲●◆
Thalassiosira symmetrica Fryxell & Hasle 1972 ▲●◆
Thalassiosira sp. A ●
Thalassiosira sp. B ●
Thalassiosira sp. Z ▲●
Thalassiosira spp. Cleve 1873 emend. Hasle 1973 ▲●◆
Thalassiothrix spp. Cleve & Grunow 1880 ▲●◆

Marine non-planktonic species (including benthic, epiphytic and epilithic species)

Achnanthes brevipes Aghardh 1824 ●
Achnanthes sp. J.B.M. Bory de St.-Vincent 1822 ●◆
Actinoptychus senarius (Ehrenberg) Ehrenberg 1843 ●◆
Actinoptychus vulgaris Schuman 1867 ●◆
Amphora spp. Ehrenberg ex Kützing 1844 ▲●◆
Ardissonea spp. De Notarsi (1870) ●
Biddulphia sp. Gray 1821 ●◆
Campylodiscus spp. Ehrenberg ex Kützing 1844 ●
Catacombas sp. Williams & Round 1986 ●
Cocconeis pseudomarginata Gregory 1857 ●
Cocconeis scutellum Ehrenberg 1838 ▲●
Cocconeis stauroneiformes (Rabenhorst) Okuno 1957 ▲
Cocconeis spp. Ehrenberg 1838 ▲●◆
Cymatonitzschia marina Simonsen 1974 ●◆
Fallacia sp. Stickle und Mann 1990 ▲●◆
Grammatophora sp. Ehrenberg 1840 ●
Glyphodesmis rhombica (Cleve) Simonsen 1974 ●
Gyrosigma spp. Hassall 1845 ▲●
Hyalodiscus sp. Ehrenberg 1845 ▲●
Lyrella sp. Karajeva 1978 ▲●◆
Mastogloia spp. Thwaites ex Smith 1856 ▲●
Membraneis sp. Paddock 1988 ▲
Navicula directa (W. Smith) Ralfs in Pritchard 1861 ▲●◆
Navicula distans (W. Smith) Ralfs in Pritchard 1861 ●
Navicula perminuta Grunow in Van Heurck 1880 ▲●◆
Navicula spp. Bory 1824 ▲●◆
Nitzschia spp. Hassall 1845 ▲●◆
Psammodiscus sp. Round & Mann 1980 ●
Surirella sp. Turpin 1828 ●◆
Toxarium spp. J.W. Bailey 1854 ●
Triceratium pentacrinus (Ehrenberg) Wallich f. *quadrata* Hustedt 1930 ●

Freshwater species
Aulacoseira granulata (Ehrenberg) Ralfs 1861 ▲●◆
Aulacoseira spp. Thwaites 1848 ▲●◆
Cymbella sp. Agardh. by Van Landingham 1969 ▲●◆
Diploneis spp. Ehrenberg ex Cleve 1894 ▲●◆
Entomoneis sp. Ehrenberg 1845 ●
Epithemia sp. Kützing 1844 ●◆
Hantzschia sp. Grunow 1877 ▲●
Luticola mutica (Kützing) D. G. Mann 1990 ▲●◆
Neidium spp. Pfitzer 1871 ▲●◆

Stephanodiscus sp. Ehrenberg 1845 ●◆
Synedra ulna (Nitzsch) Ehrenberg 1832 ●

Lumped taxa
Bacteriastrum delicatulum and *B. furcatum*
Fallacia sp. and *Lyrella* sp.
Nitzschia bicapitata as a group
Thalassiothrix spp. and *Lioloma* spp.

Silicoflagellates
Dictyocha messanensis Haeckel 1887 ▲●◆
Distephanus pulchra (Schiller) Ling & Takahashi 1985 ▲●◆

Dinoflagellates
Actiniscus pentasterias (Ehrenberg) Ehrenberg 1854 ▲●◆

Taxonomic list of species identified from the 10 net-plankton hauls (▲), 11 non-brine surface sediment samples (●) and two brine surface sediment samples (◆) from the northern Red Sea.

References

Alldredge, A.L. and Silver, M.W., 1982. Abundance and production rates of floating diatom mats (*Rhizosolenia castracanei* and *R. imbricata* var. *shrubsolei*) in the eastern Pacific ocean. Marine Biology, 66: 83-88.

Arz, H.W., Lamy, F., Pätzold, J., Müller, P.J. and Prins, M., 2003a. Mediterranean moisture source for an early-Holocene humid period in the northern Red Sea. Science, 300: 118-121.

Arz, H.W., Pätzold, J., Müller, P.J. and Moammar, M.O., 2003b. Influence of Northern Hemisphere climate and global sea level rise on the restricted Red Sea marine environment during Termination I. Paleoceanography, 18(2): 1053, doi:10.1029/2002PA000864.

Berger, W.H., 1976. Biogeneous deep-sea sediments: production, preservation and interpretation. In: J.P. Riley and R. Chester (Editors), Treatise on Chemical Oceanography. Academic Press, New York, pp. 266-388.

Bishop, J.K., Edmond, J.M., Ketten, D.R., Bacon, M.P. and Sylker, W.B., 1977. The chemistry, biology, and vertical flux of particulate matter from the upper 400 m of the equatorial Atlantic Ocean. Deep-Sea Research, 24: 511-548.

Dowidar, N.M., 1976. The phytoplankton of the Suez Canal. Acta Adriatica, 18(14): 241-256.

Dugdale, R.C., Wilkerson, F.P. and Minas, H.J., 1995. The role of a silicate pump in driving new production. Deep-Sea Research, 42: 697-719.

Edwards, F.J., 1987. Climate and Oceanography. In: A.J. Edwards and S.M. Head (Editors), Key Environments: Red Sea. Pergamon Press, Oxford, pp. 45-70.

Erba, E., 1991. Deep mid-water bacterial mats from anoxic basins of the Eastern Mediterranean. Marine Geology, 100: 83-101.

Eshel, G., Cane, M.A. and Blumenthal, M.B., 1994. Modes of subsurface, intermediate, and deep water renewal in the Red Sea. Journal of Geophysical Research, 99(C8): 15,941-15,952.

Eshel, G. and Naik, N.H., 1997. Climatological Coastal Jet Collision, Intermediate Water Formation, and the General Circulation of the Red Sea. Journal of Physical Oceanography, 27: 1233-1257.

Halim, Y., 1969. Plankton of the Red Sea. Oceanography and marine biology: an annual review, 7: 231-275.

Hartmann, M., Scholten, J.C., Stoffers, P. and Wehner, F., 1998. Hydrographic structure of brine-filled deeps in the Red Sea - new results from the Shaban, Kebrit, Atlantis II, and Discovery Deep. Marine Geology, 144: 311-330.

Kaczmarska, I. and Fryxell, G., 1994. The genus *Nitzschia*: three new species from the equatorial Pacific Ocean. Diatom Research, 9(1): 87-98.

Kemp, A.E.S., Pike, J., Pearce, R.B. and Lange, C.B., 2000. The "Fall dump"-a new perspective on the role of a "shade flora" in the annual cycle of diatom production and export flux. Deep-Sea Research II, 47: 2129-2154.

Kimor, B. and Golandsky, B., 1977. Microplankton of the Gulf of Elat: Aspects of Seasonal and Bathymetric Distribution. Marine Biology, 42: 55-67.

Lange, C.B., Treppke, U.F. and Fischer, G., 1994. Seasonal diatom fluxes in the Guinea Basin and their relationship to trade winds, hydrography and upwelling events. Deep-Sea Research I, 41: 859-878.

Lenz, J., Schneider, G., El Hag, A.G.D., Gradinger, R., Fritsche, P., Moigis, A., Pillen, T., Rolke, M. and Weisse, T., 1988. Planktological data from the central Red Sea and the Gulf of Aden; R.V. "Meteor", cruise No. 5/2, January-March 1987. Berichte aus dem Institut für Meereskunde an der Christian-Albrechts-Universität Kiel, 180: 200.

Manheim, F.T., 1974. Red Sea geochemistry. Initial Report DSDP, 23: 975-998.

Müller, P.J. and Schneider, R., 1993. An automated leaching method for determination of opal in sediments and particulate matter. Deep-Sea Research I, 40(3): 425-444.

Nelson, D.M., Tréguer, P., Brzenzinski, M.A., Leynaert, A. and Quéguiner, B., 1995. Production and dissolution of biogenic silica in the ocean: Revised global estimates, comparison with regional data and relationship to biogenic sedimentation. Global Biogeochemical Cycle, 9: 359-372.

Pätzold, J., Abd El-Wahab Farha, O., Abu-Ouf, M., Al Hazmi, Y.M.M., Al-Rousan, S., Arz, H.W., Bagabas, K.A.A., Bassek, D., Blaschek, H., Böke, W., Donner, B., Eder, W., Felis, T., Gayed, H.Y.K., Gutowski, M., Hemleben, C., Hübner, H., Hübscher, C., Kadi, K.A., Kästner, R., Klauke, S., Körner, S.O., Kuhlmann, H., Lützeler, T., Meier, S., Melegy, M.M., Moammar, M.O., Moha-

muda, A.Z., Mokhtar, T.A., Moos, C., Omar, O.M., Rasheed, M., Rosiak, U., Salem, M., Schmidt, M., Schmitt, M., Stoffers, P., Shata, A.M., Themann, S. and Weldeab, S., 2000a. Report and preliminary results of *Meteor* cruise M 44/3 Aqaba (Jordan) - Safaga (Egypt) - Dubá (Saudia Arabia) - Suez (Egypt) - Haifa (Israel). Berichte aus dem Fachbereich Geowissenschaften der Universität Bremen, 149: 135.

Pätzold, J., Halbach, P.E., Hempel, G. and Weikert, H., 2000b. Meteor-Berichte: Östliches Mittelmeer - Nördliches Rotes Meer 1999 Cruise No. 44. 00-3, Leitstelle METEOR: Institut für Meereskunde der Universität Hamburg, Hamburg.

Ragueneau, O., Tréguer, P., Leynaert, A., Anderson, R.F., Brzezinski, M.A., DeMaster, D.J., Dugdale, R.C., Dymond, J., Fischer, G., Francois, R., Heinze, C., Maier-Reimer, E., Martin-Jezequel, V., Nelson, D.M. and Queguiner, B., 2000. A review of the Si cycle in the modern ocean: recent progress and missing gaps in the application of biogenic opal as a paleoproductivity proxy. Global and Planetary Change, 26: 317-365.

Romero, O.E., Lange, C.B., Fischer, G., Treppke, U.F. and Wefer, G., 1999. Variability in export production documented by downward fluxes and species composition of marine planktonic diatoms: Observations from the tropical and equatorial Atlantic. In: G. Fischer and G. Wefer (Editors), Use of Proxies in Paleoceanography - Examples from the South Atlantic. Springer-Verlag, Berlin Heidelberg, pp. 365-392.

Rossignol-Strick, M., 1987. Rainy periods and bottom water stagnation initiating brine accumulation and metal concentrations: 1. The late Quaternary. Paleoceanography, 2: 333-360.

Rullkötter, J., 2000. Organic Matter: the driving force of early diagenesis. In: H. Schulz and M. Zabel (Editors), Marine Geochemistry. Springer Verlag, Berlin Heidelberg, pp. 129-172.

Schrader, H.J. and Gersonde, R., 1978. Diatoms and silicoflagellates. Utrecht Micropaleontology Bulletin, 17: 129-176.

Seeberg-Elverfeldt, I.A., Lange, C.B., Pike, J., Pätzold, J. and Arz, H.W., 2003. Preservation of diatoms in sediments from the northern Red Sea, EGS-AGU-EUG Joint Assembly, Nice, France.

Shaikh, E.A., Roff, J.C. and Dowidar, N.M., 1986. Phytoplankton ecology and production in the Red Sea off Jiddah, Saudi Arabia. Marine Biology, 92: 405-416.

Shannon, C. and Weaver, W., 1949. The mathematical theory of communication. University of Illinois Press, Urbana, 125 pp.

Simonsen, R., 1974. The diatom plankton of the Indian Ocean Expedition of R/V "Meteor". "Meteor" Forschungs-Ergebnisse, 19. Institut für Meeresforschung Bremerhaven, Bremerhaven, 66 pp.

Sommer, U., 2000. Scarcity of medium-sized phytoplankton in the northern Red Sea explained by strong bottom-up and weak top-down control. Marine Ecology Progress Series, 197: 19-25.

Sommer, U., Berninger, U.G., Böttger-Schnack, R., Cornils, A., Hagen, W., Hansen, T., Al-Najjar, T., Post, A.F., Schnack-Schiel, S.B., Stibor, H., Stübing, D. and Wickham, S., 2002. Grazing during early spring in the Gulf of Aqaba and the northern Red Sea. Marine Ecology Progress Series, 239: 251-261.

Taha, O.E., Abdel-Karim, M.S. and Sobhy, E.H., 2002. Vertical distribution of phytoplankton species and their cell densities in the northern region of Aqaba Gulf (St. A). Red Sea Program - Final Report: 50-51.

Takahashi, K., 1986. Seasonal fluxes of pelagic diatoms in the subarctic Pacific, 1982-1983. Deep-Sea Research, 33: 1225-1251.

Tréguer, P., Nelson, D.M., van Bennekom, A.J., DeMaster, D.J., Leynaert, A. and Queguiner, B., 1995. The silica balance in the world ocean: a reestimate. Science, 268: 375-379.

Veldhuis, M.J.W., Kraay, G.W., van Bleijswijk, J.D.L. and Baars, M.A., 1997. Seasonal and spatial variability in phytoplankton biomass, productivity and growth in the northwestern Indian Ocean: the southwest and northeast monsoon, 1992-1993. Deep-Sea Research I, 3: 425-449.

Weikert, H., 1987. Plankton and the Pelagic Environment. In: A.J. Edwards and S.M. Head (Editors), Key Environments: Red Sea. Pergamon Press, Oxford, pp. 90-111.

3.2 The significance of diatoms in the formation of laminated sediments of the Shaban Deep, Northern Red Sea

Ismene A. Seeberg-Elverfeldt[a], Carina B. Lange[b], Helge W. Arz[c], Jürgen Pätzold[a] and Jennifer Pike[d]

[a]Research Center Ocean Margins, University of Bremen, P.O. Box 330440, 28334 Bremen, Germany
[b]Departamento Oceanografía, Universidad de Concepción, Centro FONDAP-COPAS, Casilla 160-C, Concepción, Chile
[c]GFZ-Potsdam, Telegrafenberg, 14473 Potsdam, Germany
[d]School of Earth, Ocean & Planetary Sciences, Cardiff University, Cardiff, Wales, United Kingdom

Marine Geology, accepted

Abstract

Laminated sediments spanning the last 20,000 years (though not continuously) in the Shaban Deep, a brine-filled basin in the northern Red Sea, were analyzed microscopically and with backscattered electron imagery in order to determine laminae composition with emphasis on the diatomaceous component. Based on this detailed study, we present schematic models to propose paleoflux scenarios for laminae formation at different time-slices. The investigated core (GeoB 5836-2; 26°12.61'N, 35°21.56'E; water depth 1475 m) shows light and dark alternating laminae that are easily distinguishable in the mid-Holocene and at the end of the deglaciation (13-15 ka) period. Light layers are mainly composed of coccoliths, terrigenous material and diatom fragments, while dark layers consist almost exclusively of diatom frustules (monospecific or mixed assemblages). The regularity in the occurrence of coccolith/diatom couplets points to an annual deposition cycle where contrasting seasons and associated plankton blooms are represented (diatoms – fall/winter deposition; coccoliths - summer signal). We propose that for the past ~15,000 years, the laminations represent two-season annual varves. Strong dissolution of carbonate, with the concomitant loss of the coccolith-rich layer in sediments older than 15 ka prevents us from presenting a schematic model of annual deposition. However, the diatomaceous component reveals a marked switch in species composition between Last Glacial Maximum sediments (dominated by *Chaetoceros* resting spores) and sediments somewhat younger (18-19 ka; dominated by *Rhizosolenia*). We propose that different diatom assemblages reflect changing conditions in stratification in the northern Red Sea: Strong stratification conditions, such as during

two meltwater pulses at 14.5 ka and 11.4 ka, are reflected in the sediment by *Rhizosolenia* layers, while *Chaetoceros*-dominated assemblages represent deep convection conditions.

***Keywords**: Red Sea; Shaban Deep; laminated sediments; diatoms; brine*

Introduction

Laminated pelagic and hemipelagic sediments from several places around the world have been thoroughly studied during the past few decades, highlighting their use for unraveling intra- and inter-annual export flux variability. Basically, there are two fundamental requirements for their formation: a) variation of sediment composition via changes in input (chemical or biological) conditions, and b) environmental conditions (i.e. low oxygen in bottom waters or physical suppression of burrowing activity) that will preserve the laminated sediment fabric from bioturbation (see review in Kemp, 1996; Kemp et al., 2000).

Laminated sediments are found, for example, in the Santa Barbara Basin off California (e.g. Lange and Schimmelmann, 1996 and references therein), Saanich Inlet, Canada (e.g. Dean et al., 2001; McQuoid and Hobson, 2001), Cariaco Basin, Venezuela (Hughen et al., 1996), off Pakistan (e.g. von Rad et al., 1999 ; Staubwasser and Sirocko, 2001), the Gotland Deep in the Baltic Sea (e.g. Burke et al., 2002), Mejillones Bay off northern Chile (Ortlieb et al., 2000), the Black Sea (Pilskaln and Pike, 2001), and Palmer Deep off western Antarctica (Leventer et al., 2002). Several of these sites provide records with seasonal- to annual-scale temporal resolution, although this detail is not attainable in many settings.

Laminated sediments have recently been described in the Shaban Deep, a brine-filled basin in the northern Red Sea (Hemleben et al., 1996b). About 25 brine-filled deeps are found in the Red Sea along its central axis. The high salinities are due to leaching of sub-bottom Miocene evaporites (Manheim, 1974). The thickness of the brine body itself is therefore controlled by the amount of leaching salt and diffusion processes at the seawater-brine interface. The seismic data of Meteor cruise M52/3 to the northern Red Sea in 2002 showed that the top of the Miocene evaporites crops out within the brine basin (Erhardt and Hübscher in Pätzold et al., 2003). The modern level of the brine-seawater interface corresponds to the top of this so called s-reflector.

The Shaban Deep was discovered in 1981 on a cruise of the *RV Valdivia* (Cruise Reports Menor 1 and Menor 2, 1984; Hartmann et al., 1998). It consists of four sub-basins (southern, eastern, northern and western; Fig. 1) which have the brine-seawater interface at nearly the same water depth (1324.5 ± 0.5 m; Hartmann et al., 1998) and a salinity of about 260 psu. The brine body itself has a thickness of 200 m and is almost depleted in dissolved oxygen (< 0.3

mg/l; Hartmann et al., 1998). There is an absence of benthic life and bioturbation. Rossignol-Strick (1987) assumed that changes in deep and bottom water circulation may influence the development of brine bodies and stagnation of water circulation would result in a rise of the brine surface and increasing anoxic conditions. During these anoxic intervals laminated sediments can build up inside the brine basins. The presence of these laminations suggests the possibility of layers that may be deposited on an annual basis and the potential for a high-resolution proxy of climate changes.

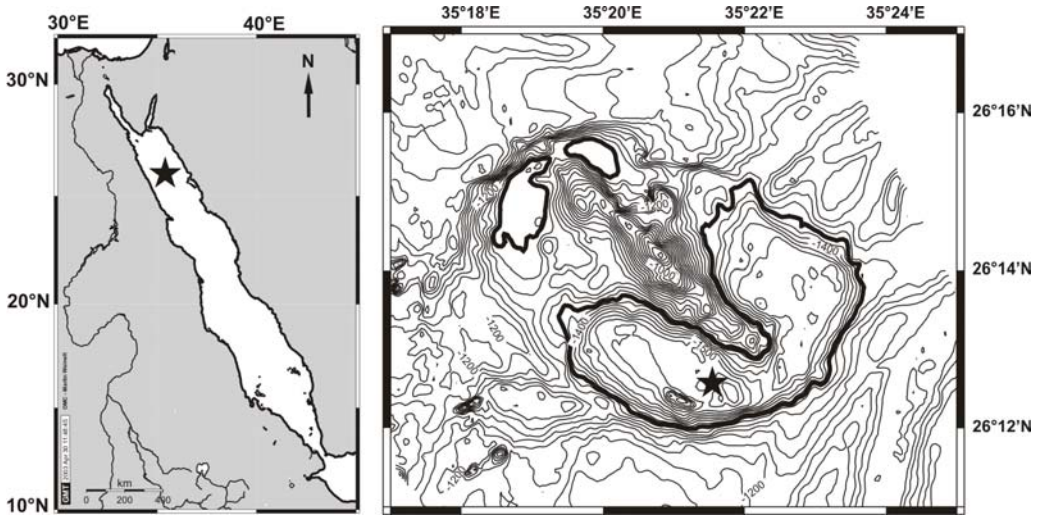

Fig. 1. Location of coring site GeoB 5836-2 (asterisk) within the Shaban Deep (northern Red Sea). Dark contour line on the right-hand panel indicates the depth of the modern brine surface.

Our objective in working with laminated sediments from the Shaban Deep is to deliver a detailed microscopic study of the laminations present, with emphasis on the diatomaceous component. These data allow an evaluation of the sediments as to a) whether the laminations carry an annual signal, b) what processes are responsible for the formation of laminations, and c) the usefulness of laminations in interpreting paleoclimatic/paleoceanographic changes at annual to decadal scale.

Three major laminated intervals characterize the last 50,000 years in the Shaban Deep (Arz and Pätzold, in prep.). These occur in the mid-Holocene (4-6 ka), the Last Glacial Maximum (LGM)-deglacial (~13-22 ka) and in Oxygen Isotope Stage 3 (sediments older than 33.7 ka). We studied sediments younger than 22,000 years in detail and propose that within the Holocene, pairs of laminae most likely represent seasonal-scale flux events with an alternation of siliceous and calcareous components. In contrast, laminations in the older section, while most likely recording productivity/deposition events, are more difficult to attribute to a seasonal signal unambiguously because of the lack of an annual terrigenous marker and dissolution of

carbonate. Finally, we present schematic models to propose paleoflux scenarios for laminae formation at different time-slices in this unique setting.

Geographical setting

Circulation

The Red Sea is a very unique environment. There are no permanent river inflows, rainfall is sparse and evaporation largely exceeds precipitation. The seawater exchange with the Arabian Sea in the south is limited due to the very shallow sill (137 m) of the Strait of Bab el Mandab.

In the Red Sea the prevailing winds are from the NW to NNW throughout the year and run parallel to its main axis. South of about 19°N, however, wind directions are reversed in winter and blow from the SSE (e.g. Edwards, 1987).

Due to high evaporation, sea surface salinity (SSS) values are high and increase from south to north, reaching up to 40 psu in the northern Red Sea (Edwards, 1987). Sea surface temperatures (SST) in the northern Red Sea are between 22-24°C in winter and up to 28°C in summer (e.g. Berman et al., 2003).

A description of the anti-estuarine circulation pattern of the Red Sea can be found in Eshel et al. (1994) and Eshel and Naik (1997). The circulation is mostly driven by thermohaline forcing while wind forcing is only of minor importance. Surface waters flow to the north in Eastern and Western Boundary Currents, getting denser on their way due to evaporation. At the northernmost end of the Red Sea basin southward-flowing intermediate and deep waters are formed. Different modes of deep-water renewal have been suggested, including a) descent plumes of the Gulf of Suez outflow contributing up to 50 % of the Red Sea deep water renewal (Woelk and Quadfasel, 1996); b) isopycnally-formed intermediate water that is injected directly beneath the pycnocline in the open northern Red Sea off the tip of the Sinai Peninsula (Cember, 1988); and c) shallow convection initiating intermediate waters at the collision site of the Western and Eastern Boundary Currents (Eshel and Naik, 1997).

Phytoplankton

The northern Red Sea is an oligotrophic environment and is stratified for most of the year. Dissolved nitrate and phosphate are depleted; silicate is low but still detectable. In winter, the depth of the thermocline exceeds 200 m north of 25°N. A shallow thermocline is observed at 30-60 m during spring and summer (Edwards, 1987).

The Red Sea plankton is characterized by the dominance of autotrophic picoplankton while larger cells are scarce in this region (Shaikh et al., 1986; Lindell and Post, 1995). Four differ-

ent groups of phytoplankton are important in the annual cycle of the Red Sea (Shaikh et al., 1986): diatoms are present most of the year and are the predominant group in winter; blue-green algae (*Trichodesmium* spp.) and nanoplankton dominate in late spring and summer, and dinoflagellates in the fall. In general, phytoplankton abundances decrease from the southern Red Sea to the Gulf of Suez (Halim, 1969).

Maximal phytoplankton growth takes place between November and March. Primary production off Jiddah (21°30'N) has a clear bimodal pattern with one maximum in December-February and a smaller one in June-August, and thus reflects the peaks of the two monsoonal seasons (Shaikh et al., 1986). The major seasonal peak of Chlorophyll (Chl) *a* starts in December at 75 m water depth (Shaikh et al., 1986) and then moves upwards in the water column during January and February. According to Shaikh et al. (1986), this winter peak is clearly dominated by diatoms (e.g. genera *Bacteriastrum*, *Chaetoceros*, *Nitzschia* and *Rhizosolenia*). Nutrient concentrations are highest at this time. Just after the decline of the major pulse of primary production, sub-surface nutrient regeneration takes place. Abundances, rate of primary production and nutrients decline and during the early summer nanoplankton dominates.

A second sub-surface Chl *a* maximum (75-100 m depth) occurs in September, just after the second peak of primary production in surface waters (June-August). During this time, seasonal stratification is at its maximum and surface water nutrient levels are minimal; blue-green algae are the main contributors. Also, diatoms of the genera *Leptocylindrus*, *Nitzschia* and *Rhizosolenia* are present during the secondary bloom.

Material and Methods

Marine sediments in the northern Red Sea consist mainly of biogenic carbonates and terrigenous material from eolian input (Arz et al., 2003b). The investigated core (GeoB 5836-2) was retrieved from the southern sub-basin of the Shaban Deep during *RV Meteor* cruise M 44/3 in 1999. The sampling site is located at 26°12.61'N and 35°21.56'E at a water depth of 1475 m (Fig. 1). Sediments are described as diatom-bearing nannofossil ooze, partly laminated, olive-gray to black, and with a very high content of hypersaline pore water (Pätzold et al., 2000). A general overview of sediment composition and texture was gained through smear slide analysis which followed standard ODP procedures. Data are available online under http://www.pangaea.de/home/iseeberg-elverfeldt/. We emphasize here that smear-slide analysis provides only rough estimates of the relative abundances of microfossils and detrital constituents in order to give a general overview of sedimentary composition. A rough assess-

ment of coccolith preservational states was done based on the system used during ODP Leg 175 (Shipboard Scientific Party, 1998, Explanatory Notes, p. 35).

Biogenic opal content was measured for selected samples (at 20, 50, 322, 370, 424, 448, 456, 480, 512 ,580, 648 cm) and determined by the basic leaching method of DeMaster (1981), modified by Müller and Schneider (1993).

We also report on total organic carbon (C_{org}) and carbonate content (Arz, unpubl. data). Total carbon (TC) and C_{org} were determined on untreated and decalcified samples by combustion at 1050°C using a Heraeus CHN-O-Rapid elemental analyzer. Carbonate was calculated from the difference and expressed as calcite ($CaCO_3$ = (TC- C_{org}) x 8.33). Additionally, we logged the sediment core using a Multi-Sensor-Core-Logger (MSCL; GEOTEK) with an attached video camera.

Cookie cutter slabs were taken within the laminated intervals (Fig. 2) following the method described by Schimmelmann et al. (1990) and Dean et al. (1999). X-radiographs of slabs were taken to record differences in sediment density and structure. In this study, the X-radiograph negatives were scanned to establish a direct relationship with the thin sections that are described below. In the scanned negatives, light bands represent layers of very dense material and dark bands indicate layers of lower density.

Polished thin sections of resin-embedded sediment were prepared at the Cardiff University, Wales following the methodology of Pike and Kemp (1996a) with a small modification: the samples were first soaked in de-ionized water to remove the salt before they were embedded. To assess lamina composition, the polished thin sections were carbon-coated and studied using scanning electron microscopy (SEM). A Leo (Cambridge Instruments) S360 SEM with an Oxford Instruments INCA Wave elemental analysis system was used at Cardiff University, and a Philips XL 30 ESEM was used at the Alfred-Wegener-Institute for Polar and Marine Research in Bremerhaven, both equipped with a backscatter detector. BSEI (backscattered electron imagery) mosaics were produced for every thin section. These photomosaics may be considered as porosity maps where porous diatomaceous sediment appears darker while terrigenous sediment is less porous and therefore brighter. After first producing low magnification (30X) BSEI photomosaics that act as basemaps of each sample, high resolution pictures at higher magnifications (up to 1900X) were taken to study the composition of individual lamina in detail and to identify the species present. Additionally, raw sediment blocks, cracked open along lamina boundaries and coated with Au/Pd were also studied to get topographic images of single laminae using SEI (secondary electron imagery). Thin sections were also analyzed using a Zeiss compound microscope. Observations from conventional light microscopy and

topographic SEM imagery were combined to facilitate identification of diatoms (to genus or species level) as well as coccoliths in cross section in the BSEI photomosaics.

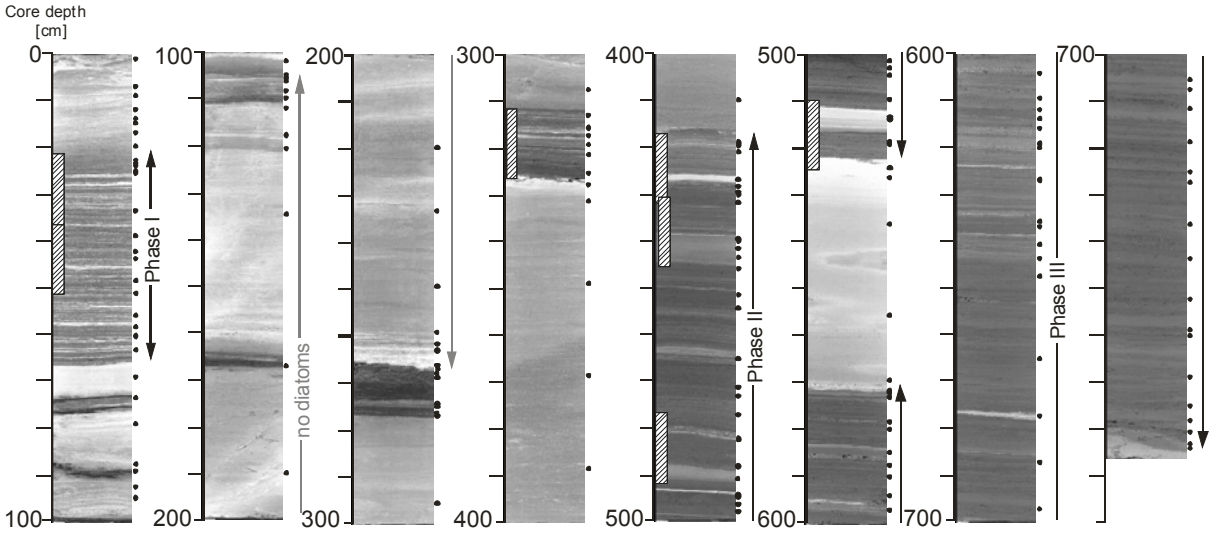

Fig. 2. General lithology of core GeoB 5836-2 (videologger data) showing the distribution of laminated and non-laminated sediments, the position of the cookie cutter slabs (hatched bars), and smear slide samples (black circles). Phases I (4-6 ka), II (14-22 ka) and III (older than ~ 34,000 cal yr BP) are indicated as well as the interval without diatoms.

Results

General characteristics of core GeoB 5836-2

A preliminary age model was developed based on planktic foraminifera $CaCO_3$ accelerator mass spectrometry ^{14}C dates (Arz and Pätzold, in prep.). The top section of the core GeoB 5836-2 was lost during recovery and thus the surface is dated 3890 cal yr BP ± 40. Age control is difficult in sediments older than 22 ka BP due to strong carbonate dissolution. Furthermore, Stoffers et al. (1990) described authigenic carbonates in Shaban Deep sediments which complicate the exact age determination even further.

Sedimentation rates are very variable in the investigated core, encompassing 0.028 cm/yr in the mid-Holocene, 0.054 cm/yr in the early Holocene, and ca. 0.016 cm/yr during Termination I. Rates are very low in sediments older than the LGM (0.004 cm/yr).

Core GeoB 5836-2 has three main laminated sections (termed "Phases" here) that are separated by homogenous intervals of variable length (Fig. 2): 1) Phase I, from 21 to 65 cm, representing 4-6 ka; 2) Phase II, from 417-525 cm, representing 13-22 ka; and 3) Phase III, from 572 to 785 cm, encompassing sediments older than ~34 ka. In addition, two small laminated intervals are present in the early Holocene (at 260-267 cm and 312.5-327.5 cm).

Total organic carbon (C_{org}), carbonate ($CaCO_3$) and opal contents reveal major differences among the three phases (Arz and Pätzold, in prep.). Phase I has high carbonate contents

(~33wt%) and good preservation, low biogenic silica (~2.6wt%), and high C_{org}-values (~1.3wt%). Phase II is characterized by the highest C_{org}-content (>1.5wt%), variable amounts of $CaCO_3$ (5-45wt%; average 15wt%), and relatively high biogenic silica (~12.4wt%). Phase III has very low C_{org}-contents (0.6wt%) and variable carbonate contents (5-30wt%; average 8wt%) with some intervals being almost carbonate-free; biogenic silica is highest (~21.2wt%).

Smear Slide Analyses

Smear slide analyses (Fig. 2) reveal that homogenous sediments of the first 20 cm of core GeoB 5836-2 are composed of abundant coccolith, diatom and silicoflagellate remains. The laminated interval that follows (23-64 cm; Phase I) has alternating dark and light layers with basically the same composition as the homogenous interval above, although fragile diatoms (e.g. *Nitzschia bicapitata*) are well preserved here. Coccolith species richness is high and preservation is very good in this mid-Holocene section. *Emiliania huxleyi* and *Gephyrocapsa oceanica* are the main contributors. Additionally, *Umbilicosphaera sibogae*, *Helicosphaera sellii* (?) and *Calcidiscus leptoporus* are abundant, and *Florisphaera profunda* is also present.

The homogenous interval between 65 and 417 cm is dominated by coccoliths. Diatoms are even absent from 105 to 267 cm, but within the two short laminated sections (260-277 cm and 312.5-327.5 cm) they become more abundant from 268 cm downcore. Diatom species of the genus *Azpeitia* (mainly *A. nodulifera*) are predominant in the homogenous sections while *Chaetoceros* vegetative cells are more abundant in the laminated intervals. Coccoliths are less abundant in laminated Phase II (417-525 cm) with *E. huxleyi* being the main contributor (*F. profunda* is absent). This interval is mainly characterized by layers of *Chaetoceros* and *Bacteriastrum* setae (in aggregates), *Azpeitia*, and *Rhizosolenia* (*R. setigera* and *R. pungens*).

Diatom preservation is poor in the short homogenous section (513.5-518.5 cm), and also in the homogenous interval (525-572 cm) that separates Phase II from laminated Phase III. In both, broken valves of *Azpeitia* are common. Phase III (572-785 cm) can be divided into two large sub-sections by their diatom composition: preservation is good between 572-620 cm and *Chaetoceros* (resting spores and setae), *Bacteriastrum*, *Azpeitia* and *Thalassionema* are abundant. Between 620 and 785 cm preservation is poor and *Azpeitia* is the main contributor to the diatom assemblage. Coccoliths are rare to few throughout Phase III. At the base of the core (785-791 cm), coccoliths again become more abundant while diatoms are absent.

Composition of laminae

Thin section 23-65 cm, within Phase I (Mid-Holocene, 4-6 ka)

As described above, the mid Holocene of core GeoB 5836-2 is strongly laminated. Thin alternating dark and light laminae can be readily seen in the X-radiograph (Fig. 3). In addition, bright thick layers are observed.

Thin section analysis reveals that the light layers are in average 123 µm thick (n = 100; Table 1), and are mainly composed of coccoliths and terrigenous material (Figs 3A, 8A), accompanied by small foraminifers and diatom fragments. The dark layers, on the other hand, are composed almost exclusively of diatoms with a minor terrigenous contribution. The average thickness of dark laminae is 119 µm (n = 100; Table 1). Laminae of *Rhizosolenia* (*R. pungens* and *R. setigera*) predominate throughout (Figs 3B, 8B), sporadically carrying pockets of *Hemiaulus hauckii* (Fig. 8C). Some of these layers can reach thicknesses of up to 500 µm. These *Rhizosolenia* layers can be replaced by a mixed assemblage composed of *Chaetoceros* vegetative cells (mainly *C. lorenzianus*; Fig. 8D) and resting spores (e.g. *C. compressus*), also containing species of *Thalassiosira*, *Nitzschia* (mainly *N. bicapitata*) and others. Silicoflagellate pockets (e.g. *Dictyocha calida*) are also present. Large foraminifers and pteropods are embedded in the sediments disturbing the dark/light layering (Fig. 3). The very bright layers in the X-radiographs are composed of coccoliths and framboidal pyrite (Fig. 3C). Their thickness is very variable, ranging from 300 µm to up to 1.5 mm. The amount of pyrite within each layer also varies so that we can distinguish layers with a large amount and others with little pyrite.

Thin section 312.5-327.5 cm, transition to Phase II (Early Holocene, ~10-11 ka)

The early Holocene is mainly homogenous with the exception of two short laminated intervals at 260-277 cm and 312.5-327.5 cm core depth. We report on the second laminated interval. In the upper half of the investigated cookie cutter slab sediments are homogenous and composed of coarse material. X-radiography reveals faintly laminated sediments in the lower half, with very bright spots at the base of the slab (Fig. 4).

Light and dark alternating layers are clearly evident in the thin sections (Fig. 4). The light layers are mainly composed of coccoliths, terrigenous material, broken valves of diatoms and small foraminifers (Fig. 4A), but in some layers, small grains of framboidal pyrite accompany this assemblage (Fig. 4B). The average thickness of these light layers is 176 µm (n = 91; Table 1) with some exceptions that reach up to 1.4 mm. The main contributor of the dark

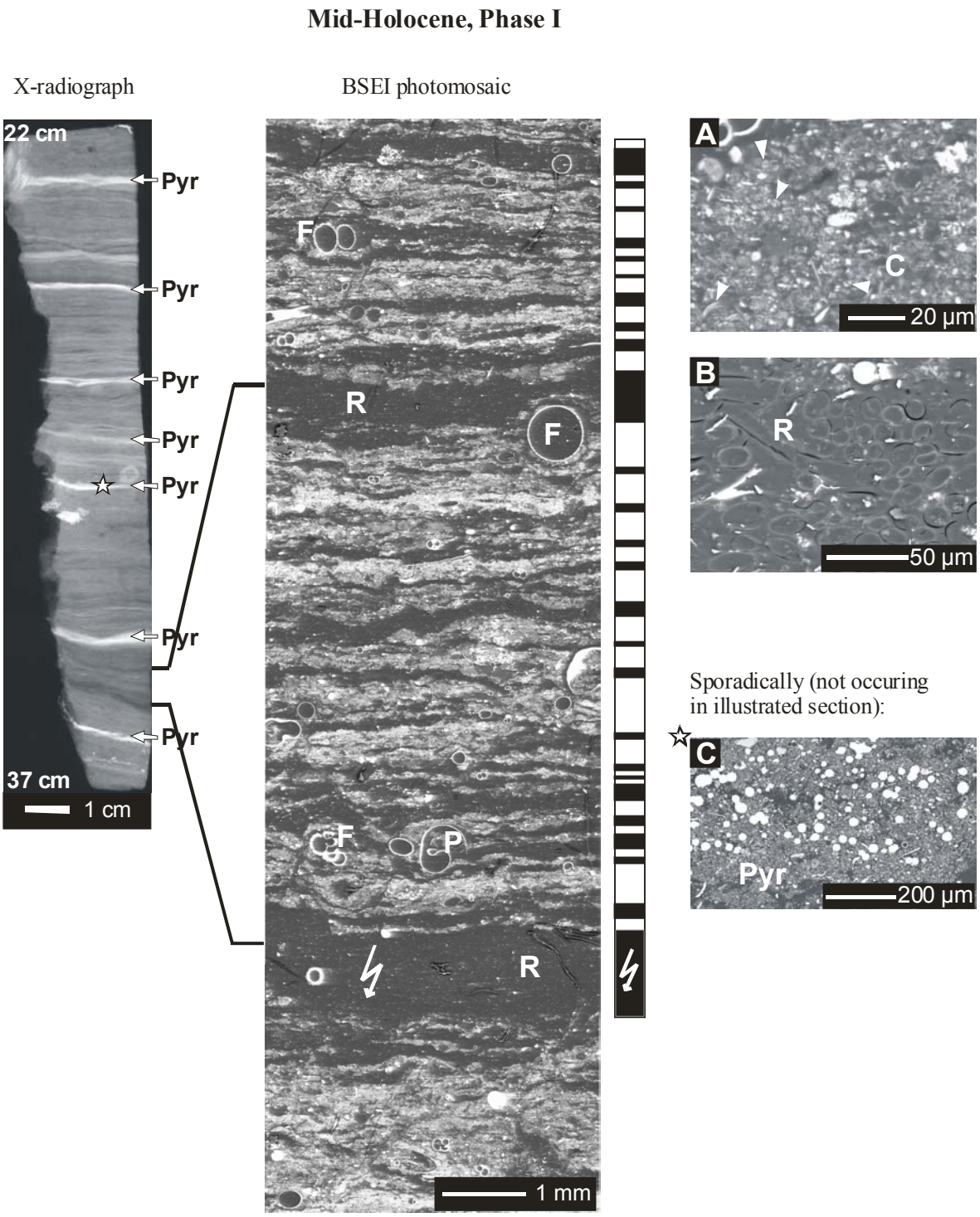

Fig. 3. Phase I, mid-Holocene. X-radiograph of slab 22-37 cm (left). Note thin laminae, and bright layers (marked with **Pyr**) which are composed of framboidal pyrite (see text). BSEI photomosaic of thin section (center). Note alternating dark and light laminae with embedded large foraminifers (**F**) and pteropods (**P**). The thickness of the bottom dark lamina is widened due to a crack in the thin section (indicated by white arrow). The log on the right side of the photomosaic illustrates the laminae succession with black representing dark layers dominated by *Rhizosolenia* and white representing light layers composed of coccoliths, terrigenous material and diatoms fragments. Note the variation in thicknesses of both lamina types. BSEI micrographs (right) showing: A. Detail of light layer with coccoliths (**C,** also pointed out by small arrowheads) and terrigenous debris; B. Dark lamina composed exclusively of *Rhizosolenia* (**R)** frustules; C. Detail of very bright layer composed of pyrite, coccoliths and terrigenous material. This pyrite layer is marked with an asterisk on the X-radiograph (left).

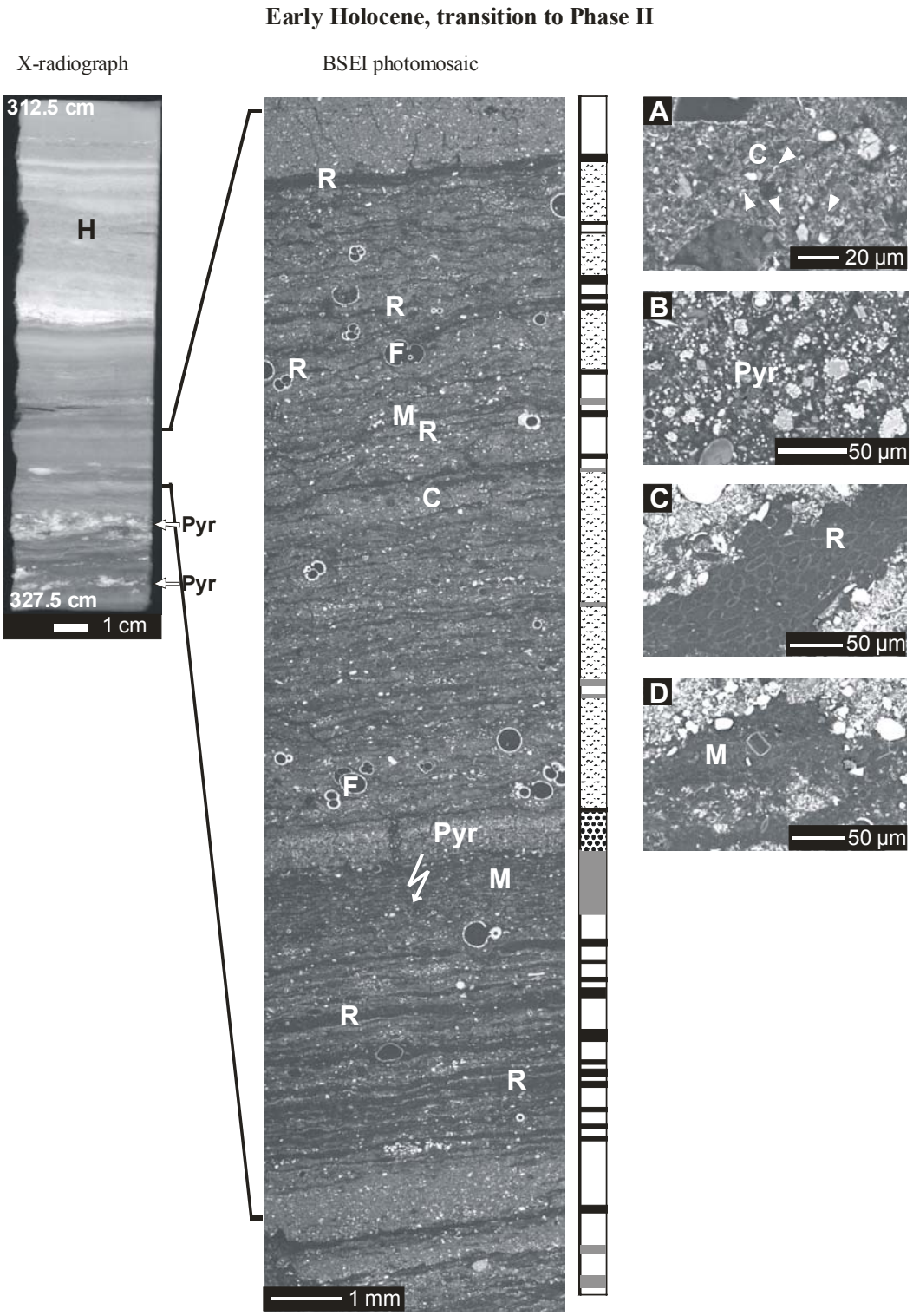

Fig. 4. Transition to Phase II, early Holocene. X-radiograph of slab 312.5-327.5 cm (left). Upper half is homogenous (**H**), and faintly laminated sediments are seen in the lower half, with very bright spots at the end of the X-radiograph. BSEI photomosaic of thin section (center). Light and dark alternating layers with embedded foraminifers (**F**) are clearly evident in the thin section. White arrow indicates a crack. The log on the right side of the photomosaic illustrates the laminae succession. This sequence shows dark continuous diatomaceous layers composed of *Rhizosolenia* in black, which are frequently replaced by dark layers composed of a mixed assemblage (grey), light layers with coccoliths, terrigenous material and diatoms fragments (white) and a pyrite layer (dotted). Thin, wispy discontinuous white and dark intermingled laminae are denoted with a wavy pattern. All lamina types show a highly variable in thickness. BSEI micrographs (right) showing: A. Detail of light layer with coccoliths (**C;** also pointed out by small arrowheads) and terrigenous debris, sometimes accompanied by (B) framboidal pyrite (**Pyr**). C-D. Dark diatomaceous laminae composed of *Rhizosolenia* (**R**) and a mixed assemblage (**M**).

layers are diatom species of the genus *Rhizosolenia* (*R. pungens* and *R. setigera*; Fig. 4C), but layers with a mixed diatom assemblage often take the place of a *Rhizosolenia* layer. Within the mixed layers, species of *Chaetoceros* vegetative cells and resting spores (mainly *C. compressus/contortus* accompanied by several other species) as well as *Nitzschia* (e.g. *N. bicapitata*, *N. interruptestriata* and *N. longicollum*) and *Thalassiosira* can be found (Fig. 4D). The average thickness of the dark layers is 76 µm (n = 61; Table 1). Pockets containing silicoflagellates (e.g. *Dictyocha calida*) are also present. As in the mid-Holocene section, larger foraminifers are embedded in the sediments, disrupting the layering, but these seem to be smaller specimens than the ones described for the mid-Holocene (Fig. 4). The bright spots at the base of the X-radiograph are large clumps of pyrite that in some cases disturb the dark/light layering.

Table 1: Lamina data for three investigated time intervals, including lamina thickness range, mean, standard deviation

time interval	lamina type	range	mean lamina thickness	standard deviation	number of laminae observed
mid-Holocene	light	34-340 µm	122.7 µm	70.8	100
	dark	34-510 µm	118.7 µm	73.4	100
early Holocene	light	34-1700 µm	175.9 µm	244.7	91
	dark	26-170 µm	76.4 µm	37.5	61
Upper Phase II	light	26-340 µm	115.5 µm	65.0	91
	dark	26-782 µm	128.1 µm	129.8	122

Thin section 417-446 cm, Upper Phase II (13-15 ka)

Two cookie cutter slabs were investigated which cover the upper Phase II (Fig. 5). There are three homogenous intervals, at 417-419.5 cm, 428.3-429.1 cm and 440.5-446 cm, while the rest of the sediment is finely laminated with alternating light and dark layers. Again, bright thick layers can be seen in the X-radiograph (Fig. 5).

SEM studies reveal that the upper homogenous section is made up of very coarse material (large fragments of terrigenous material, large foraminifers, pteropods), as well as some diatoms (Fig. 8E). In contrast, the middle non-laminated interval (428.3-429.1 cm) is composed of very fine material such as coccoliths, small foraminifers and fine silt grains. The bottom of the second cookie cutter slab (440.5-446 cm) shows a gradient from coarser material at the bottom to fine grains toward the top. It contains terrigenous material, coccoliths, small foraminifers and some diatoms.

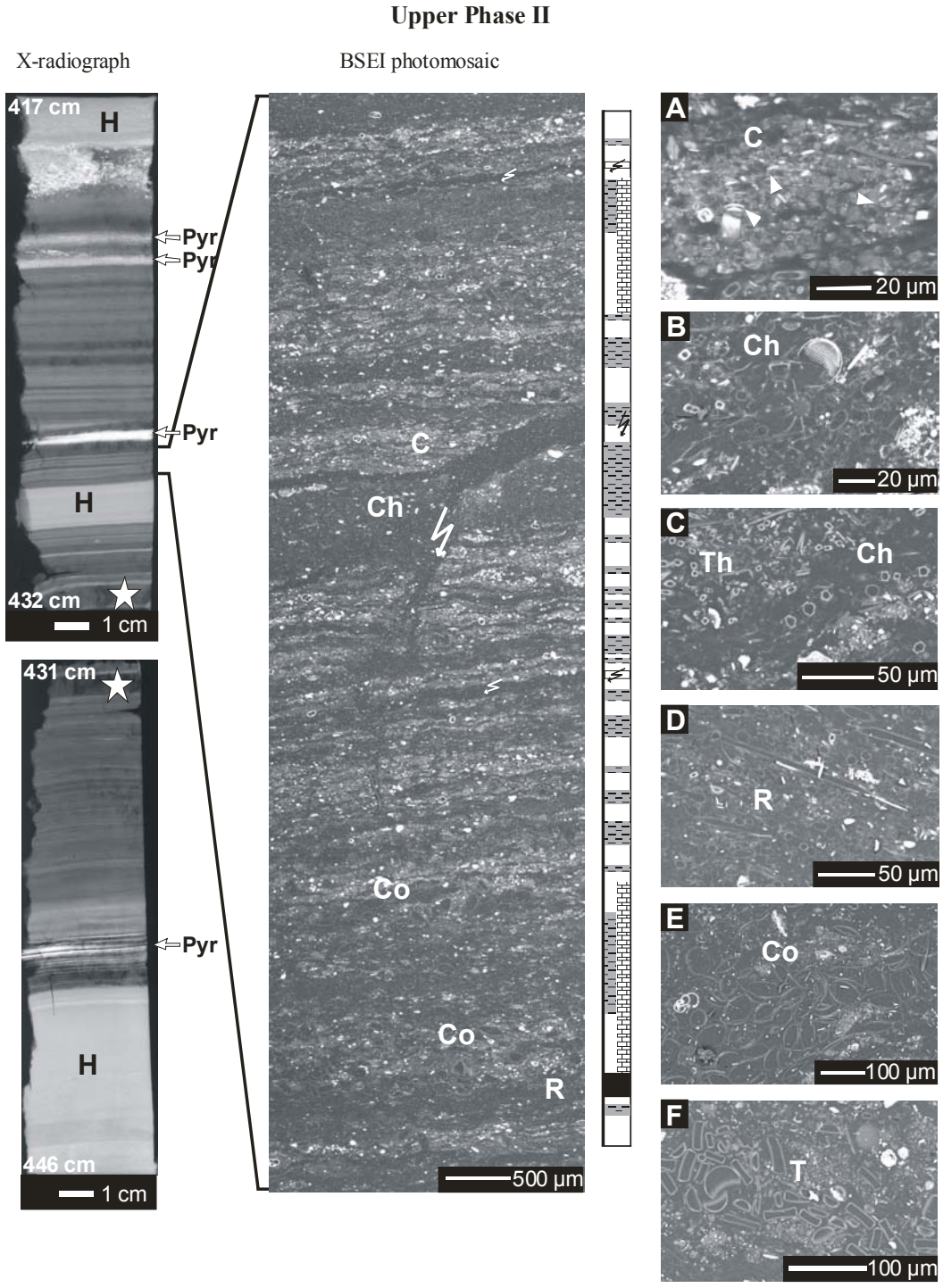

Fig. 5. Upper Phase II. X-radiograph of slabs 417-432 cm and 431-446 cm (left). Note three homogenous intervals (**H**), bright layers (**Pyr**) and distinct laminations. Asterisk marks the point of overlap between both X-radiographs. BSEI photomosaic of thin section (center) with predominance of diatom-rich layers. Small foraminifers are observed. White arrows indicate cracks. The log on the right side of the photomosaic illustrates the laminae succession. Dark layers in the photomosaic are composed of *Chaetoceros* and *Bacteriastrum* aggregates of vegetative cells and setae (grey stippled with black in log). Light layers are comprised of coccoliths, terrigenous material and diatom fragments (marked white); one *Rhizosolenia* layer is marked in black, and wide intervals with centric species such as *Coscinodiscus*, *Thalassiosira* and *Azpeitia* are denoted with bricks. Black arrows point out cracks. BSEI micrographs (right) showing: A. Light layers are comprised of coccoliths (**C**), terrigenous material and diatom fragments. B. Dark diatomaceous layer composed of aggregates of vegetative cells and setae of *Chaetoceros* (**Ch**); *Bacteriastrum* is also present. C. Dark diatomaceous layer with resting spores of *Chaetoceros compressus* (**Ch**) and *Thalassionema pseudonitzschioides* pockets (**Th**). D. *Rhizosolenia* lamina (**R**). E-F. Sporadically, layers of *Coscinodiscus* (**Co**) and/or *Thalassiosira* (**T**) are seen.

Light layers in the laminated sections are comprised of coccoliths, terrigenous material and diatom fragments (Fig. 5A), and are on average 116 µm thick (n = 91; Table 1). The dominant contributors of the dark diatomaceous layers between 417-437.5 cm are aggregates of vegetative cells and setae from different species of *Chaetoceros* (predominantly *C. lorenzianus* or *C. didymus* from about 423 cm downward) and *Bacteriastrum* (*B. elongatum*, *B. hyalinum*, *B. delicatulum*/*furcatum*) (Figs 5B, 8F, G). In some of these layers, resting spores of *Chaetoceros* (*C. compressus*/*contortus* and *C. seiracanthus*) are present and pockets of *Thalassionema* (e.g. *T. pseudonitzschioides* and *T. nitzschioides*) are occasionally embedded within the aggregates (Figs 5C, 8H). Layers of *Rhizosolenia* (*R. pungens* and *R. setigera*) also occur irregularly and have a mat-like appearance (Figs 5D, 8I). These "*Rhizosolenia* mats" become more abundant below 437.5 cm. Sporadically, layers of large *Coscinodiscus* (several species) (Fig. 5E) and/or *Thalassiosira* (*T. eccentrica*, *T. lineata*, *T. oestrupii*) (Figs 5F, 8J) are seen, but no pattern in their occurrence could be recognized. Occasionally, *Azpeitia nodulifera* can be found as well. Radiolarians are embedded in the sediments. Dark layers are 128 µm thick on average (n = 122; Table 1). The foraminifers in this interval are small and mainly present in the light layers. Here too, the bright layers seen in the X-radiograph are comprised of pyrite, coccoliths and terrigenous debris.

Thin section 477-492 cm, within Lower Phase II (18-19 ka)

Laminations in this section are much fainter than in upper Phase II and are not easily distinguished with X-radiography. This slab ends with a thin (0.5 cm) homogenous layer. Again, bright, thick layers are evident (as in Phase I) but do not seem to follow a particular frequency pattern (Fig. 6).

BSEI of thin sections reveals tightly packed valves of *Rhizosolenia* (mainly *R. setigera*) (Figs 6A, 8K) that form a background matrix within which large *Coscinodiscus* (*C.* aff. *perforatus*; Fig. 8L), *Stellarima stellaris*, several species of *Actinocyclus*, and smaller centric diatoms (e.g. *Azpeitia nodulifera* and *Thalassiosira eccentrica*) are embedded (Figs 6, 8M, N). Their distribution appears to be random. Foraminifers are absent and coccoliths are extremely scarce. The very bright layers mentioned above were analyzed with X-ray microanalysis and are composed of Ca-rhodochrosite (Fig. 6) as described by Stoffers et al. (1990). The thickness of these Ca-rhodochrosite laminae varies between 200 µm and 1 mm.

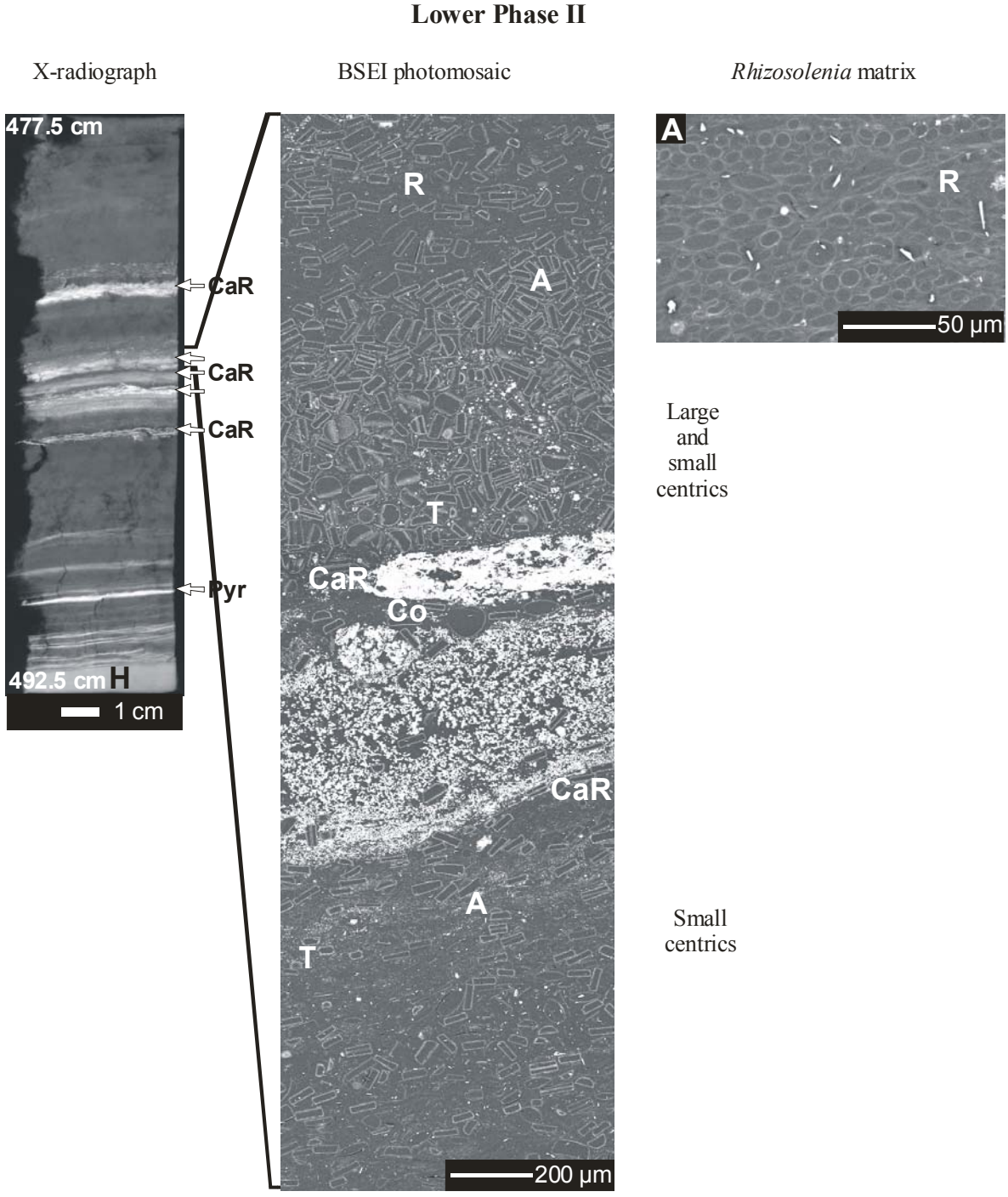

Fig. 6. Lower Phase II. X-radiograph of slab 477.5-492.5 cm (left). Laminae are faint. Bright, thick layers are evident and composed of Ca-rhodochrosite (**CaR**) or Pyrite (**Pyr**). Note homogenous interval (**H**) at bottom of slab. BSEI photomosaic of thin section (center) with diatom genera *Azpeitia* (**A**), *Thalassiosira* (**T**) and *Coscinodiscus* (**Co**). The biogenic $CaCO_3$ and terrigenous components are missing. BSEI micrograph (right) showing: A. Tightly-packed valves of *Rhizosolenia* (**R**) that form a background matrix within which the above-mentioned centric diatoms are embedded.

Thin section 510-525 cm, Lowest Phase II (Last Glacial Maximum, ~22 ka)

The laminated sediments of the cookie cutter slab taken around the LGM are interrupted by a homogenous interval seen in the X-radiograph (Fig. 7). In the BSEI, this homogenous section is composed of centric diatom species, resting spores of *Chaetoceros*, many diatom fragments and abundant terrigenous material. The upper and lower limits of this interval are abrupt.

The alternating pattern of light and dark laminae cannot be distinguished as such in the thin section (Fig. 7), and the general appearance in the SEM is darker than in younger sediments. This dark matrix is dominated by resting spores of *Chaetoceros* (mainly *C. compressus*/*contortus*; Fig. 7A). Thick non-continuous layers of *Coscinodiscus* (*C. radiatus*, *C. centralis*), *Azpeitia nodulifera*, *Stellarima stellaris*, and *Thalassiosira leptopus* are present as well (Fig. 7B). Light pockets composed of terrigenous material, diatom fragments, pyrite and very few coccoliths are intermingled within this dark matrix.

Additional smear slides analyses revealed common abundance of small *Cyclotella* specimens (~ 3-6 µm, that resemble *C. caspia*) which may have been easily overlooked in the thin sections due to their small size.

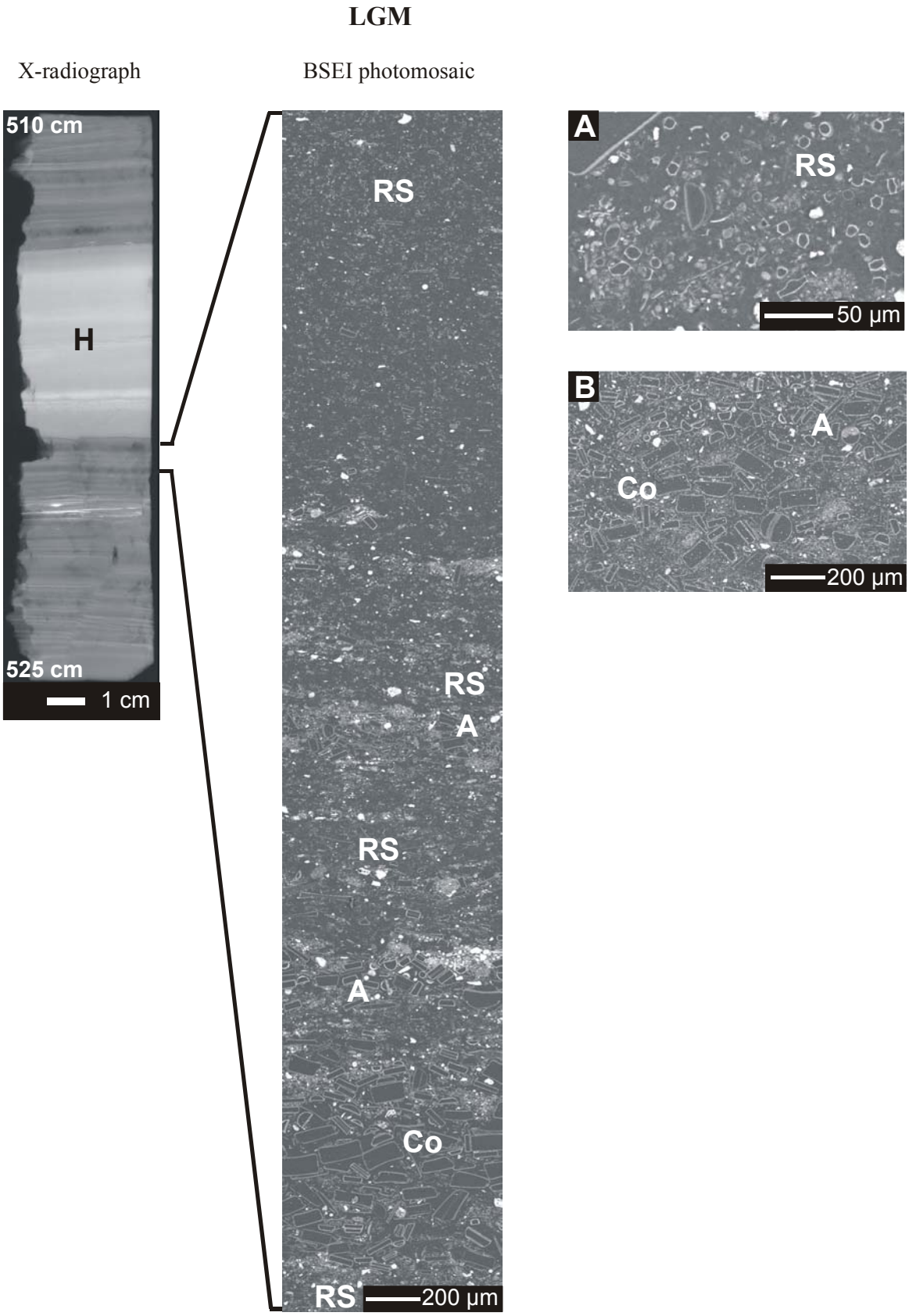

Fig. 7. LGM. X-radiograph of slab 510-525 cm (left). The laminated sediments are interrupted by a homogenous interval (**H**). BSEI photomosaic of thin section (center). It is difficult to distinguish an alternating pattern of light and dark laminae, and the sediments have a general dark appearance. BSEI micrographs (right) showing: A. Dark background is dominated by resting spores of *Chaetoceros* (**RS**). B. Thick layers of *Coscinodiscus* (**Co**) and *Azpeitia* (**A**) are present.

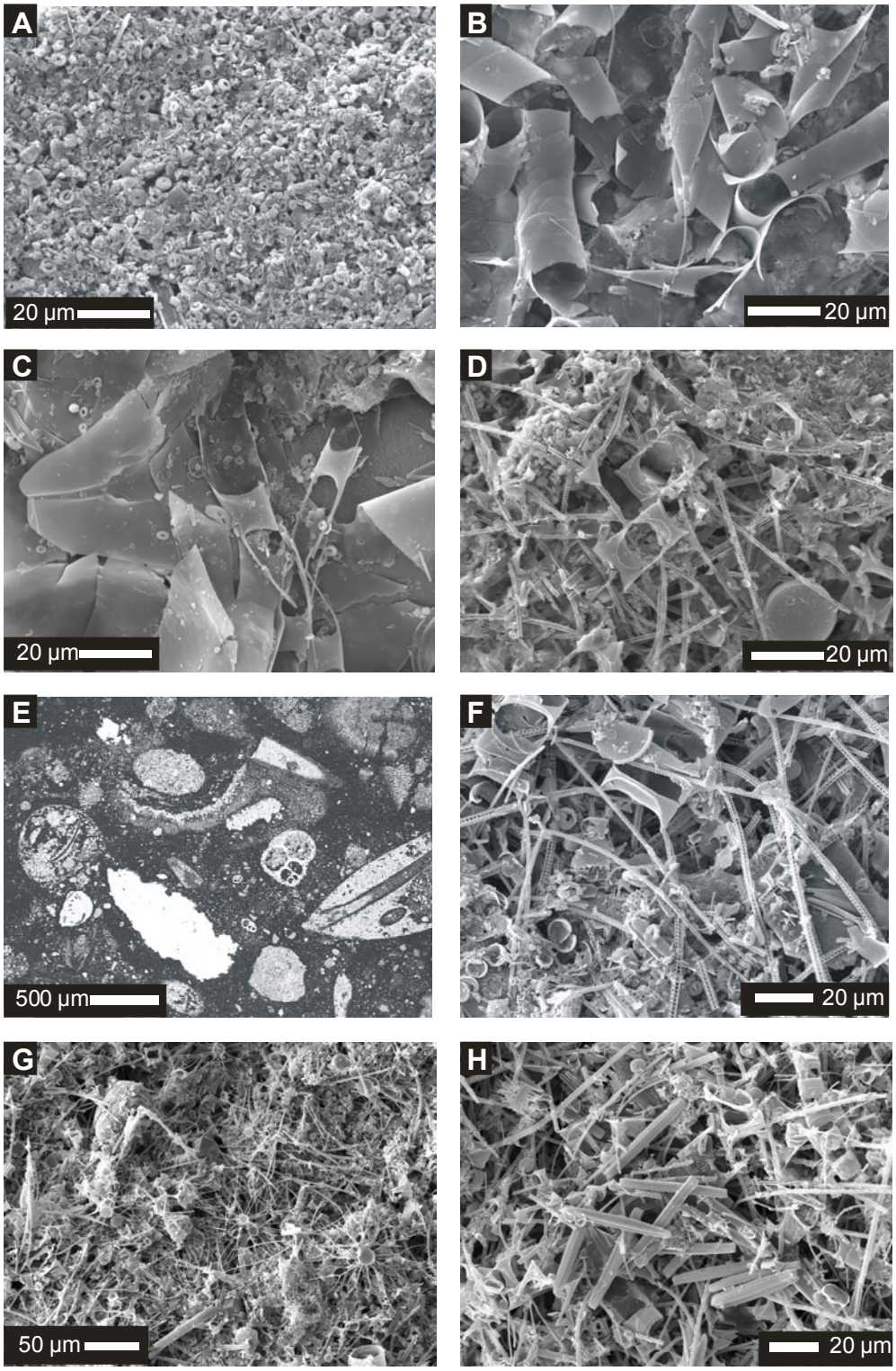

Fig. 8. Scanning electron (SEM) micrographs of selected laminae. A-D. Mid-Holocene, Phase I. A. Coccolith lamina. B. *Rhizosolenia* lamina, mainly *R. pungens*. C. Pocket of *Hemiaulus hauckii* on top of large *Rhizosolenia* girdle bands, contiguous area and claspers. D. Example of mixed assemblage with dominance of *Chaetoceros lorenzianus*. Note coccoliths on *Chaetoceros* setae, and *Thalassiosira lineata* in lower right corner. E-H. Upper Phase II. E. BSEI showing coarse material of upper homogenous interval in slab 417-432 cm (Fig. 5). F. SEM micrograph with *C. lorenzianus* and some coccoliths; small species of *Thalassiosira* are intermingled. G. Overview of aggregates with *Chaetoceros didymus* and *Bacteriastrum hyalinum* as well as *B. delicatulum*/*furcatum*. H. Pocket of *Thalassionema pseudonitzschioides*. Note the resting spore of *Chaetoceros seiracanthus* in the upper left corner.

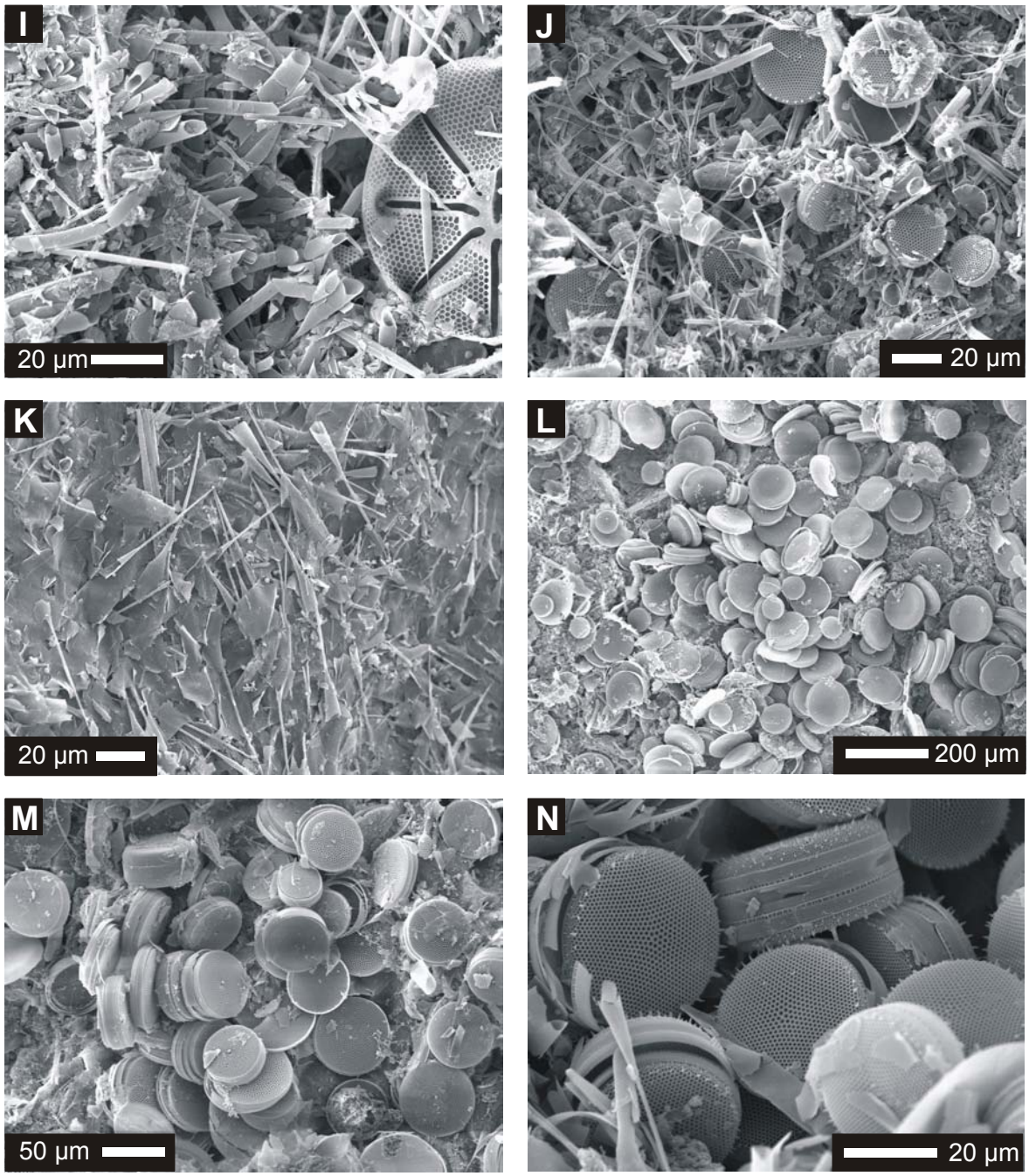

Fig. 8 (cont.). SEM micrographs of selected laminae. I-J. Upper Phase II. I. Mat-aspect of a *Rhizosolenia*-layer. J. Cluster of *Thalassiosira eccentrica*. K-N. Lower Phase II. K. Matrix of *Rhizosolenia setigera*. L. Layer of *Coscinodiscus* aff. *perforatus* and *Azpeitia nodulifera*. M. *A. nodulifera*. N. *Thalassiosira eccentrica*.

Schematic depositional models

We present schematic models of paleofluxes and their dominant components for the different time-slices presented above (Fig. 9). We base our models on what is known about the annual phytoplankton cycle in the Red Sea (see Geographical Setting, section 2.2.). We assume that coccolith-rich layers are attributable to summer deposition while diatom-rich layers represent fall/winter flux to the seafloor. The regularity in the occurrence of these alternating layers (coccolith/diatom couplets) as well as the fact that sedimentation rates for the different laminated intervals are comparable to those estimated from measuring the thickness of couplets, point to an annual deposition cycle, We therefore assume that the laminations in sediments younger than 15 ka represent two-season annual varves.

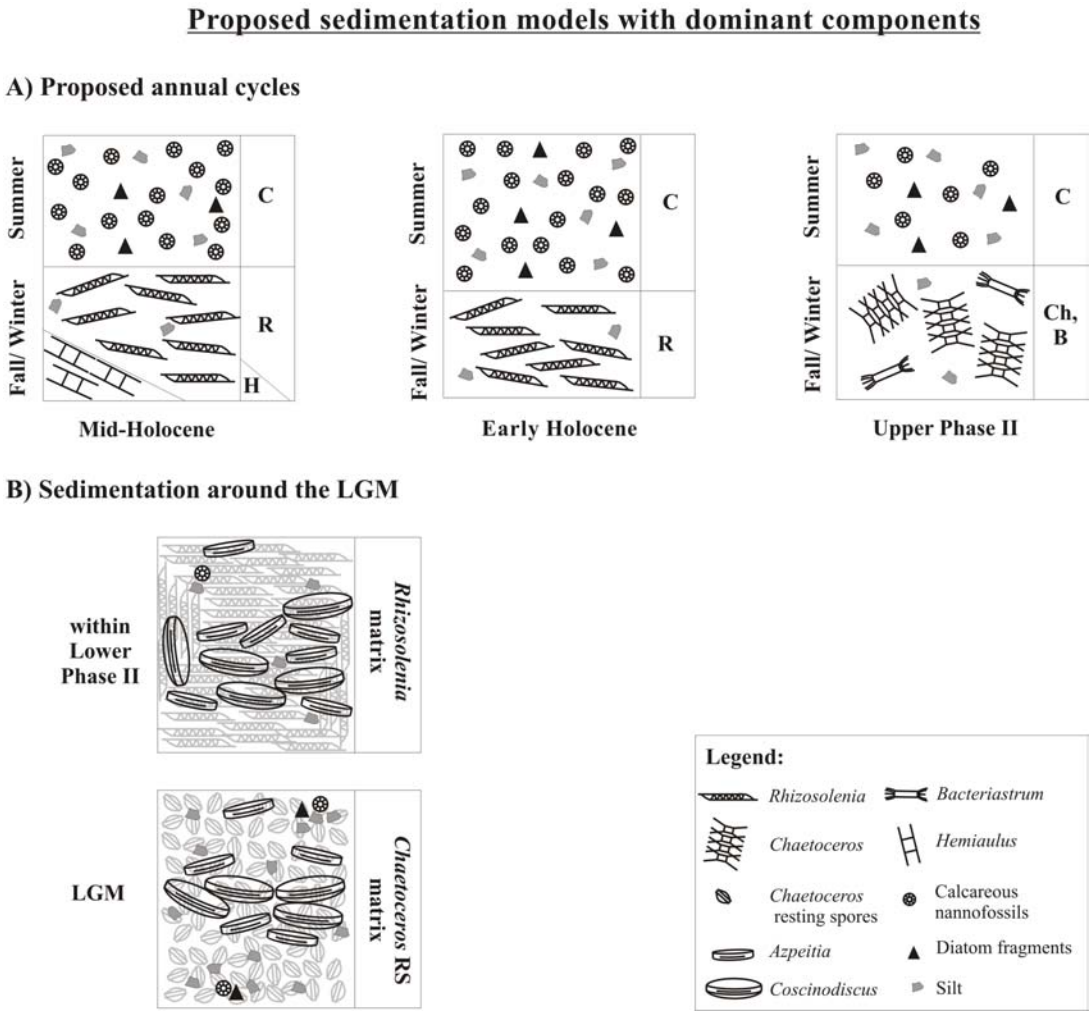

Fig. 9. Summary of schematic sedimentation models. A. Proposed annual cycle of sedimentation with dominant components in the mid-Holocene, early Holocene and Upper Phase II: light laminae result from summer flux of coccolithophorids; dark laminae represent late fall/winter production of diatoms. C = coccolith layer; R = *Rhizosolenia*; H = *Hemiaulus*; Ch, B = *Chaetoceros*/*Bacteriastrum* aggregates. *Hemiaulus hauckii* pockets can be present within the *Rhizosolenia* laminae of the mid-Holocene. Note that light layers are thicker in the early Holocene. B. Proposed sedimentation during the Last Glacial Maximum and the early phase of deglaciation. The *Chaetoceros* RS matrix during the LGM is replaced by a tightly packed *Rhizosolenia* matrix during early deglaciation. Terrigenous particles and coccoliths are more abundant in LGM sediments.

During the Mid-Holocene (Fig. 9), coccolith-rich layers (summer) alternate regularly with diatom-rich layers (fall/winter). The similarity in mean lamina thicknesses of these layers (Table 1) points to equal contribution to the sediments. Putting our detailed BSEI study in the context of the preliminary age model (see Results, section 4.1.), we observe that the lamina couplet coccoliths/*Rhizosolenia* persists over decades (average of ~ 44 years). This pattern is then replaced by one of coccoliths/mixed diatoms which lasts ~ 30 years on average. These periodicities were estimated by measuring the length on the BSEI photomosaic over which the two couplet types expand and calculating their duration by using the sedimentation rate for the mid-Holocene.

The species composition of light/dark laminae observed in BSEI in the early Holocene (Fig. 9) is basically the same as in the Mid-Holocene; light layers are thicker than dark ones. In contrast to the Mid-Holocene, the couplet coccoliths/*Rhizosolenia* in the early Holocene is frequently (roughly every 20 years) replaced by one of coccoliths/mixed diatoms which in turn only lasts for a few years.

A marked shift in the composition and texture of the dark laminae is observed at 13-15 ka (Upper Phase II; Fig. 9). Coccoliths are less abundant, and the genera *Chaetoceros* and *Bacteriastrum* overwhelm the diatom assemblage. Here, the basic light/dark pattern can be attributed to couplets of coccoliths/*Chaetoceros-Bacteriastrum*. *Rhizosolenia* is not the major diatom component anymore (as was the case in the Holocene), although *Rhizosolenia* laminae occur as thick layers with a mat-like appearance. Layers containing a variety of other centric diatoms are also observed.

The loss of the potentially coccolith-rich layer in the sections older than 15 ka prevents us from presenting a schematic model of annual deposition. However, the diatomaceous component reveals a marked switch in species composition between LGM sediments (dominated by *Chaetoceros* resting spores) and sediments from Lower Phase II (18-19 ka; dominated by *Rhizosolenia*). This shift is depicted in Fig. 9. Differences in the quantity of terrigenous particles are also observed, being more abundant in LGM sediments than in the interval just above it.

Discussion

What drives laminae formation in the Shaban Deep?

Since the investigated core GeoB 5836-2 is not laminated over the whole length and laminated sediments can only be generated under anoxic conditions, we assume that the brine body in the Shaban Deep did not persist over the last 50,000 years. The mechanisms to accu-

mulate brine within a deep are various and not fully understood to this day. Changes in deep and bottom water circulation may play a major role (Rossignol-Strick, 1987). Stagnation of water circulation could lead to a rise of the brine surface and increasing anoxic conditions within these brine basins. Arz et al. (2003b) suggested that deep water formation in the northern Red Sea could be suppressed by the additive effect of a strong warming and freshening of the surface waters, conditions that can be found during the stepwise sea-level rise described by Fairbanks et al. (1992). Arz et al. (2003b) further speculate that the resulting stagnant bottom water conditions led to the formation of two Red Sea sapropels (RS1a and RS1b) in an otherwise oxic core from the northernmost Red Sea (GeoB 5844-2; 27°42.81'N; 34°40.90'E; 963 m water depth). RS1a ended with the onset of the Younger Dryas (YD; ~12 to 13 ka) cold period which resulted in an increased rate of deep water formation and ventilation. Sapropel RS1b was terminated with the flooding of the Gulf of Suez (~11 to 10 ka) which may have led to the initiation of an additional mode of deep-water formation, terminating the stagnant bottom water conditions. The two Red Sea sapropels (RS1a and RS1b) of oxic core GeoB 5844-2 can be related to the intervals 417-440.5 cm (Upper Phase II, Fig. 5) and 313-328 cm (early Holocene, Fig. 4) of our laminated core GeoB 5836-2, respectively.

To understand the formation of laminae in the Shaban Deep it is important to comprehend the mechanisms behind brine accumulation and erosion. Increased deep water formation and resulting strong bottom currents may erode the brine body at the seawater/brine interface *via* diffusion in a couple of hundred years (Arz and Pätzold, in prep.). Shaban Deep brine formation is not the subject of this paper and will be discussed elsewhere (Arz and Pätzold, in prep.).

Composition of laminae

Over the past decade, the application of SEM techniques to the study of laminated diatomaceous sediments has shown that seasonal-scale export fluxes can be resolved as thin sublaminae (in some cases even near-monospecific) within a year's deposition record (see review in Kemp et al., 2000). Some of these layers, mainly composed of fast-growing diatoms (e.g. *Skeletonema costatum*, *Chaetoceros* spp.), have been associated with near-surface productivity due to spring upwelling (e.g. Pike and Kemp, 1996b; Grimm et al. 1996; McQuoid and Hobson, 1997). Others, composed of large diatoms (e.g. *Rhizosolenia* spp., *Thalassiothrix* spp., some *Coscinodiscus*) have recently been suggested as representing diatom production at depth within stratified waters that sinks to the sea bed with the onset of fall/winter mixing that breaks down stratification (i.e. "fall dump", Kemp et al., 2000).

Putting our detailed microscopic analysis of the laminated intervals in the Shaban Deep into the context of what is known of the annual phytoplankton production cycle in the Red Sea (Shaikh et al., 1986), we suggest that the light/dark lamina couplets of the past 15,000 years represent contrasting seasons and associated plankton blooms (Figs 9). The regularity in the occurrence of alternating light/dark layers (coccolith/diatom couplets) points to an annual deposition cycle, and thus we assume that the laminations represent two-season annual varves. We interpret the light laminae as resulting from summer flux of coccolithophorids mainly produced by *E. huxleyi* and/or *G. oceanica* blooms. The darker laminae, on the other hand, represent late fall or winter production of diatoms that sinks through the water column to the seafloor in late winter when stratification breaks down and mixing takes place (Edwards, 1987).

Because of the diatom species composition in the dark laminae, we further suggest that the winter deposition could carry the signal of either a) winter near-surface production of fast-growing species (e.g. *Chaetoceros*) in response to nutrient availability; or b) fall production at depth (deep chlorophyll maximum, DCM) of large diatoms (e.g. *Rhizosolenia*) typical of stratified conditions and representative of a "shade flora" (Kemp et al., 2000); or c) a combination of both signals. If the scenario above is correct, we propose that the degree by which each of these signals is represented in the sediments can be used to characterize stratification/mixing variability through time. Of course, factors such as intra- and inter-annual variations in production in the water column, dissolution during sinking, aggregation, and post-depositional processes at the sediment/water interface and within the upper sediments need to be considered. Indeed, diagenetic mineral formation is observed in brines of the Red Sea. Within organic-rich layers, Stoffers et al. (1990) found diagenetically formed dolomite and rhodochrosite. Pyrite occurrence has also been described for the Shaban Deep (Rossignol-Strick, 1987; Hemleben et al., 1996b).

As expected, because of sparse rainfall and no permanent river inflows into the northern Red Sea, terrigenous input is low overall; it cannot be assigned to a specific type of lamina and thus may not be primarily associated to a season in particular. However, BSEI photomosaics show that light layers seem to hold more silt particles than the dark ones. We do not have information on dust sources and frequency of dust events for our study area in particular. However, Léon and Legrand (2003) in their study on the possible sources of eolian-transported terrigenous material influencing north Indian Ocean sediments, propose the Nubian desert, the Arabian peninsula, Iran, Pakistan and Afghanistan, and Northwest India as the main dust sources for that region. We believe that some of these source areas are likely to

influence the northern Red Sea sediments as well. Léon and Legrand (op. cit.) also point to the spring and summer as the times with highest dust frequency. This would coincide with our findings that light layers, as representatives of summer sedimentation, carry the main signal of eolian input.

Interpretation of paleofluxes

Recently, Arz et al. (2003b) combined stable oxygen isotope measurements on multiple planktic and benthic foraminifers with alkenone paleothermometry, and reconstructed sea surface temperatures (SST) and salinities (SSS) as well as vertical gradients in $\delta^{18}O$ ($\Delta\ \delta^{18}O$) for the last 22 ka from a non-laminated core (GeoB 5844-2) retrieved in the northern Red Sea off the tip of the Sinai Peninsula. We will now attempt to interpret the observed changes in laminae composition (Figs 3-7) and associated schematic paleoflux models (Figs 9) by putting the stratification/mixing assumption based on diatoms presented above into the context of Arz et al.'s (2003b) results (Fig. 10). Our interpretation includes only those time intervals between the LGM and the mid-Holocene for which detailed BSEI photomosaics are available.

Last Glacial Maximum: The LGM is documented in the northern Red Sea as a so-called "aplanktic (or aplanktonic) zone" (e.g. Winter et al., 1983; Almogi-Labin et al., 1991; Hemleben et al., 1996a; Fenton et al., 2000). During this period, planktic foraminifers became extinct due to the high salinity levels (~ 50 psu) and an almost monospecific pteropod fauna (*Creseis acicula*) was established at that time (Winter et al., 1983; Almogi-Labin et al., 1991). During this interval, carbonate dissolution was severe (Arz et al., 2003b) which resulted in the loss of the coccolith-rich layers in these sediments. The anomalously high salinity values (Fig. 10) are attributed to a drastic reduction of water exchange between the Red Sea and the Indian Ocean through the Strait of Bab el Mandab due to lowered glacial sea level (see Fig. 1 in Sirocko, 2003), greater evaporation, and to some extent also due to an increased aridity in the area (e.g. Hemleben et al., 1996a; Arz et al., 2003a; Siddal et al., 2003). Arz et al.'s (2003b) reconstruction of the LGM scenario suggests a drop of 4°C in SST from present-day values in the northern Red Sea (Fig. 10), a slightly increased productivity, as well as an enhanced input of eolian-transported terrigenous material.

Within the diatomaceous component of the sediment, there is a very clear switch from a *Chaetoceros* resting spore matrix (~22 ka, LGM) to a *Rhizosolenia* matrix (~19 ka, end of LGM, lower Phase II) (Fig. 9) as well as a marked difference in the amount of terrigenous

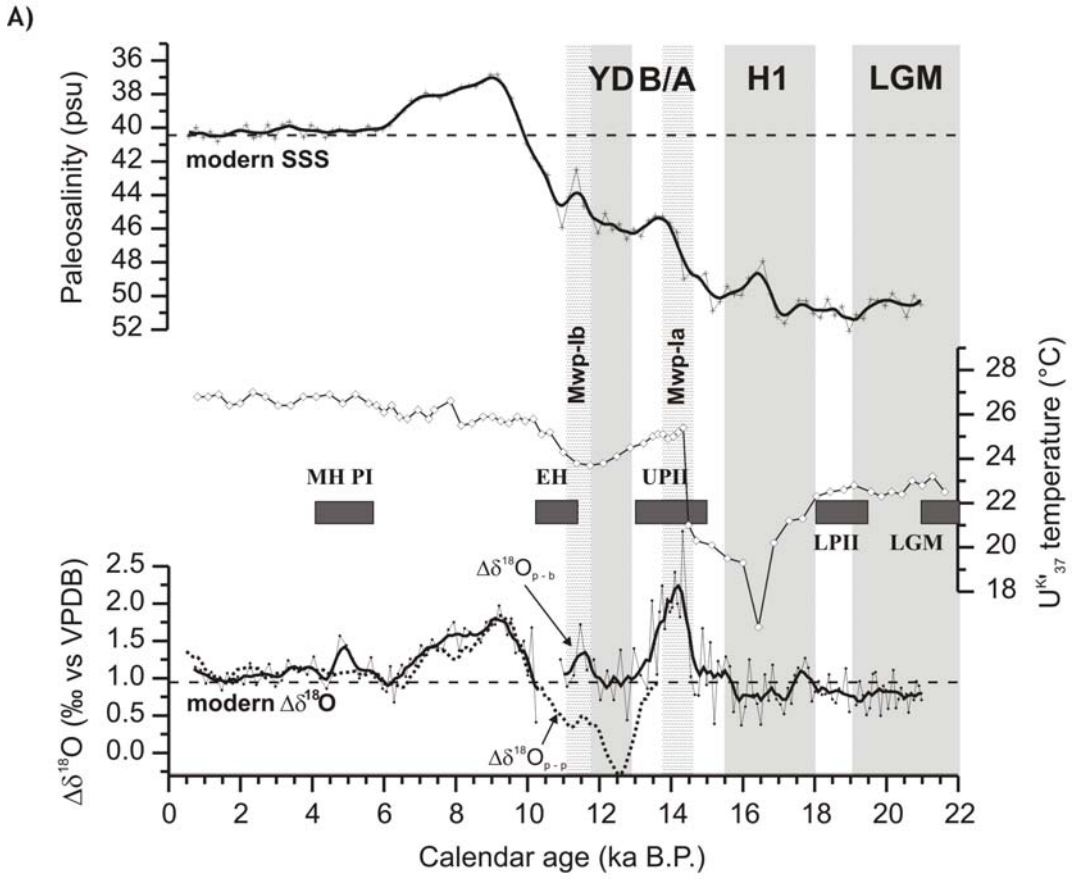

B) Summary of laminated intervals

Abbreviation	MH PI	EH	UPII	LPII	LGM
Age/Phase	Mid-Holocene, Phase I	Early Holocene	Upper Phase II, across Bølling/Allerød	Lower Phase II	Last Glacial Maximum
	4-6 ka	~10-11 ka	13-15 ka	18-19 ka	~22 ka
Dominant diatom flora	*Rhizosolenia*	*Rhizosolenia* and mixed	switch from *Rhizosolenia* to *Chaetoceros-Bacteriastrum*	*Rhizosolenia* matrix	*Chaetoceros* resting spore matrix
Interpretation	stratified, multi-decadal variability in stratification and mixing events	increasing stratification, high variability between stratification and mixing events	switch from stratification to well-mixed	stratified ? or less nutrients ?	well-mixed water column, increased eolian influence, increased nutrients

Fig. 10. A. Investigated cookie cutters samples (black bars) of core GeoB 5836-2 (this study) put into the context of reconstructed sea surface paleosalinities, $U^{k'}_{37}$ paleotemperatures and the vertical gradients in $\delta^{18}O$ (calculated as the difference between planktic and benthic records, $\Delta\ \delta^{18}O_{p\text{-}b}$, and between shallow planktic and deep planktic records, $\Delta\ \delta^{18}O_{p\text{-}p}$) from core GeoB 5844-2 (27°42.81'N; 34°40.90'E; 963 m water depth) described by Arz et al. (2003a) and Arz et al. (2003b). Dotted vertical bars mark the melt water pulses 1a and 1b (Fairbanks et al., 1992), and gray shaded vertical bars show the duration of the Younger Dryas (YD), Heinrich event 1 (H1) and the Last Glacial Maximum (LGM); B/A corresponds to the Bølling/Allerød. B. Summary of the results for the investigated laminated intervals.

particles which are more abundant in LGM sediments (Fig. 7) compared to ~19 ka sediments (Fig. 6). We can only speculate that this species switch may point to a well-mixed water column during the LGM (*Chaetoceros*) which then becomes stratified (*Rhizosolenia*) towards the end of the LGM. However, no dramatic changes in SST, SSS and the $\Delta\delta^{18}O_{p\text{-}b}$ gradient (as a proxy of water column stratification) can be observed in the 19-22 ka time window (Fig. 10). Another explanation for the change in the background diatom assemblage that does not involve a change in stratification may be related to higher nutrient availability in surface waters during the LGM which in turn could have been associated with the increased eolian-transported terrigenous material. The co-occurrence of thick non-continuous layers of *Coscinodiscus*, *Azpeitia* and other large centric diatoms within glacial sediments may indicate a more pronounced seasonal contrast between summer stratification and winter deep mixing at that time, as was assumed by Arz et al. (2003b) for glacial sediments of core GeoB 5844-2.

Bølling/Allerød: The warm Bølling/Allerød period in the Red Sea is characterized by an abrupt rise in SST and a decrease in SSS (Fig. 10) which have been interpreted by Arz et al. (2003b) as a surface freshening and a strongly stratified water column centered at around 14.5 ka. The authors relate this to the postglacial melt water pulse MWP 1a (Fairbanks et al., 1992). They further suggest that the combined effect of a strong warming and freshening of the surface waters that relates to the step-wise sea level rise could have suppressed regular deep water formation, and that the resulting stagnant bottom water conditions would have led to the formation of the RS 1a sapropel in core GeoB 5844-2.

The laminated sediments in core GeoB 5836-2 representing the ~13-15 ka time period (Upper Phase II, Figs 5 and 9) can be correlated with sapropel RS1a of core GeoB 5844-2. The sediments show a marked change in the dominant diatom assemblages at about 437.5 cm core depth. While the dominant pattern involves an alternation of coccoliths and *Rhizosolenia* laminae below that depth, the couplets coccoliths/*Chaetoceros*-*Bacteriastrum* characterize the sediments above it. We attribute the former pattern to stratification maximum during MWP 1a and the latter to the decline in stratification that followed (Fig. 10). This period that led to the YD, characterized by surface water cooling, slightly increased SSS and a $\Delta\delta^{18}O_{p\text{-}b}$ gradient that points to an increased rate of deep-water formation and ventilation (Arz et al., 2003b; Fig. 10).

The Holocene: The laminated section of Upper Phase II (Fig. 5) terminates with a homogenous interval that extends to ca. 327 cm depth in the core (Fig. 2) which contains the YD cold period. This is followed by a short laminated section of the early Holocene (Figs 2 and 4) which can be correlated with sapropel RS 1b of core GeoB 5844-2, and was documented as a

minor freshening peak around 11.4 ka (Arz et al., 2003b) associated with MWP 1b (Fairbanks et al., 1992). It was related to another phase of increased, although less pronounced, stratification of the uppermost water column (Arz et al., 2003b; Fig. 10). The investigated cookie-cutter sample (Fig. 4) picks up this increased stratification which, we believe, is reflected by a pattern of coccoliths/*Rhizosolenia* couplets (Fig. 9). The frequent replacement (every ~ 20 years) of this pattern by coccoliths/mixed diatoms couplets (lasting for only few years) suggests high variability between stratification and mixing events. High frequency changes may well have taken place at this time (11-9 ka) which marks a transition from relatively high to much lower salinities and weaker to stronger stratification (Fig. 10). These conditions became established during a northern Red Sea humid interval between ~9 and 7 ka and were explained by enhancement and southward extension of rainfall from Mediterranean sources; they terminated at about 6.25 ka (Arz et al., 2003a).

The Mid-Holocene laminated interval (starting at ~6 ka, shortly after the end of the humid phase), is characterized by temperatures, salinities and stratification conditions similar to modern values (Fig. 10). The observed switch from a coccoliths/*Rhizosolenia* to a coccoliths/mixed diatom pattern seems to happen every 3 to 146 years with an average of 44 years. This suggests decadal variability in stratification and mixing with the former pattern representing a mode of stratification and the latter one mixing, each lasting several years.

Conclusions

- Laminated sediments spanning the last 22,000 years (though not continuously) in the Shaban Deep (core GeoB 5836-2; 26°12.61'N, 35°21.56'E; water depth 1475 m) can be used for reconstructing paleoceanographic and paleoclimatic changes in the region at high resolution.
- Laminated sediments encompassing the period 4-15 ka show a clear alternating light/dark pattern (coccoliths/diatom couplets) in the BSEI photomosaics and are interpreted as carrying a signal of contrasting seasons and associated plankton blooms: Light, coccolith-rich layers represent the summer flux; dark diatomaceous layers correspond to late fall and/or winter production. We thus suggest that the laminations in this time interval represent two-season annual varves.
- The main contributors to the diatomaceous layers are species of the genus *Rhizosolenia* (in the early and mid-Holocene) and *Chaetoceros* (during the deglaciation and the Last Glacial Maximum). The most important species within the coccolith layers are *E. huxleyi* and *G. oceanica*.

- The lack of coccolith-rich layers within LGM sediments is assumed to be due to strong carbonate dissolution ("aplanktic interval"). This dissolution prevents identification of an annual cycle of sedimentation. However, a marked and abrupt switch in diatom species can be observed between LGM sediments with a background matrix of *Chaetoceros* resting spores (~22 ka) and sediments from the lower Phase II with a background matrix of *Rhizosolenia* (~19 ka). Differences in the amount of terrigenous particles are also observed between these two time intervals, being more abundant in LGM sediments.
- We propose that the different diatom assemblages that characterize each of the time-intervals analyzed (from the mid-Holocene to the LGM) reflect changing conditions in stratification in the northern Red Sea: *Rhizosolenia* dominance points to strong stratification of the water column (i.e. at the beginning of meltwater pulse MWP 1a, at 14.5 ka). The genus *Rhizosolenia* has been suggested as representing a deep diatom production and associated with a "shade flora". In contrast, sediments dominated by *Chaetoceros* reflect mixing conditions (e.g. LGM). This genus is composed of fast-growing diatoms and has been associated with near-surface productivity due to upwelling.
- *Rhizosolenia* and a more stratified water column seem to have played the dominant role in the northern Red Sea since the Last Glacial Maximum, at least during times when the brine in the Shaban Deep was present.

Acknowledgements

We thank the captain and crew of *R/V Meteor* for their efforts and support at sea. We also acknowledge the generous grant of permission for conducting research in the territorial waters of the Kingdom of Saudi Arabia. Thanks are extended to Martin Čepek for his help with the identification of coccoliths; to Marco Klann for opal analysis, and to the technicians of the Cardiff University (Peter Fisher and Lawrence Badham) and the Alfred-Wegener-Institute for Polar and Marine Research (Ute Bock) for their technical assistance during preparation of thin sections and the endless hours at the SEM. We also want to thank Axel Ehrhardt from the Centre for Marine and Climate Research Institute for Geophysics (University of Hamburg) for creating the bathymetric map of the Shaban Deep (Fig. 1) from bathymetric grid data of *RV Meteor* Cruises 44/3 and 52/3. Two anonymous referees are acknowledged for their comments and suggestions that have greatly improved the final form of this manuscript. We are very grateful to the Hanse Institute of Advanced Study, Delmenhorst, Germany, for the Fellowship awarded to C. B. Lange. This is Contribution No. XXX of Cardiff School of Earth, Ocean and Planetary Sciences. This work was supported by the Deutsche Forschungsgemeinschaft as part of the DFG-Research Center "Ocean Margins" at the University of Bremen, No. RCOM0105.

References

Almogi-Labin, A., Hemleben, C., Meischner, D. and Erlenkeuser, H., 1991. Paleoenvironmental events during the last 13,000 years in the central Red Sea as recorded in Pteropoda. Paleoceanography, 6(1): 83-98.

Arz, H. and Pätzold, J., in prep. Late Quaternary climate impact on brine formation in the Shaban Deep, northern Red Sea.

Arz, H.W., Lamy, F., Pätzold, J., Müller, P.J. and Prins, M., 2003a. Mediterranean moisture source for an early-Holocene humid period in the northern Red Sea. Science, 300: 118-121.

Arz, H.W., Pätzold, J., Müller, P.J. and Moammar, M.O., 2003b. Influence of Northern Hemisphere climate and global sea level rise on the restricted Red Sea marine environment during Termination I. Paleoceanography, 18(2): 1053, doi:10.1029/2002PA000864.

Berman, T., Paldor, N. and Brenner, S., 2003. Annual SST cycle in the Eastern Mediterranean, Red Sea and Gulf of Elat. Geophysical research letters, 30(5): 1261, doi: 10.1029/2002GL15860.

Burke, I.T., Grigorov, I. and Kemp, A.E.S., 2002. Microfabric study of diatomaceous and lithogenic deposition in laminated sediments from the Gotland Deep, Baltic Sea. Marine Geology, 183: 89-105.

Cember, R.P., 1988. On the sources, formation and circulation of Red Sea Deep Water. Journal of Geophysical Research, 93: 8175-8191.

Cruise Reports Menor 1 and Menor 2, 1984. Preussag Meerestechnik. Confidential Reports PREE-CR-03-4 and PREE-CR-05-4, Ministry of Petroleum and Mineral Resources, Deputy Ministry for Mineral Resources, Jeddah, Kingdom of Saudi Arabia.

Dean, J.M., Kemp, A.E.S., Bull, D., Pike, J., Patterson, G. and Zolitschka, B., 1999. Taking varves to bits: Scanning electron microscopy in the study of laminated sediments and varves. Journal of Paleolimnology, 22: 121-136.

Dean, J.M., Kemp, A.E.S. and Pearce, R.B., 2001. Palaeo-flux records from electron microscope studies of Holocene laminated sediments, Saanich Inlet, British Columbia. Marine Geology, 174: 139-158.

DeMaster, D.J., 1981. The supply and accumulation of silica in the marine environment. Geochimica et Cosmochimica Acta, 45(2): 1715-1732.

Edwards, F.J., 1987. Climate and Oceanography. In: A.J. Edwards and S.M. Head (Editors), Key Environments: Red Sea. Pergamon Press, Oxford, pp. 45-70.

Eshel, G., Cane, M.A. and Blumenthal, M.B., 1994. Modes of subsurface, intermediate, and deep water renewal in the Red Sea. Journal of Geophysical Research, 99(C8): 15,941-15,952.

Eshel, G. and Naik, N.H., 1997. Climatological Coastal Jet Collision, Intermediate Water Formation, and the General Circulation of the Red Sea. Journal of Physical Oceanography, 27: 1233-1257.

Fairbanks, R.G., Charles, C.D. and Wright, J.D., 1992. Origin of global Meltwater Pulses. In: R.E. Taylor, A. Long and R. Kra (Editors), Radiocarbon after four decades; an interdisciplinary perspective. Springer Verlag, New York, pp. 473-500.

Fenton, M., Geiselhart, S., Rohling, E.J. and Hemleben, C., 2000. Aplanktic zones in the Red Sea. Marine Micropaleontology, 40: 277-294.

Grimm, K.A., Lange, C.B. and Gill, A.S., 1996. Biological forcing of hemipelagic sedimentary laminae: evidence from ODP Site 893, Santa Barbara Basin, California. Journal of Sedimentary Research, 66(3): 613-324.

Halim, Y., 1969. Plankton of the Red Sea. Oceanography and marine biology: an annual review, 7: 231-275.

Hartmann, M., Scholten, J.C., Stoffers, P. and Wehner, F., 1998. Hydrographic structure of brine-filled deeps in the Red Sea - new results from the Shaban, Kebrit, Atlantis II, and Discovery Deep. Marine Geology, 144: 311-330.

Hemleben, C., Meischner, D., Zahn, R., Almogi-Labin, A., Erlenkeuser, H. and Hiller, B., 1996a. Three hundred eighty thousand year long stable isotope and faunal records from the Red Sea: Influence of global sea level change on hydrography. Paleoceanography, 11(2): 147-156.

Hemleben, C., Roether, W. and Stoffers, P., 1996b. Östliches Mittelmeer, Rotes Meer, Arabisches Meer; Cruise No. 31, 30 December 1994 - 22 March 1995, Leitstelle METEOR, Institut für Meereskunde der Universität Hamburg, Hamburg.

Hughen, K.A., Overpeck, J.T., Peterson, L.C. and Anderson, R.F., 1996. The nature of varved sedimentation in the Cariaco Basin, Venezuela, and its palaeoclimatic significance. In: A.E.S. Kemp (Editor), Palaeoclimatology and Palaeoceanography from laminated sediments. Geological Society, Special Publication, pp. 171-184.

Kemp, A.E.S., 1996. Laminated sediments as palaeo-indicators. In: A.E.S. Kemp (Editor), Palaeoclimatology and Palaeoceanography from laminated sediments. Geological Society, Special Publication.

Kemp, A.E.S., Pike, J., Pearce, R.B. and Lange, C.B., 2000. The "Fall dump"-a new perspective on the role of a "shade flora" in the annual cycle of diatom production and export flux. Deep-Sea Research II, 47: 2129-2154.

Lange, C.B., Schimmelmann, A., Yasuda, M.K. and Berger, W.H., 1996. Marine varves off southern California. In: C.B. Lange, A. Schimmelmann, M.K. Yasuda and W.H. Berger (Editors), Scripps Institution of Oceanography, Reference Series. University of California, San Diego, pp. 1-55.

Léon, J.-F. and Legrand, M., 2003. Mineral dust sources in the surroundings of the north Indian Ocean. Geophysical Research Letters, 30(6): 1309, doi:10.1029/2002GL016690.

Leventer, A., Domack, E., Barkoukis, A., McAndrews, B. and Murray, J., 2002. Laminations from the Palmer Deep: A diatom-based interpretation. Paleoceanography, 17(2): 10.1029/2001PA000624.

Lindell, D. and Post, A.F., 1995. Ultraphytoplankton succession is triggered by deep winter mixing in the Gulf of Aqaba (Eilat), Red Sea. Limnology and Oceanography, 40(6): 1130-1141.

Manheim, F.T., 1974. Red Sea geochemistry. Initial Report DSDP, 23: 975-998.

McQuoid, M.R. and Hobson, L.A., 1997. A 91-year record of seasonal and interannual variability of diatoms from laminated sediments in Saanich Inlet, British Columbia. Journal of Plankton Research, 19(1): 173-194.

McQuoid, M.R. and Hobson, L.A., 2001. A Holocene record of diatom and silicoflagellate microfossils in sediments of Saanich Inlet, ODP Leg 169S. Marine Geology, 174: 111-123.

Müller, P.J. and Schneider, R., 1993. An automated leaching method for determination of opal in sediments and particulate matter. Deep-Sea Research I, 40(3): 425-444.

Ortlieb, L., Escribano, R., Follegati, R., Zuniga, O., Kong, I., Rodriguez, L., Valdés, J., Guzman, N. and Iratchet, P., 2000. Recording of ocean-climate changes during the last 2,000 years in a hypoxic marine environment off northern Chile (23°S). Revista Chilena de Historia Natural, 73: 221-242.

Pätzold, J., Abd El-Wahab Farha, O., Abu-Ouf, M., Al Hazmi, Y.M.M., Al-Rousan, S., Arz, H.W., Bagabas, K.A.A., Bassek, D., Blaschek, H., Böke, W., Donner, B., Eder, W., Felis, T., Gayed, H.Y.K., Gutowski, M., Hemleben, C., Hübner, H., Hübscher, C., Kadi, K.A., Kästner, R., Klauke, S., Körner, S.O., Kuhlmann, H., Lützeler, T., Meier, S., Melegy, M.M., Moammar, M.O., Mohamuda, A.Z., Mokhtar, T.A., Moos, C., Omar, O.M., Rasheed, M., Rosiak, U., Salem, M., Schmidt, M., Schmitt, M., Stoffers, P., Shata, A.M., Themann, S. and Weldeab, S., 2000. Report and preliminary results of *Meteor* cruise M 44/3 Aqaba (Jordan) - Safaga (Egypt) - Dubá (Saudia Arabia) - Suez (Egypt) - Haifa (Israel). Berichte aus dem Fachbereich Geowissenschaften der Universität Bremen, 149: 135.

Pätzold, J., Moammar, M.O., Al Farawati, R., Al Hazmi, Y.M.M., Al Otibi, A., Antunes, A., Arz, H.W., Berger, J., Botz, R., Donner, B., Erhardt, A., Garbe-Schönberg, C.-D., Ghandourah, M., Hübscher, C., Kahl, G., Klann, M., Klauke, S., Klitzke, U., Legge, H.L., Lichowski, F., Schewe, F., Schmidt, M., Schmitt, M., Seeberg-Elverfeldt, I.A. and Truscheit, T., 2003. Black Sea - Mediterranean - Red Sea, Part 3, Cruise No. 52, Leg 3, March 10 - March 27, 2002, Limassol-Limassol. In: J. Pätzold, G. Bohrmann and C. Hübscher (Editors), METEOR-Berichte, Black Sea - Mediterranean - Red Sea, Cruise No. 52, January 2 - March 27, 2002. Universität Hamburg, Hamburg, pp. 62; available under http://www.marum.de/M52_-_Schwarzes_Meer_-_Mittelmeer_-_Rotes_Meer.html.

Pike, J. and Kemp, A.E.S., 1996a. Preparation and analysis techniques for studies of laminated sediments. In: A.E.S. Kemp (Editor), Palaeoclimatology and Palaeoceanography from laminated sediments. Geological Society, Special Publication, pp. 37-48.

Pike, J. and Kemp, A.E.S., 1996b. Records of seasonal flux in Holocene laminated sediments, Gulf of California. In: A.E.S. Kemp (Editor), Palaeoclimatology and Palaeoceanography from laminated sediments. Geological Society, Special Publication, pp. 157-170.

Pilskaln, C.H. and Pike, J., 2001. Formation of Holocene sedimentary laminae in the Black Sea and the role of the benthic flocculent layer. Paleoceanography, 16(1): 1-19.

Rossignol-Strick, M., 1987. Rainy periods and bottom water stagnation initiating brine accumulation and metal concentrations: 1. The late Quaternary. Paleoceanography, 2: 333-360.

Schimmelmann, A., Lange, C.B. and Berger, W.H., 1990. Climatically controlled marker layers in Santa Barbara Basin sediments and fine-scale core-to-core correlation. Limnology and Oceanography, 35(1): 165-173.

Shaikh, E.A., Roff, J.C. and Dowidar, N.M., 1986. Phytoplankton ecology and production in the Red Sea off Jiddah, Saudi Arabia. Marine Biology, 92: 405-416.

Shipboard Scientific Party, 1998. Explanatory notes. In: G. Wefer, W.H. Berger, C. Richter and et al. (Editors), Proceedings of the Ocean Drilling Program, Initial Reports. Ocean Drilling Program, College Station, TX, pp. 27-46.

Siddall, M., Rohling, E.J., Almogi-Labin, A., Hemleben, C., Meischner, D., Schmelzer, I. and Smeed, D.A., 2003. Sea-level fluctuations during the last glacial cycle. Nature, 423: 853-858.

Sirocko, F., 2003. Ups and downs in the Red Sea. Nature, 423: 813-814.

Staubwasser, M. and Sirocko, F., 2001. On the formation of laminated sediments on the continental margin off Pakistan: the effects of sediment provenance and sediment redistribution. Marine Geology, 172: 43-56.

Stoffers, P., Botz, R. and Scholten, J., 1990. Isotope Geochemistry of Primary and Secondary Carbonate Minerals in the Shaban-Deep (Red Sea). In: D. Helnig, P. Rothe, U. Förster and P. Stoffers (Editors), Sediments and Environmental Geochemistry. Springer, Berlin, pp. 83-94.

von Rad, U., Schaaf, M., Michels, K.H., Schulz, H., Berger, W.H. and Sirocko, F., 1999. A 5000-yr record of climate change in varved sediments from the oxygen minimum zone off Pakistan, northeastern Arabian Sea. Quaternary Research, 51: 39-53.

Winter, A., Almogi-Labin, A., Erez, Y., Halicz, E., Luz, B. and Reiss, Z., 1983. Salinity tolerance or marine organisms deduced from Red Sea quaternary record. Marine Geology, 53: M17-M22.

Woelk, S. and Quadfasel, D., 1996. Renewal of deep water in the Red Sea during 1982-1987. Journal of Geophysical Research - Oceans, 101(C8): 18155-18165.

3.3 Laminae type and possible mechanisms for the formation of laminated sediments in the Shaban Deep, Northern Red Sea

Ismene A. Seeberg-Elverfeldt[a], Carina B. Lange[b] and Jürgen Pätzold[a]

[a]Research Center Ocean Margins, University of Bremen, P.O. Box 330440, 28334 Bremen, Germany
[b]Departamento Oceanografía, Universidad de Concepción, Centro FONDAP-COPAS, Casilla 160-C, Concepción, Chile

Manuscript in Preparation

Abstract

Laminated sediments in the Shaban Deep, a brine-filled basin in the northern Red Sea, were analyzed with backscattered electron imagery. Here we present possible mechanisms involved in the formation of laminae of various types and homogenous intervals arising from the detailed investigation of multicore GeoB 7805-1 (26°13.9'N, 35°22.6'E; water depth 1447 m) and gravity core GeoB 5836-2 (26°12.61'N, 35°21.56'E; water depth 1475 m). Sediment structure includes six types: a) a laminated structure with alternating light (mainly coccoliths) and dark (diatom frustules) layers, where the diatom component is indicative of the intra-annual variability between stratification and mixing events; b) a pocket-like structure attributed to the sinking of particles within fecal pellets and aggregates; c) a matrix of tightly packed diatoms that relates to extended stratification/mixing periods of the water column; d) homogenous intervals that result from turbidity deposition; e) silt accumulations which origin may lie in agglutinated foraminifers; and f) pyrite layers with pyrite formation possibly initiated at the seawater-brine interface

***Keywords**: laminated sediments; diatoms; Red Sea; Shaban Deep; brine;*

Introduction

Our research has focused on using laminated sediments of the Shaban Deep (a brine-filled deep in the northern Red Sea) as recorders of abrupt changes in productivity and circulation. Previous work by our team has dealt with the detailed composition of mid-Holocene to Last Glacial Maximum (LGM) laminated sediments from the southern basin of the Shaban Deep (core GeoB 5836-2; 26°12.61'N, 35°21.56'E; 1475 m water depth) (Seeberg-Elverfeldt et al., accepted). We showed that sediments encompassing the period 4-15 ka have a light and dark alternating pattern where light layers are mainly composed of coccoliths, terrigenous material of eolian origin and diatom fragments, and dark layers consist of almost exclusively diatom frustules (monospecific or mixed assemblage). It was further proposed that different diatom assemblages reflect changing conditions in stratification/mixing in the northern Red Sea (Seeberg-Elverfeldt et al., accepted). This was discussed against the background of already existing paleoceanographic data from an oxic core from the northernmost Red Sea (GeoB 5844-2; 27°42.81'N; 34°40.90'E; 963 m water depth) (Arz et al., 2003). It was concluded that brine sediments from the Shaban Deep can be used for reconstructing paleoceanographic and paleoclimatic changes in the region at high resolution.

One of our goals has also been the understanding of the effects of preservation in the sediments of the northern Red Sea in order to assess the accuracy with which the sedimentary record reproduces the original living assemblage. For that, we also studied microplankton assemblages (mainly diatoms) from plankton tows and surface sediments along a N-S transect in the northern Red Sea between 28° and 21°N (Seeberg-Elverfeldt et al., 2004), with special attention on the comparison between two different types of sediment: oxic, non-brine sediments and anoxic, brine sediments from the Shaban Deep. We showed that the preservation of biogenic opal and siliceous microplankton assemblages is by far better than in non-brine sediments (Seeberg-Elverfeldt et al., 2004).

Based on our former detailed studies, schematic models of paleoflux scenarios for laminae formation at different time-slices were proposed. In this study, we extend the previous records into the late Holocene and move one step further in our understanding of laminae formation. We summarize the different types of sediment structure preserved in Shaban Deep sediments of late Holocene through LGM age, and deliver possible mechanisms involved in their genesis.

Study area

As it is known from the literature, the Red Sea is a very unique environment. There are no permanent river inflows, rainfall is sparse and evaporation largely exceeds precipitation. The seawater exchange with the Arabian Sea in the south is limited due to the very shallow sill (137 m) of the Strait of Bab el Mandab (e.g. Edwards, 1987). The circulation is mostly driven by thermohaline forcing while wind forcing is only of minor importance. A description of the anti-estuarine circulation pattern of the Red Sea can be found in Eshel et al. (1994) and Eshel and Naik (1997).

The Red Sea plankton is characterized by the dominance of autotrophic picoplankton while larger cells are scarce in this region (Shaikh et al., 1986; Lindell and Post, 1995). Four different groups of phytoplankton are important in the annual cycle of the Red Sea (Shaikh et al., 1986): diatoms are present most of the year and are the predominant group in winter; blue-green algae (*Trichodesmium* spp.) and nanoplankton dominate in late spring and summer, and dinoflagellates in the fall. The diatom winter peak (December-February) is clearly dominated by *Bacteriastrum*, *Chaetoceros*, *Nitzschia* and *Rhizosolenia* (Shaikh et al., 1986). While the plankton is dominated by fragile forms (e.g. *Nitzschia bicapitata* group) surface sediments of oxic settings are enriched in robust taxa (e.g. *Alveus marinus*, *Azpeitia neocrenulata*, *A. nodulifera* and *Roperia tesselata*), and only anoxic brine sediments preserve the fragile diatoms to some extend (up to 26% of the assemblage; Seeberg-Elverfeldt et al. 2004).

The Shaban Deep

About 25 brine-filled deeps are found along the central axis of the Red Sea. The Shaban Deep (formerly named Jean Charcot Deep, Pautot et al., 1984) is one of these axial depressions in the northern Red Sea. It consists of four small basins (southern, eastern, northern and western; Fig. 1) that are separated by two ridges running N-S and W-E, respectively (Pautot et al., 1984; Hartmann et al., 1998). The basins have the seawater-brine interface at nearly the same water depth (~1325 m; Hartmann et al., 1998) and a salinity of about 260 psu. The high salinities are due to leaching of sub-bottom Miocene evaporites (Manheim, 1974). The top of Miocene evaporites (so called S-reflector) crops out within the brine basin at the modern level of the seawater-brine interface (Pautot et al., 1984; Pätzold et al., 2003). The temperature within the brine is only slightly higher (~ 3°C) than the surrounding seawater (Hartmann et al., 1998). There is only minimal exchange (diffusion and convection) at the seawater-brine interface (Hartmann et al., 1998). The brine body itself has a thickness of up to 200 m, is almost depleted in dissolved oxygen (< 0.3 mg L^{-1}), and sulphide is absent (Hartmann et al.,

1998); its density is ~1.2 gr cm^{-3} (Millero et al., 1982). Methane concentrations increase sharply at the seawater-brine interface and are several orders of magnitude higher within the brine that in the overlying seawater (Faber et al., 1998). No evidence for benthic life has been found, although a rich prokaryotic community has been described to thrive at the seawater-brine interface (Eder et al., 2002; Antunes et al., 2003). The Shaban Deep has been described as being hydrothermally active (e.g. Pautot et al., 1984), and Stoffers et al. (1990) found diagenetically-formed dolomite and rhodochrosite within organic rich layers in the sediments.

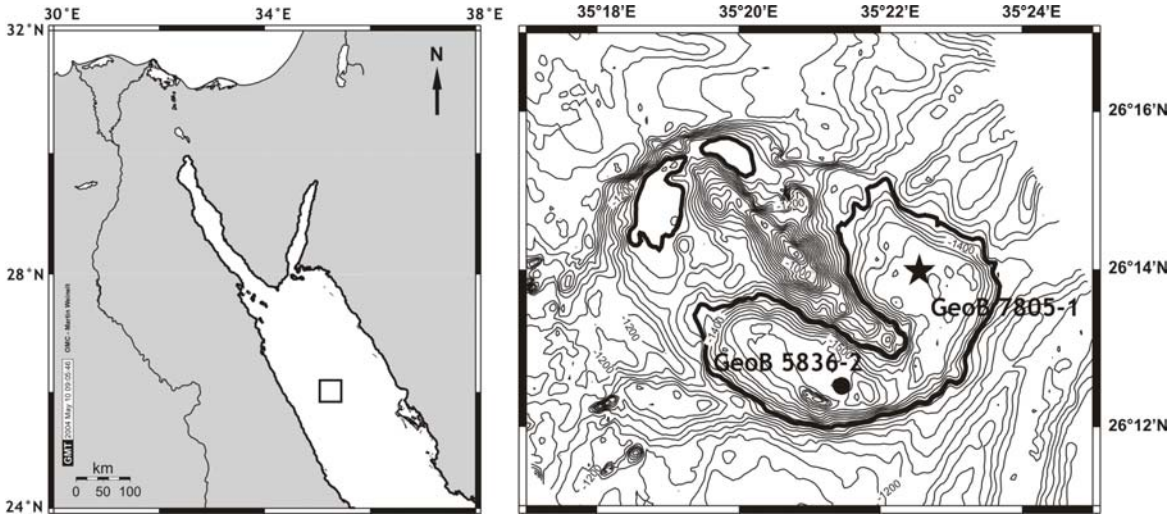

Fig. 1: Location of the Shaban Deep in the northern Red Sea (square, left panel) and of coring sites GeoB 7805-1 (asterisk) in the eastern basin and GeoB 5836-2 (filled circle) in the southern basin (right panel). Dark contour line on the right-hand panel indicates the depth of the modern brine surface.

Material and Methods

Two cores from the Shaban Deep were used in this study (Fig. 1): Gravity core GeoB 5836-2 was retrieved from the southern basin (26°12.61'N, 35°21.56'E; 1475 m water depth ; total length of core = 790 cm) during *RV Meteor* cruise M 44/3 in 1999 (Pätzold et al., 2000). This core was used in previous investigations (Seeberg-Elverfeldt et al., accepted), and results are re-analyzed here. Multicore GeoB 7805-1 from the eastern basin of the Shaban Deep (26°13.9'N and 35°22.6'E; 1447 m water depth; total length of core = 60 cm) was collected during *RV Meteor* cruise M 52/3 in 2002 (Pätzold et al., 2003). Because of its high water content and soupy texture, the multicore was left in cold storage (4°C) for ~ 12 months. After this period, it had compacted down to 48 cm in length.

Both cores were logged with a Multi Sensor-Core-Logger (MSCL) with 3 Linescan CCD's Digital Imaging for determination of the color scale (Fig. 2). In addition, Fe was measured every 0.2 cm with an X-ray fluorescence (XRF) scanner on multicore GeoB 7805-1 (Fig. 3).

A general overview of sediment composition and texture was gained through smear slide analysis which followed standard ODP procedures.

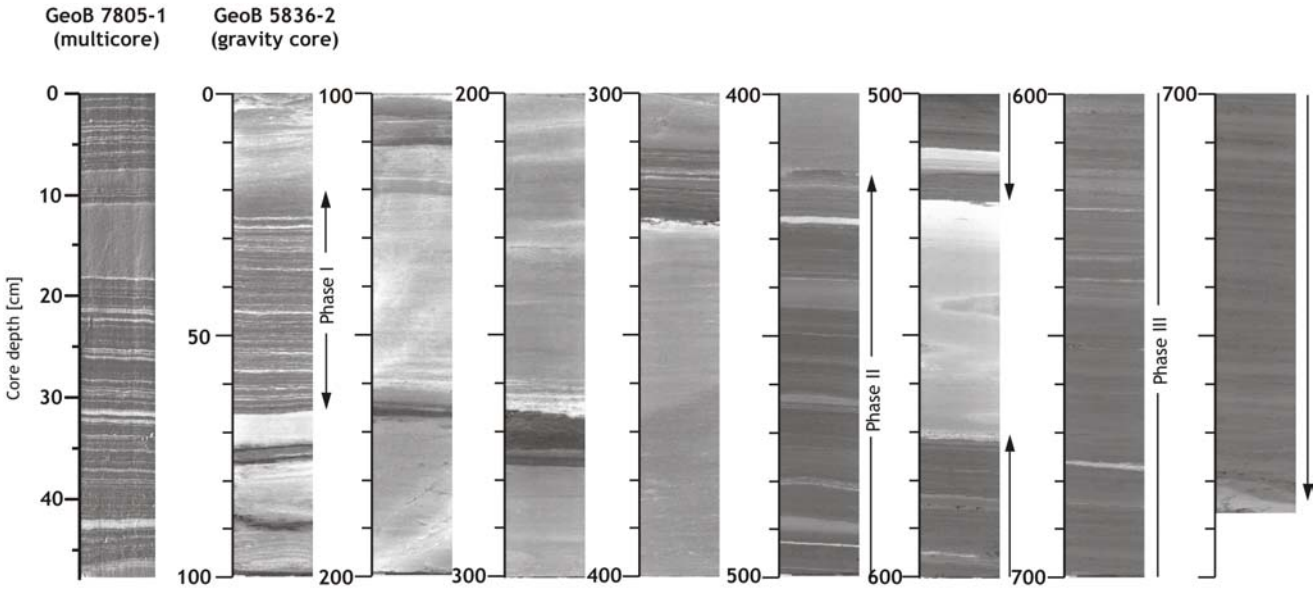

Fig. 2: General lithology of multicore GeoB 7805-1 (core photograph; 48 cm long) and gravity core GeoB 5836-2 (videologger data; 790 cm long) showing the distribution of laminated and non-laminated sediments. Phases I (4-6 ka), II (14-22 ka) and III (older than ~ 34 ka) are indicated. Multicore GeoB 7805-1 encompasses the late Holocene.

The working halves of both cores were first sampled with "cookie cutters" of 15 cm (L) x 1 cm (W) x 5 cm (D) following the method described by Schimmelmann et al. (1990) and Dean et al. (1999). X-radiographs of slabs were taken to record differences in sediment density and structure. In this study, the X-radiograph negatives were scanned to establish a direct relationship with the thin sections that are described below. In the scanned negatives, light bands represent layers of very dense material and dark bands indicate layers of lower density.

Polished thin sections of resin-embedded sediment for gravity core GeoB 5836-2 were prepared from the cookie cutter slabs at the Cardiff University, Wales, following the methodology of Pike and Kemp (1996a) with one small modification: the samples were first soaked in deionized water to remove the salt before they were embedded. Details can be found in Seeberg-Elverfeldt et al. (accepted).

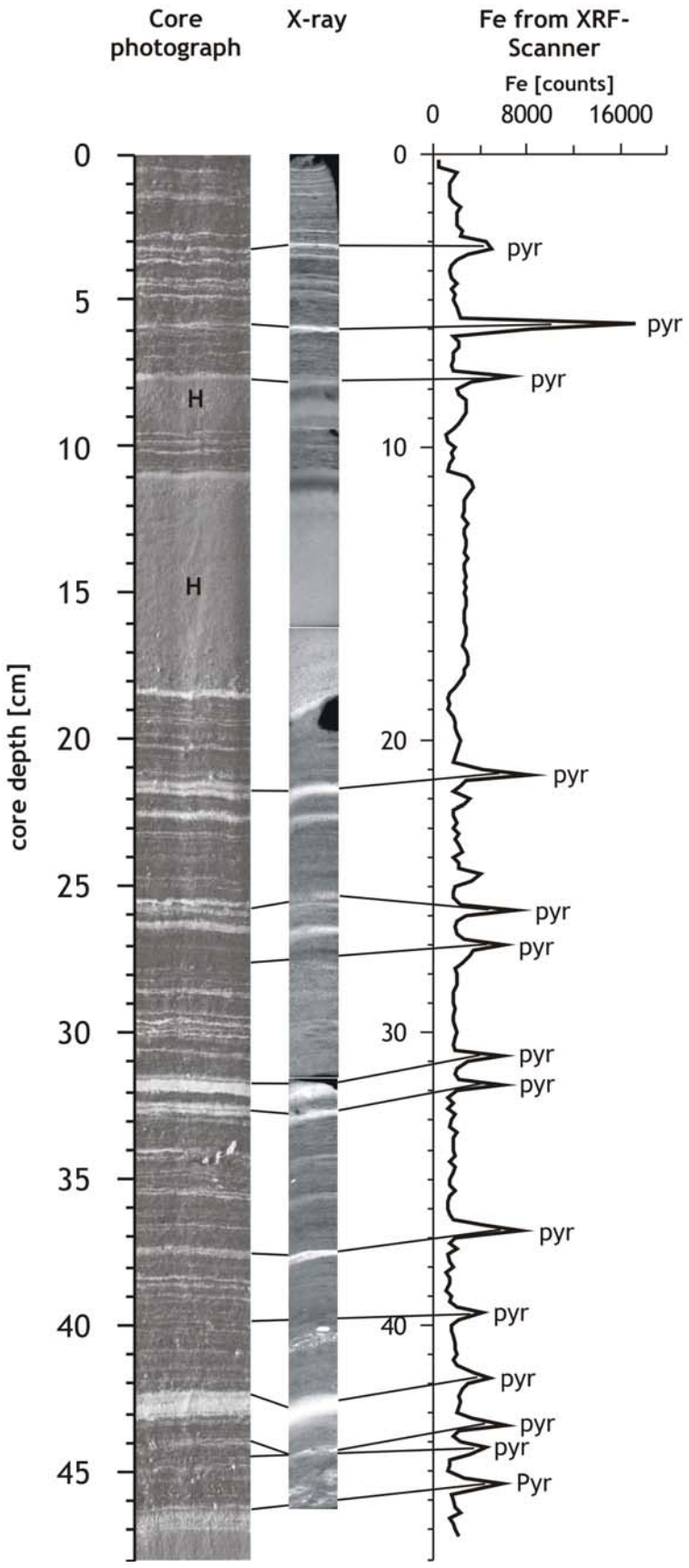

Fig. 3: Correlation between general lithology (left), X-radiography (middle) and Fe-intensities (right) measured by XRF-scanner on multicore GeoB 7805-1. Pyrite layers (**pyr**) are located within prominent white layers (left); they are light in X-radiography (middle) and coincide with high Fe-intensities (right). H = homogenous intervals within the late Holocene.

Polished thin sections of resin-embedded sediments from multicore GeoB 7805-1 were prepared at the GeoForschungsZentrum Potsdam, Germany (Köhler and Berger, pers. comm.). There, 7 cm long samples were taken with a 3 cm overlap to the adjacent samples, shock-frozen with liquid nitrogen and freeze-dried for 48 hours. Afterward these sediment blocks were embedded stepwise under vacuum in Araldit 2020, a two-component epoxy resin.

All polished thin sections were carbon coated and studied using scanning electron microscopy (SEM). A Leo (Cambridge Instruments) S360 SEM with an Oxford Instruments INCA Wave elemental analysis system was used at Cardiff University and a Philips XL 30 ESEM was used at the Alfred-Wegener-Institute for Polar and Marine Research in Bremerhaven, Germany, both equipped with a backscatter detector. BSEI (backscattered electron imagery) mosaics were produced for every thin section. These photomosaics may be considered as porosity maps where porous diatomaceous sediment appears darker while terrigenous and calcareous sediment is less porous and therefore brighter. After first producing low magnification (30X for GeoB 5836-2 and 80X for GeoB 7805-1) BSEI photomosaics that act as basemaps of each sample, high resolution pictures at higher magnifications (up to 3500X) were taken to study the composition of individual lamina in detail and to identify the species present.

Results

General characteristics of Shaban Deep sediments

Brine sediments from the Shaban Deep are "diatom-bearing nannofossil ooze, partly laminated, olive-gray to black, with varying contents of carbonate, opal, and terrigenous material, and with a very high content of hypersaline pore water" (Pätzold et al., 2000). Smear slide analysis reveal that sediments of both cores mainly consist of varying contents of coccoliths (sometimes coccospheres), diatoms, and terrigenous material. Foraminifers, pteropods, silicoflagellates and radiolarians are also present. Dominant coccolith species are *Emiliania huxleyi, Gephyrocapsa oceanica* and *Aligosphaera robusta*, while *Umbilicosphaera sibogae*, *Helicosphaera sellii* (?), *Calcidiscus leptoporus* and *Florisphaera profunda* are also present. The genus *Amaurolithus* is spread throughout the sediments, always sparse. The diatom assemblage is dominated by the genera *Azpeitia*, *Bacteriastrum*, *Chaetoceros*, *Coscinodiscus*, *Nitzschia, Rhizosolenia* and *Thalassionema*.

Analyzed sediments of gravity core GeoB 5836-2 cover the time interval between 4 and 22 ka (Seeberg-Elverfeldt et al., accepted) while multicore GeoB 7805-1 encompasses the last ~2000 years (Seeberg-Elverfeldt et al. in prep.).

Multicore GeoB 7805-1 is laminated with two prominent homogenous intervals between 7.6-9.5 cm and 10.9–18.4 cm (Fig. 3). Both homogenous intervals are bound at the top by a distinct bright layer and a slightly darker interval directly beneath it; the rest of each homogenous interval is lighter (greyish) than the laminated intervals in the core. Several prominent, very bright white layers of variable thickness are observed at 18.4-18.7 cm, 21.7-22.1 cm, 22.7-22.9 cm, 26.5-26.7 cm, 31.7-32.3 cm, 32.7-33 cm and 42.2-43 cm. Some of them contain a blue/black layer which is located directly in the middle of the white layer or shifted towards the top. These blue/black layers show up white in the X-radiographs and correspond well with Fe-intensities measured with XRF (Fig. 3). It was previously established (Seeberg-Elverfeldt et al., accepted) that these layers (dark within the sediment and light in X-radiograph and BSEI) are composed of coccoliths and framboidal pyrite. In addition, there are several yellowish layers present. The core ends with another homogenous interval starting at 46.2 cm. This one also carries a bright layer at the top and a pyrite layer directly beneath it.

Core GeoB 5836-2 has three main laminated sections: 1) Phase I, from 21 to 65 cm, representing 4-6 ka; 2) Phase II, from 417-525 cm, representing 13-22 ka; and 3) Phase III, from 572 to 785 cm, encompassing sediments older than ~34 ka. In addition, two small laminated intervals are present in the early Holocene (at 260-267 cm and 312.5-327.5 cm). The laminated sections are separated by homogenous intervals of variable length. Moreover, several smaller homogenous layers are found within laminated Phase II (13 and 22 ka) (Fig. 2). In general, laminations are clearly visible in the mid-Holocene while they are fainter in Phases II and III (Fig. 2).

Pyrite layers are observed throughout the cores and their occurrence is more frequent in younger sediments. Also, some layers of Ca-rhodochrosite are seen in Lower Phase II sediments (18-19 ka) (Seeberg-Elverfeldt et al., accepted).

Detailed Composition of Shaban Deep sediments

Biogenic components

Dark and light layers/ pocket structure/matrix

Thin section analysis revealed that the laminated (faint-prominent) sediments of the Shaban Deep present three basic structures: a) alternating light and dark continuous layers (Fig. 4); b) a pocket-like structure where dark, discontinuous “layers” are embedded within the light material (Fig. 5); and c) a matrix of tightly packed diatoms (Seeberg-Elverfeldt et al., accepted). The first two types are found in sediments younger than 15 ka while the matrix type is characteristic of sediments dated 18-22 ka.

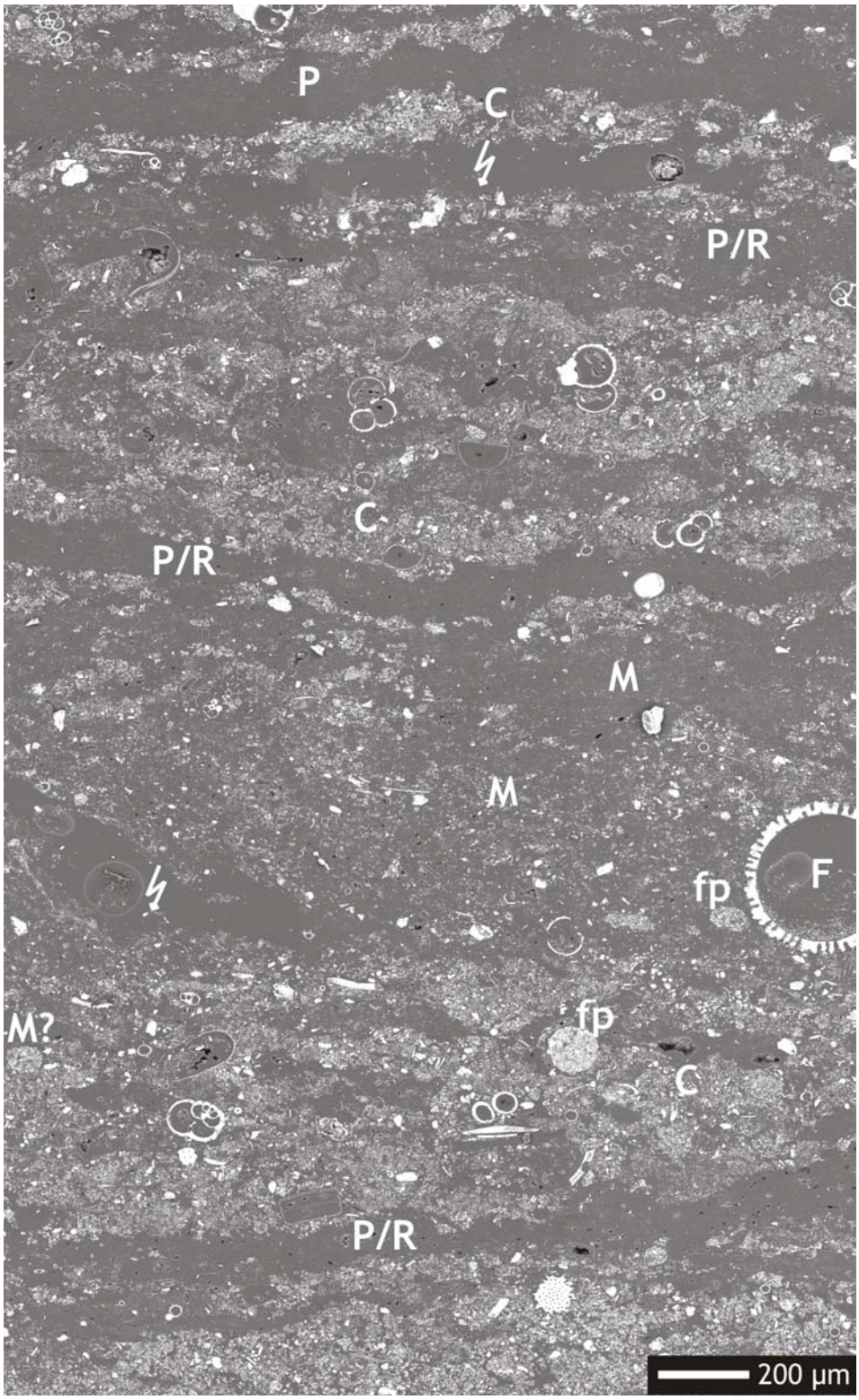

Fig. 4: BSEI photomosaic of thin section at 23.5 cm in multicore GeoB 7805-1. Alternating dark/light layers are shown which consist of *Proboscia*/*Rhizosolenia* (**P**/**R**), coccoliths, terrigenous material and diatom fragments (**C**). Note that P/R layers are continuous while "layers" with a mixed assemblage (**M**) are not. Fecal pellets (**fp**) and foraminifers (**F**) are present as well. White arrows indicate cracks.

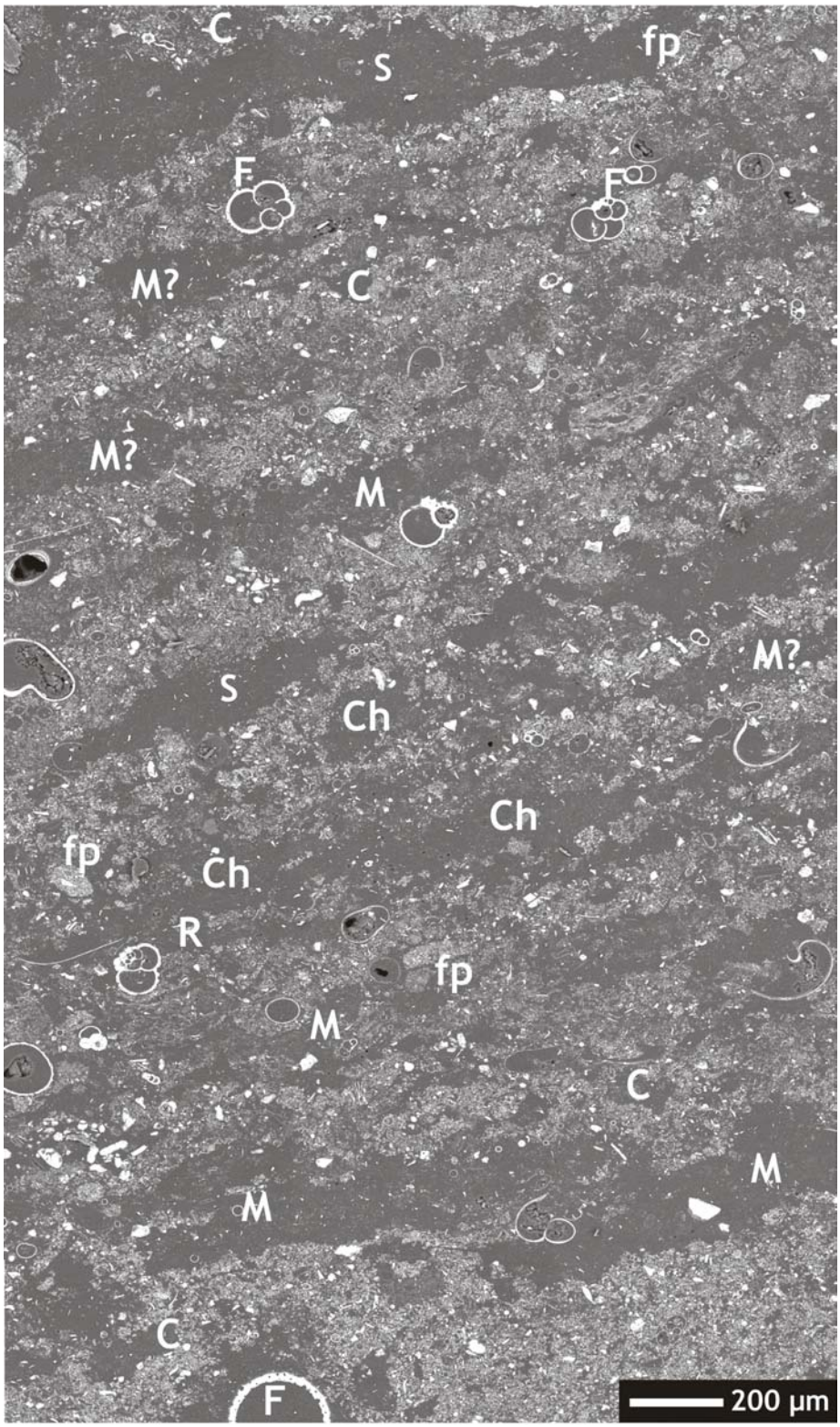

Fig. 5: BSEI photomosaic of thin section at 43.5 cm in multicore GeoB 7805-1, demonstrating pocket-like structure of the sediment. Dark pockets with a mixed assemblage (**M**), *Chaetoceros* vegetative cells (**Ch**) or setae (**S**) can be easily distinguished and are embedded within a light background (**C**) composed of coccoliths, terrigenous material and diatom fragments. Fecal pellets (**fp**), foraminifers (**F**) and one small cluster of Rhizosolenia (**R**) are also observed.

Large foraminifers, pteropods and radiolaria are embedded in late and mid-Holocene sediments disturbing the lamina fabric. Foraminifers decrease in number and size downcore and are absent from the matrix type sediments of 18 ka to LGM age.

a) Type alternating light and dark continuous layers (Fig. 4*)*

Light layers are comprised of coccoliths (sometimes coccospheres), terrigenous particles and diatom fragments (Fig. 6A). Dark layers on the other hand are comprised of either *Proboscia*/*Rhizosolenia* mats (Fig. 6B), aggregates of vegetative cells and setae from different species of *Chaetoceros* and *Bacteriastrum,* or a mixed *Chaetoceros/Nitzschia/Thalassiosira* assemblage (Fig. 6C) (Seeberg-Elverfeldt et al., accepted).

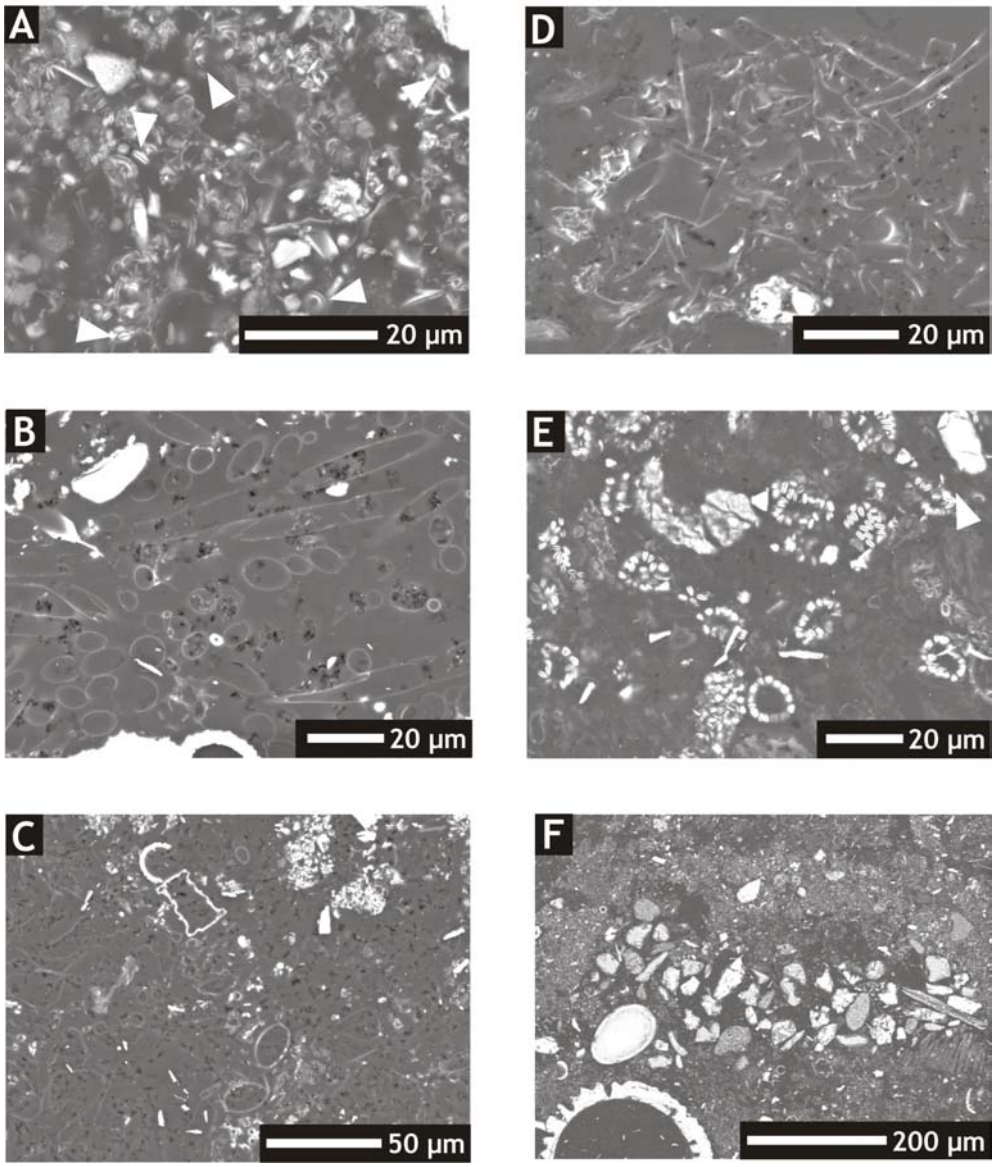

Fig. 6: BSEI photographs of selected laminae of multicore GeoB 7805-1 (A-E) and gravity core GeoB 5836-2 (F) showing examples of: A. Coccoliths (arrowheads), terrigenous particles and diatom fragments within a light layer. B. *Proboscia*, dark layer. C. Example of mixed assemblage. D. Chitinous remains of copepods. Small arrowhead points to antennae (or leg). E. Coccospheres of *Aligosphaera robusta* within a "gray" pocket. F. Silt accumulation.

*b) Type pocket-like structure (*Fig. 5*)*

Dark pockets are intermingled within the light material. These pockets contain either a mixed diatom assemblage or an assemblage that is clearly dominated by *Chaetoceros*. The species that define the mixed assemblage are mostly delicate forms and are often hard to distinguish within the BSEI photomosaic (Fig. 6C).

Some dark pockets, especially within sediments from the late Holocene, are filled with material of unknown origin. At least in two cases that could be properly photographed, structures that resembled copepod remains could be recognized. Figure 6D shows this kind of material where part of a leg or maybe an antenna is observed. We therefore define these structures as chitinous copepod remains.

In addition to the diatom-dominated dark pockets or layers mentioned above there are others which appear light gray in the BSEI photomosaics; they are filled with well preserved coccospheres and coccolith plates as well as some diatoms (Fig. 6E).

c) Type matrix

Sediments are characterized by a matrix of tightly packed *Rhizosolenia* frustules (18-19 ka) or by a matrix dominated by resting spores of *Chaetoceros* (LGM) within which thick non-continuous layers of large centric diatoms (*Coscinodiscus*, *Azpeitia*, *Stellarima* and *Thalassiosira*) and/or light pockets of coccoliths, terrigenous material and diatom fragments are embedded (Seeberg-Elverfeldt et al., accepted).

Fecal pellets

Light layers or pockets (coccolith/terrigenous) of all time intervals carry various amounts of fecal pellets ("fp" in Figs 4 and 5). They are most abundant within late Holocene sediments where they sometimes appear in clusters (Fig. 7A); their number decreases sharply within Lower Phase II and LGM sediments. Two morphological types of fecal pellets can be distinguished: elliptical and small spheroids (Fig. 7A, B). Elliptical pellets are the most common type; they vary from circular/oval to elongate in cross section. They are mainly composed of coccolith plates, diatom fragments and small amounts of terrigenous particles (Fig. 7C).

We observed elliptical pellets in different stages of disintegration; while their shape and outline is clearly defined within younger sediments (Fig. 7D) they become quite diffuse in the older sections (Fig. 7E). Finally, when their structure breaks apart, they seem to blend into the light background (Fig. 7F).

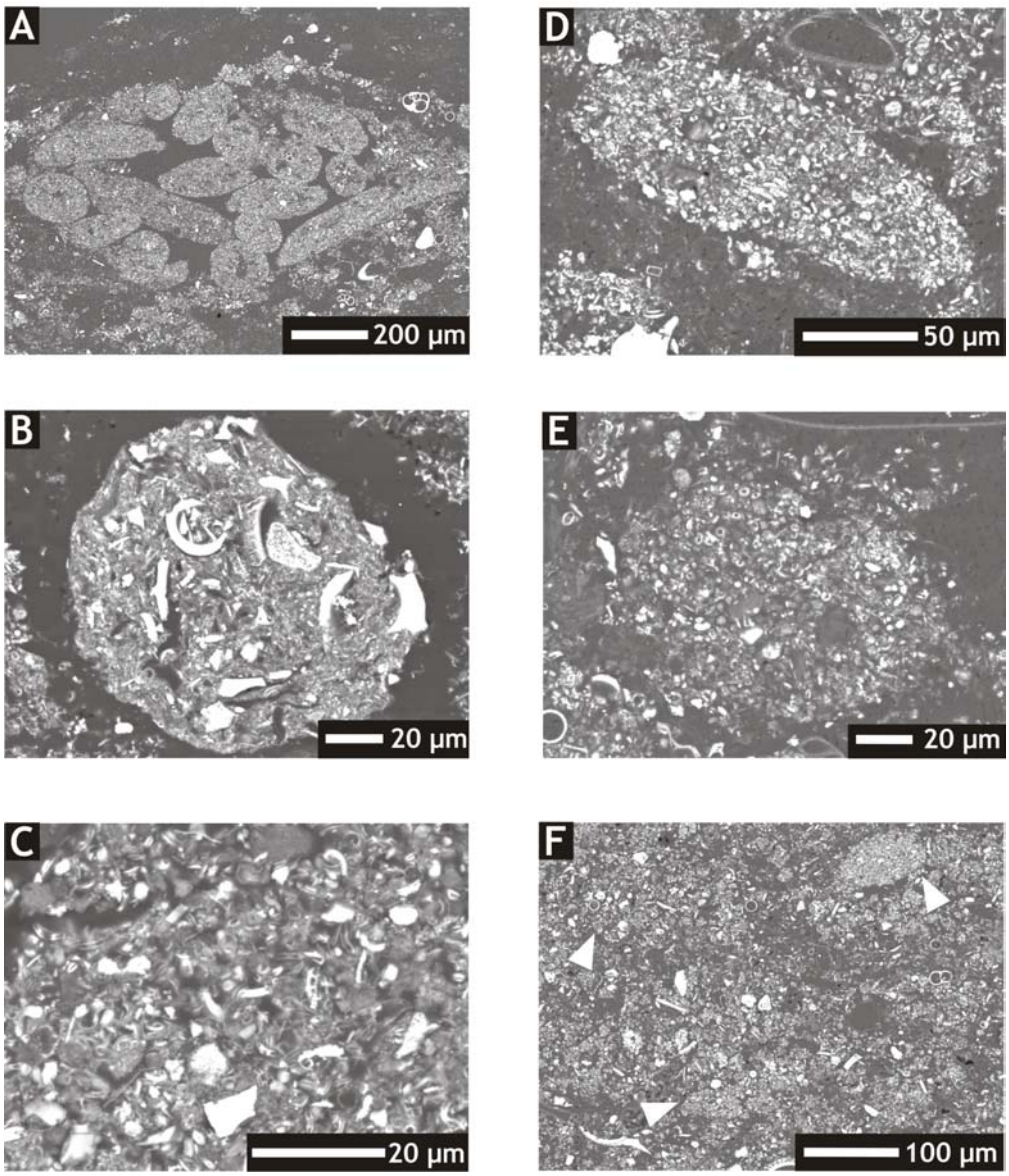

Fig. 7: BSEI photographs of fecal pellet types and composition in multicore GeoB 7805-1. A. Cluster of elliptical fecal pellets. B. Densely packed spheroid fecal pellet, composed of coccoliths, terrigenous particles and diatom fragments, as well as some material of unknown origin. C. Detail of composition of elliptical pellet (coccoliths, terrigenous material and diatom fragments). D-F. Sequence of disintegration of fecal pellets proposed as the mechanism to generate light layers. D. Intact elliptical fecal pellet. E. Disintegrating pellet. F. Resulting light layer where the original shape of fecal pellet can still be recognized (arrowheads).

The second type of pellet (spherical) contains more densely packed material. Again coccoliths and diatom fragments can be found within these pellets but also some material of unknown origin (Fig. 7B). Spheroids occur individually in all time intervals but most frequently in younger sediments.

Although we are not able to assign an origin to the pellets (they could have been produced by copepods and Appendicularia (Humberto Gonzalez, pers. comm.)), the fact that copepod remains were found within our sediments supports our hypothesis of their pelagic origin.

Homogenous intervals

As stated above, several homogenous intervals are present within laminated sections (Fig. 2). In general, we distinguish two types of homogenous intervals. One type contains a mixture of coccoliths, terrigenous material, large centric diatoms and small foraminifers without sorting. The other type shows a gradation from coarser material at the bottom to finer grains at the top. One such example from the late Holocene is given in Fig. 8. Here, we observe that large particles (foraminifers and pteropods) concentrate at the bottom of the homogenous interval. This is followed by a mixture of coccoliths, diatoms, terrigenous material and small foraminifers which occupies the largest part of the homogenous section. Above the mixed interval many large centric diatoms (e.g. *Coscinodiscus* spp.), coccoliths and terrigenous material occur; this has a darker appearance in the BSEI photomosaics. The homogenous interval ends with very fine grained material that consists of almost exclusively coccolith plates. This represents the distinct bright top boundary of the homogenous interval.

Abiogenic components

Silt accumulations

A type of particle accumulation that is also present throughout the analyzed cores consists of clusters of larger silt grains, without developing the character of a lamina. Boundaries of these types are seldom sharp but they are easily distinguishable from the background material (Fig. 6F). These accumulations are composed of either a wide range of particle sizes (unsorted) or all the particles belong more or less to the same size fraction (sorted).

Pyrite layers

Episodic, up to 1 mm thick pyrite layers are present at all times except in the LGM. They are most frequent in younger sediments. Thin section analysis confirms the association of pyrite with BSEI light layers (Seeberg-Elverfeldt et al., accepted). Pyrite grains can be positioned in the middle of a light layer or shifted towards the top of it (as in Holocene and Upper Phase II (13-15 ka) sediments), or they can be distributed randomly over the whole light material (as in Lower Phase II (18-19 ka) sediments). The amount and size of framboidal pyrite grains varies within these layers.

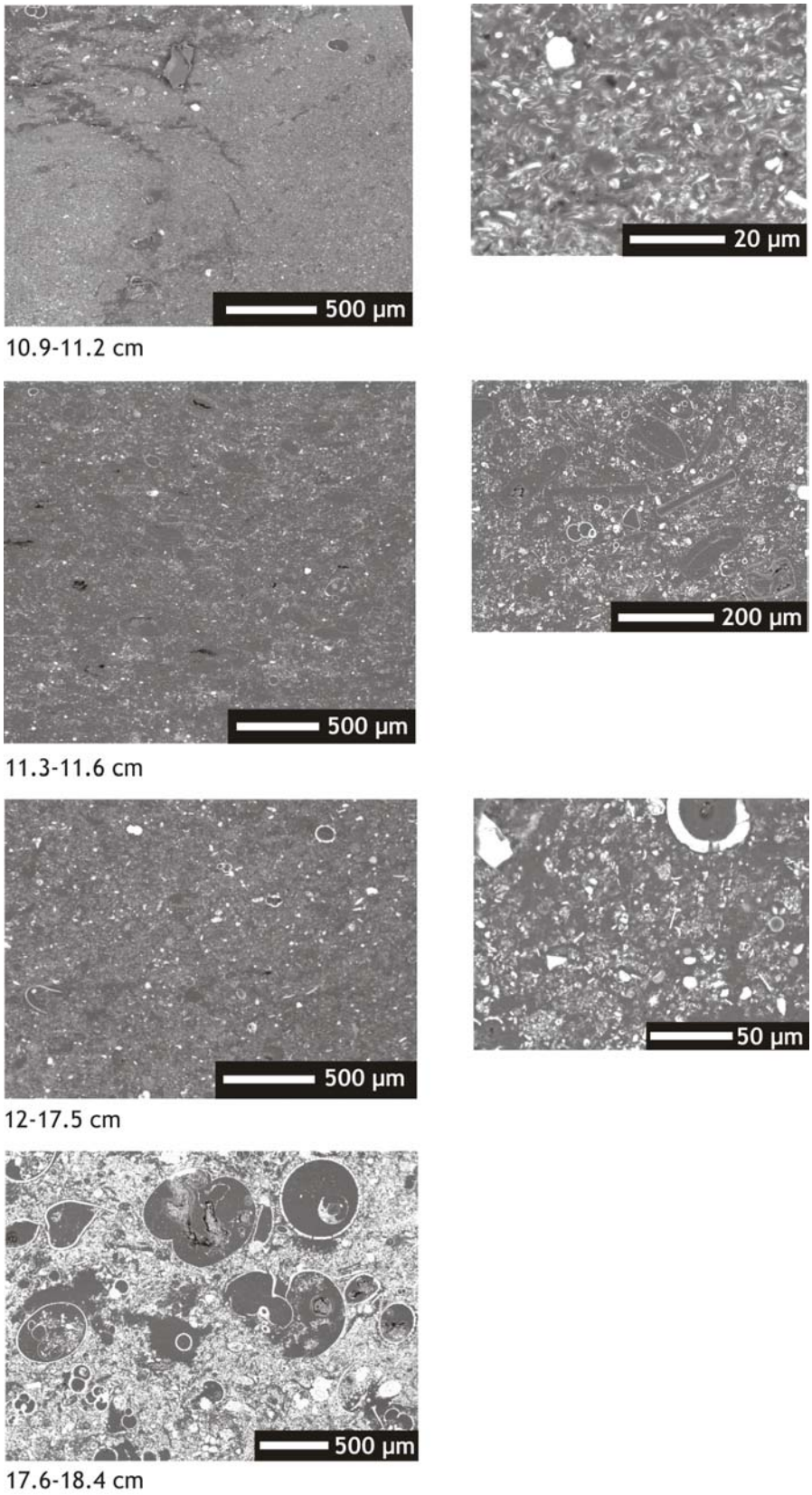

Fig. 8: BSEI photographs of homogenous interval in the late Holocene (10.9-18.4 cm, multicore GeoB 7805-1). Left-hand panel shows the four different sequences discussed in the text (from bottom to top): coarse material (large foraminifers and pteropods) at the bottom, a mixture of coccoliths, diatoms, terrigenous material and small foraminifers on top of it, followed by a darker layer enriched in large centric diatoms. A pure coccolith layer bounds the homogenous interval at the top. High magnification photographs revealing detailed composition of the coccolith, diatom and mixed sequences are given on right-hand panel.

Discussion

In our previous study (Seeberg-Elverfeldt et al., accepted) we were able to develop annual sedimentation models for Shaban Deep sediments of age 4-15 ka. We proposed that for the past ~15,000 years, the laminations represent two-season annual varves with light, coccolith-rich layers representing the summer flux and dark diatomaceous layers corresponding to late fall and winter production . Furthermore, it was suggested that *Rhizosolenia*-dominated layers are related to stratification of the water column while *Chaetoceros*-dominated layers account for mixing events. The frequency with which the pattern coccolith/*Rhizosolenia* couplets would be replaced by coccolith/*Chaetoceros* couplets was further used as indicative of the variability between stratification and mixing events (Seeberg-Elverfeldt et al., accepted). The new results for the late Holocene included here also suggest that an annual signal is being preserved, and point to prevailing mixed conditions during this time. The dominant pattern in the late Holocene is that of dark pockets with a mixed diatom assemblage or a *Chaetoceros*-dominated assemblage being interrupted by short periods of stratification (*Proboscia*/*Rhizosolenia* layers).

For older sediments, where the carbonate signal is missing, we were not able to introduce an annual sedimentation model (Seeberg-Elverfeldt et al., accepted).

Possible mechanisms for the formation of biogenic laminae

Below we present possible mechanisms involved in the formation of laminae of various types and homogenous intervals in Shaban Deep sediments (Figs. 9, 10). Our rationale behind the suggested scenarios includes several assumptions regarding transport processes through the water column and interpretation of the lamina fabric under BSEI: 1) particulate matter sinks relatively fast through the water column as fecal pellets, aggregates and/or diatom mats; 2) particulate matter then concentrates at the seawater-brine interface due to the density gradi ent – until they are dense enough to break the interface - before sinking through the brine; 3) all particles that have accumulated at this interface might be subject to bacterial decomposition; 4) sorting may occur during accumulation at the seawater-brine interface and during transport to the seafloor; 5) BSEI light layers are generated by the disintegration of fecal pellets carrying mainly coccoliths (and sometimes coccospheres); and 6) the paleoflux scenarios presented earlier (Seeberg-Elverfeldt et al., accepted) are correct.

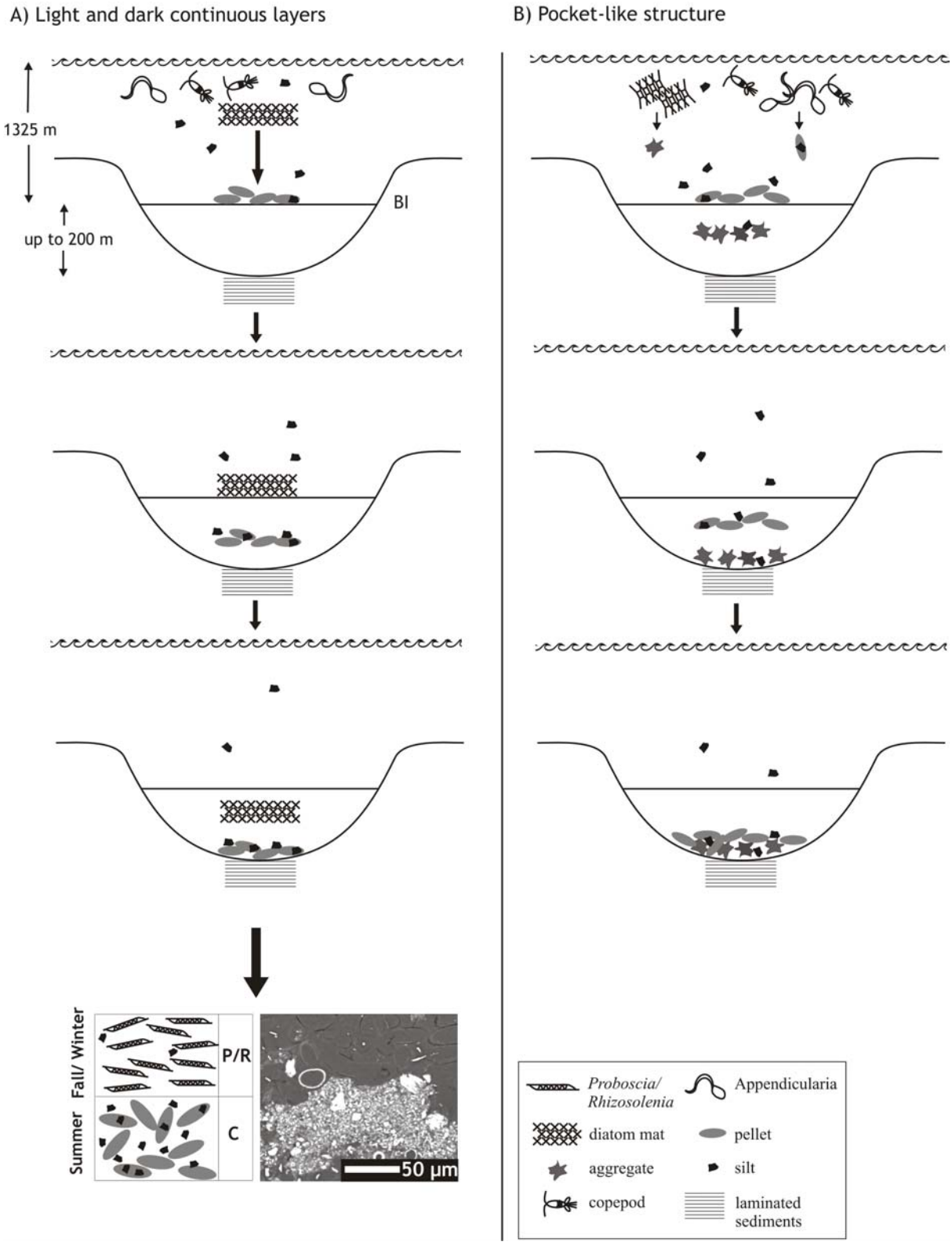

Fig. 9: Schematic diagrams of the proposed mechanism involved in the formation of light and dark continuous layers of coccolith/*Rhizosolenia* (*Proboscia*) couplets (A), and pocket-like structure (B) in laminated sediments of the Shaban Deep, northern Red Sea. See text for details. Specifications on water column depth, brine thickness and seawater-brine interface (BI) are given in the first diagram only but also apply to Fig. 10.

Our first type of sediment fabric, dark *Rhizosolenia* or *Proboscia* laminae coupled with light coccolith-rich ones, are found within the Holocene and the Upper Phase II sediments. The species in the diatomaceous lamina have been associated with mat development in a stratified water column and deposition during winter mixing (shade flora and fall dump of Kemp et al., 2000) while the calcareous type of lamina has been referred to as representing the summer flux of coccolithophorid blooms (Seeberg-Elverfeldt et al., accepted).

Several steps are involved in the mechanism in reaching the **alternating light and dark continuous lamina structure** (Fig. 9A) of the sediments. We suggest that first, the summer bloom of coccolithophorids is consumed by copepods and/or Appendicularia that produce fecal pellets. These sink through the water column at speeds of 27-160 m d^{-1} (Yoon et al., 2001) and accumulate at the seawater-brine interface until they become heavy enough to sink through it. Secondly, *Proboscia*/*Rhizosolenia* mats that have developed during the late fall, descend through the water column in winter when stratification breaks down. Mats sink fast (1-4 m h^{-1}; Tracy Villareal, pers. comm.) until they reach the seawater-brine interface and accumulate there until they are able to break the interface. When mats are deposited on top of the fecal pellets lying on the basin-floor, the annually laminated sediments within the Shaban Deep are generated.

Our second sediment fabric is the **pocket-like structure** found mainly within late Holocene sediments, resulting from the deposition of diatomaceous aggregates and coccolith-rich fecal pellets. As it was stated before, these pockets contain a mixed diatom assemblage that is mainly associated with species of *Chaetoceros*. This genus is known for polysaccharide exudation and aggregation into transparent exopolymer particles (TEPs) (Alldredge et al., 1993). Flocs of *Chaetoceros* sink through the water column with speeds of 50-200 m d^{-1} (two orders of magnitude faster than unaggregated *Chaetoceros* cells) (Alldredge and Gotschalk, 1989).

The basic mechanisms involving sinking and deposition explained above can also be applied for the formation of the pocket-like structure (Fig. 9B) with *Chaetoceros*-aggregates (that also include other diatom species) representing the winter production and fecal pellets the consumption of the summer bloom of coccolithophorids. Since the deposited material is a mixture of different transporting agents, no clear continuous laminae can develop. However, we suggest that over time, this pocket-like structure gets compacted to generate the coccolith/*Chaetoceros* laminae observed in Upper Phase II (13-15 ka) sediments.

The third type of structure, a **matrix** of tightly packed diatom frustules characteristic of sediments of age 18 ka – LGM, relies on the same overall mechanisms described above but due to the lack of the coccolith carbonate component an annual signal could not be defined

(Seeberg-Elverfeldt et al., accepted). It is known that during this time frame Red Sea sediments are characterized by a so-called "aplanktic zone" attributed to high salinities (> 50 psu; Arz et al., 2003) not favorable for planktonic foraminifer growth (e.g. Hemleben et al., 1996), and severe carbonate dissolution (Arz et al., 2003). Taking this into account, we would expect that fecal pellets rich in coccolithophorids were still produced in the water column but due to the severe conditions for carbonate preservation most of them would have been dissolved.

For the *Rhizosolenia* matrix (Fig. 10A) characteristic of Lower Phase II (18-19 ka) sediments, we suggest that the transportation pathway via mats to the brine-floor is the same as in the Holocene. For generating the *Chaetoceros* matrix characteristic of LGM sediments, long periods of intense mixing and/or higher nutrient availability was assumed (Seeberg-Elverfeldt et al., accepted). We suggest that large flocs (possibly TEPs) of *Chaetoceros* resting spores were produced in the water column and after accumulation on the seawater-brine interface sank down to the basin floor (Fig. 10B). Both time intervals also show thick non-continuous layers of large centric diatoms that could have either first accumulated on the seawater-brine interface or have descended directly to the bottom as large aggregates (Fig. 10A, B).

Possible depositional sequence of homogenous intervals

Some of the investigated homogenous intervals showed a clear gradation while others were more an assortment of unsorted material. Especially the two homogenous intervals during the late Holocene show the clear characteristics of turbidites (Reineck and Singh, 1980).

The Shaban Deep is part of the tectonically active axial depression where the African and Arabian plate are slowly drifting apart (e.g. Braithwaite, 1987). These movements cause underwater earthquakes that mobilize the sediment that is deposited on the slope.

The southern and eastern basins of the Shaban Deep itself have very steep slopes along the central ridge. The other slopes are gentler in the eastern basin (Fig. 1). Both basins are surrounded by a carbonate crust which possibly originates from oxidation of methane around the seawater-brine interface (Pätzold et al., 2003). Only a small amount of sediment can collect on this crust. We suggest that even small tectonic movements can cause this material to slide down the slope. This turbidity current could either a) slide right into the brine pool as a slump; or b) flow separation may occur with coarse material flowing downslope and finer material moving on top of the seawater-brine interface (McCave, 1972). This will disturb the interface and sinking turbiditic material will collect the biogenic particles that have already accumulated on the seawater-brine interface. The scenario of flow separation of turbidites was earlier described for the brine-filled Bannock Basin (Eastern Mediterranean) by Corselli and McCoy

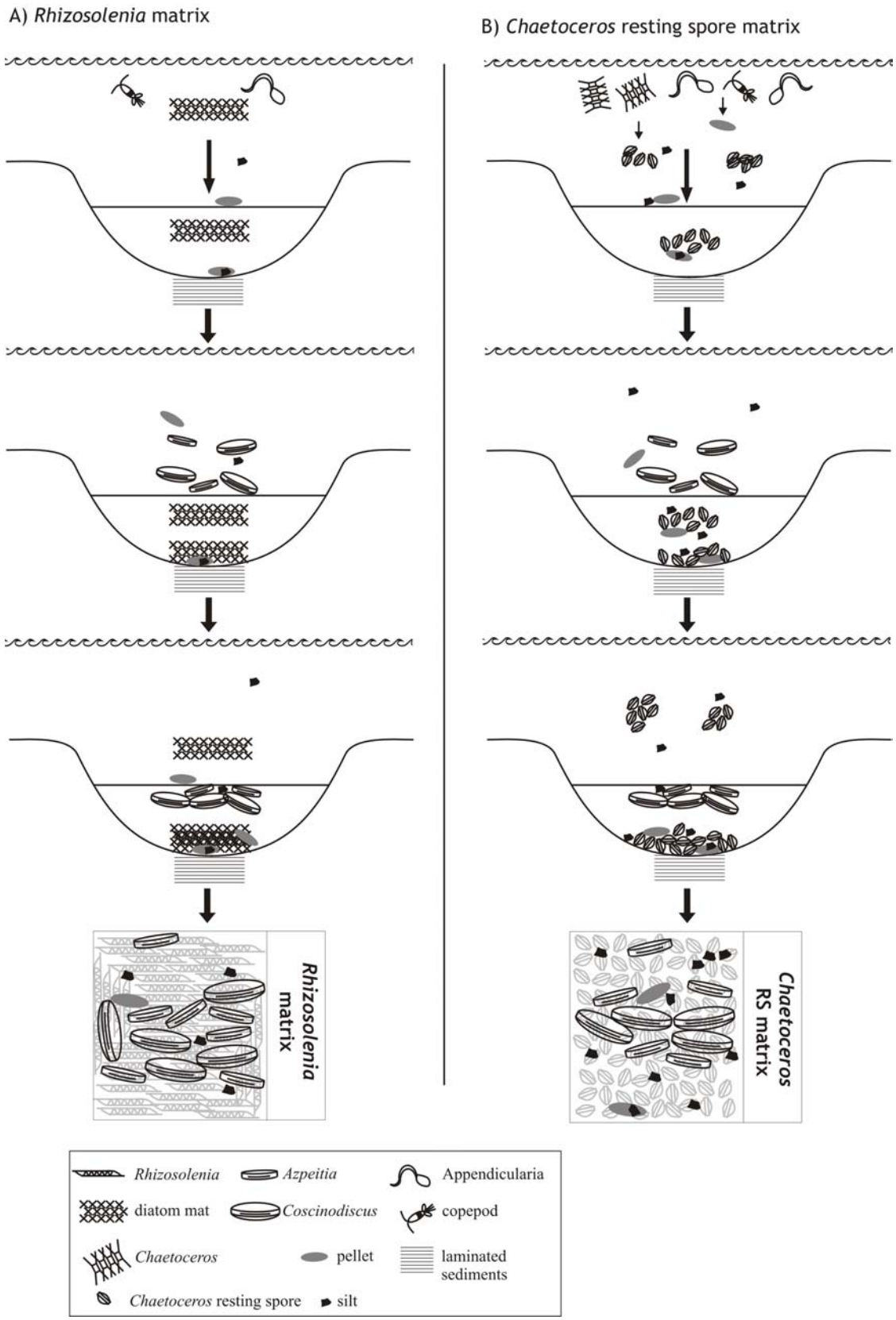

Fig. 10: Schematic diagrams of the proposed mechanism involved in the formation of a *Rhizosolenia* matrix characteristic of Lower Phase II (18-19 ka) sediments (A) and a *Chaetoceros* resting spore matrix found in LGM sediments (B). See text for detail. Specifications on water column depth, brine thickness and seawater-brine interface (BI) are given in Fig. 9A.

(1989), and would explain the gradation of homogenous intervals within late Holocene and LGM Shaban Deep sediments (Fig. 8).

Possible origin of silt accumulations

The above described accumulations of silt particles (sorted and unsorted) could be associated with abandoned detritic covers of agglutinated foraminifers (Jennifer Pike, pers. comm.). Berggren and Boersma (1969) found some benthic foraminifers (including agglutinated species) within Red Sea brine cores in low abundances. However, preserved agglutinated foraminifers were not found within any of our investigated sediments from the Red Sea.

Pike and Kemp (1996b) identified silt aggregates in anoxic laminated sediments from Guaymas Basin (Gulf of California) and Santa Barbara Basin as remains of agglutinated foraminifera. Brodie and Kemp (1995) also found "silt pellets" within the Peruvian upwelling sediments that show the same characteristics as our accumulations of silt grains. These authors describe them as either consisting of "a wide range of grain sizes, or almost exclusively of small grains (under 20 µm in size)" and assigned their origin to remains of agglutinated foraminifers.

Pike and Kemp (1996b) describe a model of the formation of these accumulations that includes the collection of silt grains of different sizes by the individual foraminifer into a detritic cover where smaller grains are used to build a new chamber while larger particles are used for protection. After finishing the new chamber, the foraminifer leaves a pile of coarser grains behind which are then preserved within the sediment (Pike and Kemp, 1996b). This model is based upon investigations of Bender (1992) about the chamber formation of *Textularia candeiana*. Bender (1992) also states that the detritic cover gets abandoned when agglutinated foraminifera are disturbed during the building process and the new chamber is left inside this detritic cover.

Possible origin of pyrite layers

Pyrite layers of all investigated intervals were always associated with coccolith layers and secondary formed carbonate was not present. Hübner (2002) investigated sediments from the brine-filled Urania Basin (eastern Mediterranean) and suggested that pyrite formation started at the seawater-brine interface. Filter samples from Meteor cruise M 52/3 (2002) from the seawater-brine interface contained amorphous Fe-oxides but no Fe-monosulfides were found (M. Schmidt, pers. comm.).

Although we are unable to deliver a specific model for the formation of pyrite layers we suggest that the first step in the formation of pyrite occurs at the seawater-brine interface under certain environmental conditions that permit the formation of amorphous monosulfides. These conditions include a) a high content of organic matter; b) hydrogen sulfide, produced during sulfate reduction; c) elemental sulfur availability; and d) bacterial oxidation of methane at the seawater-brine interface. The final transformation of monosulfides to framboidal pyrite takes place either at the brine-sediment interface or within the sediment after deposition.

Conclusions

Backscattered electron microscopy of polished thin sections reveal that Shaban Deep sediments include six different types of sediment fabric:

- Alternating light and dark continuous layers composed of coccoliths/diatom couplets;
- A pocket-like structure composed of diatom aggregates embedded within light material (coccoliths and terrigenous material);
- A matrix of tightly packed diatoms;
- Homogenous intervals due to turbidity events;
- Silt accumulations; and
- Pyrite layers

The former three structures and their composition result from a combination of biogenic production in the water column and eolian input into the Red Sea, and a sequence of events that include a) fast sinking through the water column in the form of aggregates, fecal pellets and diatom mats; b) accumulation of particles at the seawater-brine interface; c) sorting during settling through the brine and d) preservation in the sediment.

Silt accumulations are thought to be the remains of agglutinated foraminifers. The formation of framboidal pyrite may be initiated at the seawater-brine interface.

Acknowledgements

We thank the captain and crew of *R/V Meteor* for their efforts and support at sea. We also acknowledge the generous grant of permission for conducting research in the territorial waters of the Kingdom of Saudi Arabia. Thanks are extended to the technicians of the GFZ Potsdam and the Cardiff University for the preparation of thin sections and to Ute Bock (AWI) and Peter Fisher (Cardiff University) for their help with the SEM. We thank Heike Pfletschinger

for her help with XRF measurements. Special thanks go to Dr. Sabine Kasten for her helpful comments on the topic of pyrite formation. We also want to thank Axel Ehrhardt from the Center for Marine and Climate Research Institute for Geophysics (University of Hamburg) for creating the bathymetric map of the Shaban Deep (Fig. 1) from bathymetric grid data of *RV Meteor* Cruises 44/3 and 52/3. We are very grateful to the Hanse Institute of Advanced Study, Delmenhorst, Germany, for the Fellowship awarded to C. B. Lange. This work was supported by the Deutsche Forschungsgemeinschaft as part of the DFG-Research Center "Ocean Margins" at the University of Bremen, No. RCOM0XXX.

References

Alldredge, A.L. and Gotschalk, C.C., 1989. Direct observations of the mass flocculation of diatom bloom: characteristics, settling velocities and formation of diatom aggregates. Deep-Sea Research, 36(2): 159-171.

Alldredge, A.L., Passow, U. and Logan, B.E., 1993. The abundance and significance of a class of large, transparent organic particles in the ocean. Deep-Sea Research I, 40(6): 1131-1140.

Antunes, A., Eder, W., Fareleira, P., Santos, H. and Huber, R., 2003. *Salinisphaera shabanensis* gen. nov., sp. nov., a novel, moderately halophilic bacterium from the brine-seawater interface of the Shaban Deep, Red Sea. Extremophiles, 7: 29-34.

Arz, H.W., Pätzold, J., Müller, P.J. and Moammar, M.O., 2003. Influence of Northern Hemisphere climate and global sea level rise on the restricted Red Sea marine environment during Termination I. Paleoceanography, 18(2): 1053, doi:10.1029/2002PA000864.

Bender, H., 1992. Chamber formation and biomineralization in *Textularia candeiana* D'Orbigny (Sarcodina: Textulariina). Journal of Foraminiferal Research, 22(3): 229-241.

Berggren, W.A. and Boersma, A., 1969. Late Pleistocene and Holocene Planktonic Foraminifera from the Red Sea. In: E.T. Degens and D.A. Ross (Editors), Hot Brines and Recent Heavy Metal Deposits in the Red Sea. Springer Verlag, New York, pp. 282-298.

Braithwaite, C.J.R., 1987. Geology and Palaeogeography of the Red Sea Region. In: A.J. Edwards and S.M. Head (Editors), Key Environments: Red Sea. Pergamon Press, Oxford, pp. 22-44.

Brodie, I. and Kemp, A.E.S., 1995. Pelletal structures in Peruvian upwelling sediments. Journal of Geological Society, 152: 141-150.

Corselli, C. and McCoy, F.W., 1989. Sedimentation of organic matter, Bacino Bannock. In: M.B. Cita, A. Camerlenghi and C. Corselli (Editors), Anoxic Basins of the Eastern Mediterranean. Ric. Sci., Suppl., 72, pp. 50-53.

Dean, J.M., Kemp, A.E.S., Bull, D., Pike, J., Patterson, G. and Zolitschka, B., 1999. Taking varves to bits: Scanning electron microscopy in the study of laminated sediments and varves. Journal of Paleolimnology, 22: 121-136.

Eder, W., Schmidt, M., Koch, M., Garbe-Schönberg, D. and Huber, R., 2002. Prokaryotic phylogenetic diversity and corresponding geochemical data of the brine-seawater interface of the Shaban Deep, Red Sea. Environmental Microbiology, 4(11): 758-763.

Edwards, F.J., 1987. Climate and Oceanography. In: A.J. Edwards and S.M. Head (Editors), Key Environments: Red Sea. Pergamon Press, Oxford, pp. 45-70.

Eshel, G., Cane, M.A. and Blumenthal, M.B., 1994. Modes of subsurface, intermediate, and deep water renewal in the Red Sea. Journal of Geophysical Research, 99(C8): 15,941-15,952.

Eshel, G. and Naik, N.H., 1997. Climatological Coastal Jet Collision, Intermediate Water Formation, and the General Circulation of the Red Sea. Journal of Physical Oceanography, 27: 1233-1257.

Faber, E., Botz, R., Poggenburg, J., Schmidt, M., Stoffers, P. and Hartmann, M., 1998. Methane in Red Sea brines. Organic Geochemistry, 29(1-3): 363-379.

Hartmann, M., Scholten, J.C., Stoffers, P. and Wehner, F., 1998. Hydrographic structure of brine-filled deeps in the Red Sea - new results from the Shaban, Kebrit, Atlantis II, and Discovery Deep. Marine Geology, 144: 311-330.

Hemleben, C., Meischner, D., Zahn, R., Almogi-Labin, A., Erlenkeuser, H. and Hiller, B., 1996. Three hundred eighty thousand year long stable isotope and faunal records from the Red Sea: Influence of global sea level change on hydrography. Paleoceanography, 11(2): 147-156.

Hübner, A., 2002. Geochemische und mineralogische Untersuchung von Sedimenten aus dem Bereich des anoxischen, hypersalinen Urania-Beckens (östliches Mittelmeer) zur Charakterisierung von mariner Sedimentation unter extremen Bedingungen. PhD Thesis, Free University of Berlin, Berlin, 104 pp.

Kemp, A.E.S., Pike, J., Pearce, R.B. and Lange, C.B., 2000. The "Fall dump"-a new perspective on the role of a "shade flora" in the annual cycle of diatom production and export flux. Deep-Sea Research II, 47: 2129-2154.

Lindell, D. and Post, A.F., 1995. Ultraphytoplankton succession is triggered by deep winter mixing in the Gulf of Aqaba (Eilat), Red Sea. Limnology and Oceanography, 40(6): 1130-1141.

Manheim, F.T., 1974. Red Sea geochemistry. Initial Report DSDP, 23: 975-998.

McCave, I.N., 1972. Transport and escape of fine-grained sediment from shelf areas. In: D.J.P. Swift, D.B. Duane and O.H. Pilkey (Editors), Shelf sediment transport. Dowden, Hutchinson, Ross, Stroudsburg, PA, pp. 225-248.

Millero, F.J., Mucci, A., Zullig, J. and Chetirkin, P., 1982. The density of Red Sea brines. Marine Chemistry, 11: 463-475.

Pätzold, J., Abd El-Wahab Farha, O., Abu-Ouf, M., Al Hazmi, Y.M.M., Al-Rousan, S., Arz, H.W., Bagabas, K.A.A., Bassek, D., Blaschek, H., Böke, W., Donner, B., Eder, W., Felis, T., Gayed, H.Y.K., Gutowski, M., Hemleben, C., Hübner, H., Hübscher, C., Kadi, K.A., Kästner, R., Klauke, S., Körner, S.O., Kuhlmann, H., Lützeler, T., Meier, S., Melegy, M.M., Moammar, M.O., Mohamuda, A.Z., Mokhtar, T.A., Moos, C., Omar, O.M., Rasheed, M., Rosiak, U., Salem, M., Schmidt, M., Schmitt, M., Stoffers, P., Shata, A.M., Themann, S. and Weldeab, S., 2000. Report and preliminary results of *Meteor* cruise M 44/3 Aqaba (Jordan) - Safaga (Egypt) - Dubá (Saudia Arabia) - Suez (Egypt) - Haifa (Israel). Berichte aus dem Fachbereich Geowissenschaften der Universität Bremen, 149: 135.

Pätzold, J., Moammar, M.O., Al Farawati, R., Al Hazmi, Y.M.M., Al Otibi, A., Antunes, A., Arz, H.W., Berger, J., Botz, R., Donner, B., Erhardt, A., Garbe-Schönberg, C.-D., Ghandourah, M., Hübscher, C., Kahl, G., Klann, M., Klauke, S., Klitzke, U., Legge, H.L., Lichowski, F., Schewe, F., Schmidt, M., Schmitt, M., Seeberg-Elverfeldt, I.A. and Truscheit, T., 2003. Black Sea - Mediterranean - Red Sea, Part 3, Cruise No. 52, Leg 3, March 10 - March 27, 2002, Limassol-Limassol. In: J. Pätzold, G. Bohrmann and C. Hübscher (Editors), METEOR-Berichte, Black Sea - Mediterranean - Red Sea, Cruise No. 52, January 2 - March 27, 2002. Universität Hamburg, Hamburg, pp. 62; available under http://www.marum.de/M52_-_Schwarzes_Meer_-_Mittelmeer_-_Rotes_Meer.html.

Pautot, G., Guennoc, P., Coutelle, A. and Lyberis, N., 1984. Discovery of a large brine deep in the northern Red Sea. Nature, 310: 133-136.

Pike, J. and Kemp, A.E.S., 1996a. Preparation and analysis techniques for studies of laminated sediments. In: A.E.S. Kemp (Editor), Palaeoclimatology and Palaeoceanography from laminated sediments. Geological Society, Special Publication, pp. 37-48.

Pike, J. and Kemp, A.E.S., 1996b. Silt aggregates in laminated marine sediment produced by agglutinated foraminifera. Journal of Sedimentary Reseach, 66(3): 625-631.

Reineck, H.-E. and Singh, I.B., 1980. Depositional Sedimentary Environments. Springer-Verlag, Berlin Heidelberg.

Schimmelmann, A., Lange, C.B. and Berger, W.H., 1990. Climatically controlled marker layers in Santa Barbara Basin sediments and fine-scale core-to-core correlation. Limnology and Oceanography, 35(1): 165-173.

Seeberg-Elverfeldt, I.A., Lange, C.B., Arz, H.W., Pätzold, J. and Pike, J., accepted. The significance of diatoms in the formation of laminated sediments in the Shaban Deep, Northern Red Sea. Marine Geology.

Seeberg-Elverfeldt, I.A., Lange, C.B. and Pätzold, J., 2004. Preservation of siliceous microplankton in surface sediments of the northern Red Sea. Marine Micropaleontology, 51(3/4): 193-211.

Shaikh, E.A., Roff, J.C. and Dowidar, N.M., 1986. Phytoplankton ecology and production in the Red Sea off Jiddah, Saudi Arabia. Marine Biology, 92: 405-416.

Stoffers, P., Botz, R. and Scholten, J., 1990. Isotope Geochemistry of Primary and Secondary Carbonate Minerals in the Shaban-Deep (Red Sea). In: D. Helnig, P. Rothe, U. Förster and P. Stoffers (Editors), Sediments and Environmental Geochemistry. Springer, Berlin, pp. 83-94.

Yoon, W.D., Kim, S.K. and Han, K.N., 2001. Morphology and sinking velocities of fecal pellets of copepod, molluscan, euphausiid, and salp taxa in the northeastern tropical Atlantic. Marine Biology, 139: 923-928; DOI 10.1007/s002270100630.

Chapter 4: Conclusions and outlook

4.1 Conclusions

The plankton and surface sediments of the northern Red Sea are characterized by a diatom flora that is typical of tropical/subtropical environments. Comparisons between plankton and surface sediments reveal that:

- Dissolution of diatom frustules is evident. Fragile forms that dominate the plankton assemblage are a minor contributor to the sedimentary record which is enriched in robust species.
- Assemblages in surface brine sediments are much better preserved than in non-brine sediments.

The sediments underlying the Shaban Deep brine are laminated (though not continuously) over the past 50,000 years. Detailed back-scattered electron imagery of polished thin sections reveal that:

- Sediment structure includes six types: a) a laminated structure with alternating light (mainly coccoliths) and dark (diatom frustules) layers, where the diatom component is indicative of the intra-annual variability between stratification and mixing events; b) a pocket-like structure attributed to the sinking of particles within fecal pellets and aggregates; c) a matrix of tightly packed diatoms that relates to extended stratification/mixing periods of the water column; d) homogenous intervals that result from turbidity deposition; e) silt accumulations which origin may lie in agglutinated foraminifers; and f) pyrite layers with pyrite formation possibly initiated at the seawater-brine interface.
- Sediments encompassing the period 4-15 ka show a clear alternating light/dark pattern (coccoliths/diatom couplets) and are interpreted as carrying a signal of contrasting seasons and associated plankton blooms: Light, coccolith-rich layers represent the summer flux; dark diatomaceous layers correspond to late fall and/or winter production.
- The main contributors to the diatomaceous layers are species of the genus *Rhizosolenia* (in the early and mid-Holocene) and *Chaetoceros* (during the deglaciation and the Last Glacial Maximum).

- The dominant pattern in the late Holocene is that of a mixed diatom assemblage or a *Chaeoceros*-dominated assemblage being interrupted by short periods of stratification (*Proboscia*/*Rhizosolenia* layers).
- Strong carbonate dissolution during the LGM prevents identification of an annual cycle of sedimentation. However, a marked and abrupt switch in diatom species can be observed between LGM sediments with a background matrix of *Chaetoceros* resting spores (~22 ka) and sediments from the lower Phase II with a background matrix of *Rhizosolenia* (~19 ka).
- Different diatom assemblages reflect changing conditions in stratification in the northern Red Sea: *Rhizosolenia* dominance points to strong stratification of the water column (i.e. at the beginning of meltwater pulse MWP 1a, at 14.5 ka). In contrast, sediments dominated by *Chaetoceros* reflect mixing conditions (e.g. LGM).
- *Rhizosolenia* and a more stratified water column seem to have played the dominant role in the northern Red Sea since the Last Glacial Maximum, at least during times when the brine in the Shaban Deep was present.
- We found no indication for hydrothermal influence in our laminated sediments from the Shaban Deep; although the basin is described in the literature as hydrothermally active (see Chapter 1).

Thus, laminated sediments in the Shaban Deep can be used for reconstructing paleoceanographic and paleoclimatic changes in the region at high resolution.

4.2 Outlook

Marine laminated sediments are presently one of the major tools for high-resolution investigations. Others include, for example tree-ring data (e.g. Cook et al., 1998; Esper et al., 2002), ice core record (e.g. Dansgaard et al., 1993) and coral growth bands (e.g. Felis et al., 2000). All these tools can be used for unraveling the climate history regionally on an annual or maybe even seasonal scale but larger climatic cycles can also be established.

Laminated sediments of the Shaban Deep (northern Red Sea) carry an annual signal which we were able to resolve with the help of diatom assemblages and coccolithophorids since these two groups of organisms are produced in the water column at different times of the year. In addition, the shift in diatom assemblages records changing conditions in the water column in the northern Red Sea during the last 22 kyr. Stratified conditions are reflected by diatoms

commonly found associated with a deep chlorophyll maximum (DCM; rhizosolenoid diatoms; Kemp et al., 2000) located at a water depth of > 200 m (Seeberg-Elverfeldt et al., 2004) while mixed conditions favor the presence of species typical of upwelling regions (*Chaetoceros*).

Although the northern Red Sea is described as an oligotrophic area, where autotrophic picoplankton dominate the plankton community (Lindell and Post, 1995), we were able to prove that the role of diatoms in primary production was underestimated so far. The assessment that Chl *a* values in the northern Red Sea are low were mainly established through satellite data which only record the top of the surface waters. Hence, the contribution of rhizosolenoid diatoms to the overall productivity of the northern Red Sea has been overlooked.

Future work should include the deployment of moored sediment traps within the northern Red Sea to better estimate the amount and fate of diatom mats in this oligotrophic environment and to further establish the seasonal cycle of the Red Sea plankton. In addition, observations with a remotely operated vehicle (ROV) would be of uttermost importance for assessing whether particulate matter gets first accumulated on the seawater-brine interface before sinking through the brine as suggested in this thesis. In this context, samples from the seawater-brine interface should be investigated to ascertain the presence of fecal pellets and aggregates as well as mats on the interface.

A second step could be to investigate laminated sediments from core GeoB 5836-2 that are older than ~34 kyr (Phase III) with the same SEM techniques as the rest of the core. Observations in the light microscope indicate a different diatom assemblage at that time. Further work can be done on new core material which was retrieved during *RV Meteor* cruise M 52/3. A first comparison between multicores of the eastern and southern basin of the Shaban Deep show that sediment sequences from at least the Late Holocene can be nicely correlated between these sub-basins. Hemleben (1996) stated that cores that were retrieved from the southern basin show some similarities in their upper parts but not further down in the record. It would be interesting to compare our newer core material from M 52/3 with the older core GeoB 5836-2 (from *RV Meteor* cruise M 44/3) and see if correlations can be established. These correlations can then be used to further examine homogenous layers that result from turbidity flows. We may be able to establish a better model for the formation of these layers.

Another task would be to study more closely the geochemical processes involved in the formation of authigenic minerals like pyrite or Ca-rhodochrosite. This could be done in cooperation with scientist from the IfGK (Institut für Geowissenschaften der Christian-Albrechts-Universität, Kiel) who are working on the geochemistry of the Shaban Deep brine.

In addition, the role of bacteria (known to thrive at the interface; Eder et al., 2002; Antunes et al., 2003) in both lamina formation and pyrite precipitation needs to be assessed.

A major, still open question is how the brine is formed and how it changes through time. We believe that the brine was not always present within the last 50,000 years since laminated phases in core GeoB 5836-2 were interrupted by non-turbiditic homogenous intervals. These questions might be solved by the analysis of sediments from other brine-filled basins in that region. There are two more deeps north of the Shaban Deep (Oceanographer and Conrad Deep) which might hold keys for the understanding of the history of these brine basins.

References

Antunes, A., Eder, W., Fareleira, P., Santos, H. and Huber, R., 2003. *Salinisphaera shabanensis* gen. nov., sp. nov., a novel, moderately halophilic bacterium from the brine-seawater interface of the Shaban Deep, Red Sea. Extremophiles, 7: 29-34.

Cook, E.R., D'Arrigo, R.D. and Briffa, K.R., 1998. A reconstruction of the North Atlantic Oscillation using tree-ring chronologies from North America and Europe. The Holocene, 8(1): 9-17.

Dansgaard, W., Johnson, S.J., Clausen, H.B., Dahl-Jensen, D., Gundestrup, N.S., Hammer, C.U., Hvidberg, C.S., Steffersen, J.P., Sveinbjörnsdottir, A.E., Jouzel, J. and Bond, G., 1993. Evidence for general instability of past climate from a 250-kyr ice-core record. Nature, 364: 218-220.

Eder, W., Schmidt, M., Koch, M., Garbe-Schönberg, D. and Huber, R., 2002. Prokaryotic phylogenetic diversity and corresponding geochemical data of the brine-seawater interface of the Shaban Deep, Red Sea. Environmental Microbiology, 4(11): 758-763.

Esper, J., Cook, E.R. and Schweingruber, F.H., 2002. Low-Frequency Signals in Long Tree-Ring Chronologies for Reconstructing Past Temperature Variability. Science, 295: 2250-2253.

Felis, T., Pätzold, J., Loya, Y., Fine, M., Nawar, A.H. and Wefer, G., 2000. A coral oxygen isotope record from the northern Red Sea documenting NAO, ENSO, and North Pacific teleconnections on Middle East climate variability since the year 1750. Paleoceanography, 15(6): 679-694.

Hemleben, C., Roether, W. and Stoffers, P., 1996. Östliches Mittelmeer, Rotes Meer, Arabisches Meer; Cruise No. 31, 30 December 1994 - 22 March 1995, Leitstelle METEOR, Institut für Meereskunde der Universität Hamburg, Hamburg.

Kemp, A.E.S., Pike, J., Pearce, R.B. and Lange, C.B., 2000. The "Fall dump"-a new perspective on the role of a "shade flora" in the annual cycle of diatom production and export flux. Deep-Sea Research II, 47: 2129-2154.

Lindell, D. and Post, A.F., 1995. Ultraphytoplankton succession is triggered by deep winter mixing in the Gulf of Aqaba (Eilat), Red Sea. Limnology and Oceanography, 40(6): 1130-1141.

Seeberg-Elverfeldt, I.A., Lange, C.B. and Pätzold, J., 2004. Preservation of siliceous microplankton in surface sediments of the northern Red Sea. Marine Micropaleontology, 51(3/4): 193-211.

Appendix

Smear slide analysis of core GeoB 5836-2 from chapter 3.2: Seeberg-Elverfeldt et al., „The significance of diatoms in the formation of laminated sediments of the Shaban Deep, Northern Red Sea".

Depth in core [cm]	Colour	Texture	Description
1	olive	soupy	Abundant coccoliths, broken pieces of diatoms (***Azpeitia***, ***Thalassionema***, ***Thalassiosira***) and silicoflagellates; calcite grains
7	olive		Common coccoliths, diatoms (***Azpeitia***, ***Coscinodiscus***, ***Thalassiosira***) and silicoflagellates present
9	olive		Common coccoliths, diatoms and silicoflagellates; also fragile species present few ***Azpeitia***; mainly ***Thalassiosira***, some ***Rhizosolenia***
12	olive		Common coccoliths, diatoms and silicoflagellates present
14	olive		little material; assemblage as before; less diatoms
15	olive		Common coccoliths, diatoms and silicoflagellates present fewer diatoms than in 17 cm and 20 cm
17	olive		Common coccoliths, diatoms well preserved (***Chaetoceros*** veg. cells, ***Hemiaulus***)
20	olive		Frequent coccoliths, diatoms and silicoflagellates present bad preservation; few ***Rhizosolenia***
23	olive	**laminated (very thin laminations)**	Frequent coccoliths, diatoms (***N. bicapitata***; few ***Azpeitia*** and ***Coscinodiscus***) and silicoflagellates present, weakly silicified species; ***Rhizosolenia***
23.5	light		Common coccoliths, diatoms and silicoflagellates present, bad preservation (few ***N. bicapitata***; few ***Azpeitia***)
24	dark		Frequent coccoliths, frequent diatoms, silicoflagellates; good preservation
25.3	light		Frequent coccoliths, diatoms and silicoflagellates; good preservation
25.6	dark		Frequent coccoliths, diatoms (***Chaetoceros*** setae, ***Rhizosolenia***), silicoflagellates, radiolarians; better preseration than in light lamina
33.8	light		Frequent coccoliths, few diatoms
39	dark		Frequent coccoliths, more diatoms than in 42.7 cm, (no *Azpeitia*); very good preservation
42.7	light		Common coccoliths, less diatoms (no *Azpeitia*)
44	dark		Few coccoliths, few diatoms (no *Azpeitia*); bad preservation
49	dark		Few coccoliths, few diatoms (some *Azpeitia*); bad preservation
51.8	dark-olive		Frequent coccoliths, few diatoms; bad preservation
56.4	light		Common coccoliths, few diatoms

59	dark		Frequent coccoliths (more than in 70 cm); frequent diatoms (no *Azpeitia*)
61	dark-olive		Frequent coccoliths (but fewer than in 64 cm), few diatoms
64	dark		Frequent coccoliths; frequent diatoms (***Azpeitia***; ***Thalassionema***)
70	light-olive		Common coccoliths (more than in 74.5 cm), frequent diatoms (***Azpeitia***, ***Thalassionema***)
74.5	dark-olive		Frequent coccoliths; frequent diatoms (mainly ***Azpeitia***, ***Thalassionema***); bad preservation
80	light-olive		Frequent coccoliths; frequent diatoms (mainly ***Azpeitia***, few ***Chaetoceros* RS**)
88.5	dark		Few coccoliths, few diatoms (mainly ***Azpeitia***)
90	dark		Frequent coccoliths, few diatoms, broken valves
93.5	olive		Frequent coccoliths, few diatoms; bad preservation
96	olive		Common coccoliths, frequent diatoms (***Azpeitia)***; bad preservation
101	olive		Abundant coccoliths, few diatoms (***Azpeitia***); bad preservation
104	dark-olive		Common coccoliths, frequent diatoms
104.5	dark-olive		Common coccoliths, frequent diatoms
105	dark		Common coccoliths, few diatoms
105.5	light		Common coccoliths, no diatoms
107.5	light		Abundant coccoliths, no diatoms
109	olive		Abundant coccoliths, no diatoms
111.3	black		Common coccoliths, no diatoms
117	greyish	**no diatoms**	Common coccoliths, no diatoms
120	dark-grey		Common coccoliths, no diatoms
134	grey		Common coccoliths, no diatoms
167	dark		Frequent coccoliths; foraminifera present, no diatoms; calcite grains
190	grey		Common coccoliths; no diatoms
220	olive-grey		Frequent coccoliths, clay, no diatoms; calcite grains
233.3	dark		Frequent coccoliths, no diatoms
250	olive-grey		Frequent coccoliths, no diatoms; calcite grains
260			Frequent coccoliths, no diatoms
262.5	dark-grey		Common coccoliths, no diatoms
263.8	lighter		Few coccoliths, no diatoms
267	light		Few coccoliths, foraminifera present, no diatoms

268	black	laminated	Few coccoliths, diatoms present, broken valves
269	dark-olive		Few coccoliths, few diatoms
270	dark		Few coccoliths, frequent diatoms (***Azpeitia***, ***Alveus marinus***); calcite grains
275.3	dark-olive		Few coccoliths, few diatoms, broken valves, bad preservation; common calcite grains
276	dark		Few coccoliths, few diatoms, broken valves, bad preservation
277.3	dark		Frequent coccoliths (but fewer than in 278 cm), few diatoms
278	dark-olive		Frequent coccoliths, frequent diatoms (***Chaetoceros*** setae and **RS**; ***Rhizosolenia***)
297	light-olive		Frequent coccoliths, few diatoms; bad preservation
308	olive		Frequent coccoliths, rare diatoms
313.6		laminated	Frequent coccoliths, few diatoms
316.5	dark		Frequent coccoliths, few diatoms
318	light		Frequent coccoliths, few diatoms
320	light		Frequent coccoliths, frequent diatoms (***Chaetoceros* RS**)
322			little material; ***Azpeitia***; warm water assemblage (***Lauderia***); good preservation
326	dark		Few coccoliths, frequent diatoms (***Chaetoceros*** veg. cells and **RS**, ***C. affinis***, ***C. compressus C. lorenzianus***), fewer ***Azpeitia;*** different assemblage
328.5	light-beige		Frequent coccoliths, few diatoms, broken valves, bad preservation
332	olive		Frequent coccoliths, frequent diatoms
350	olive-grey		Frequent coccoliths, few diatoms
370	olive		Frequent coccoliths, frequent diatoms (mainly ***Azpeitia***)
390	olive		Frequent coccoliths, few diatoms (***Thalassionema nitzschioides* var. *nitzsch.***); bad preservation
410	dark-olive		Frequent coccoliths, frequent diatoms (***Chaetoceros***)
419	light		Frequent coccoliths, few diatoms (***Chaetoceros***)
419.5	light		Frequent coccoliths, few diatoms
420	dark-olive		Few coccoliths, frequent diatoms, ***Chaetoceros* setae** (***C. compressus*** with **RS**, ***C. debilis***); **aggregates**; good preservation
421.2	light		Frequent coccoliths; frequent diatoms, ***Chaetoceros*** setae; also ***T. nitzschioides***, ***Nitzschia sicula***
427	dark-olive		Frequent coccoliths; frequent diatoms, ***Chaetoceros*** setae; also ***T. nitzschioides***, ***Nitzschia sicula***
428.5	light, clay		Frequent coccoliths, few diatoms, broken valves; calcite grains

429.8	dark	laminated	Few coccoliths, few diatoms, some ***Rhizosolenia***
430.3	light		Few coccoliths, frequent diatoms, broken valves; some ***Rhizosolenia***
432	black		Few coccoliths, common diatoms, mainly ***Rhizosolenia***
440	dark-olive		Few coccoliths, abundant diatoms, ***Rhizosolenia*-mat**
440.5	light		Frequent coccoliths, few diatoms, some ***Rhizosolenia***
442	olive		Frequent coccoliths, few diatoms, broken valves
444	olive		Frequent coccoliths, few diatoms, broken valves; calcite grains and clay
446.6	dark		Few coccoliths, frequent diatoms, also ***Rhizosolenia***
452	light		Few coccoliths, few diatoms, mainly ***Rhizosolenia***; calcite grains
455	dark		Few coccoliths, abundant diatoms; ***Rhizosolenia*-mat**; also many ***Thalassionema schraderi***
466	light		Frequent coccoliths, few diatoms, ***Rhizosolenia***; calcite grains
472	dark		Rare coccoliths, abundant diatoms, ***Rhizosolenia*-mat**
474			Abundant diatoms, ***Rhizosolenia*-mat** (**R.*setigera*, *R. pungens***)
478	dark		Few coccoliths, few diatoms, but mainly ***Rhizosolenia***
483	dark		Frequent coccoliths, frequent diatoms, diverse assemblage (e.g. ***Azpeitia, Actinocyclus Coscinodiscus radiatus*, *Proboscia alata*, *Rhizosolenia setigera***)
483.3	light-yellow		Few coccoliths, frequent diatoms (***Actinocyclus*, *Azpeitia, Rhizosolenia setigera***); calcite grains
489	dark		Rare coccoliths, abundant diatoms, ***Rhizosolenia*-mat**
492	light-olive		Frequent coccoliths, frequent diatoms, some ***Rhizosolenia*** but mainly ***Azpeitia***
495.5	light		Frequent coccoliths, few diatoms, ***Rhizosolenia*** *and* ***Azpeitia***; calcite grains
496	light		Frequent coccoliths, few diatoms; calcite grains
497.5	black		Rare coccoliths, abundant diatoms, ***Rhizosolenia*-mat**
499	dark		Rare coccoliths, abundant diatoms, ***Rhizosolenia*-mat**
501	dark		Few coccoliths, few diatoms, broken valves
502.5	dark		Rare coccoliths, common diatoms, **aggregates *Bacteriastrum***
504	black		Few coccoliths, few diatoms; bad preservation
509.3	light		Few coccoliths, frequent diatoms, **aggregates *Bacteriastrum, Chaetoceros*** setae
513.2	dark		Few coccoliths, frequent diatoms, **aggregates *Bacteriastrum, Chaetoceros*** setae
513.7	light-olive		Few coccoliths, frequent diatoms, mainly ***Azpeitia,*** broken valves
518.4	dark-olive		Few coccoliths, few diatoms, mainly ***Azpeitia***, broken valves
519	dark		Few coccoliths, few diatoms, aggregates ***Chaetoceros*** setae; ***Cyclotella*** aff. ***caspia*** abundant
524	dark		Few coccoliths, frequent diatoms, mainly **RS *Chaetoceros*** and **aggregates** of

			Chaetoceros setae; ***Cyclotella caspia*** abundant
526	light-olive		Few coccoliths, common diatoms, mainly ***Azpeitia*** and **RS *Chaetoceros***
536	olive		Frequent coccoliths, few diatoms, mainly ***Azpeitia***, broken valves
556	olive		Frequent coccoliths, few diatoms, mainly ***Azpeitia***, broken valves
570	dark-olive		Frequent coccoliths, frequent diatoms, ***Azpeitia***, some **RS *Chaetoceros***
572.5	light-olive		Frequent coccoliths, few diatoms, broken valves
572.8	light-olive		Few coccoliths, few diatoms, mixed assemblage
573.8	dark-olive		Rare coccoliths, common diatoms, mainly ***Azpeitia***
579	dark		Rare coccoliths, common diatoms, **mixed assemblage** and **RS *Chaetoceros***
580.6	dark	**laminated**	Rare coccoliths, common diatoms, almost only **RS *Chaetoceros***
585.6	light		Rare coccoliths, frequent diatoms, ***Azpeitia*** and **RS *Chaetoceros***
588.2	light		Rare coccoliths, common diatoms, almost only ***Chaetoceros*** setae**, *Bacteriastrum* aggregates**; some **RS *Chaetoceros***
591	dark		Rare coccoliths, common diatoms, almost only **RS *Chaetoceros***
595	lighter		Rare coccoliths, frequent diatoms, less ***Azpeitia***, but abundant **RS *Chaetoceros, Chaetoceros*** setae and ***Bacteriastrum***
598	light		Frequent coccoliths, common diatoms, ***Azpeitia*** and **RS *Chaetoceros***
604	dark		Rare coccoliths, common diatoms, ***Azpeitia*** and **RS *Chaetoceros***
609.5	light		Rare coccoliths, frequent diatoms, mainly ***Azpeitia***
612	dark		Rare coccoliths, common diatoms, **RS *Chaetoceros*** and ***Thalassionema***
614	dark		Rare coccoliths, common diatoms (***Azpeitia***)
616	lighter		Rare coccoliths, common diatoms, mainly ***Chaetoceros*** setae and ***Bacteriastrum* aggregates**
619.5	lighter		Frequent coccoliths, frequent diatoms, also **RS** and setae ***Chaetoceros***
620.3	dark		Rare coccoliths, common diatoms, almost only **RS *Chaetoceros***
627	light		Frequent coccoliths, frequent diatoms, ***Azpeitia*** and **RS *Chaetoceros***
636	dark		Frequent coccoliths, frequent diatoms, ***Azpeitia*** and **RS *Chaetoceros***
637.3	light	**laminated**	Few coccoliths, frequent diatoms (***Bacteriastrum)***
641.3	light	**sometimes**	Frequent coccoliths, frequent diatoms, mainly ***Azpeitia***; broken valves
644.5	dark	**not**	Frequent coccoliths, common diatoms, mainly ***Azpeitia***; broken valves
648	light	**obvious**	Few coccoliths, frequent diatoms, mainly ***Azpeitia;*** broken valves
666	black		Few coccoliths, frequent diatoms, mainly ***Azpeitia;*** broken valves
678.3	dark		Few coccoliths, frequent diatoms, mainly ***Azpeitia;*** broken valves

688.3	light		Frequent coccoliths, frequent diatoms, mainly ***Azpeitia;*** broken valves
698.6	dark		Few coccoliths, frequent diatoms, mainly ***Azpeitia;*** broken valves
706.4	dark		Few coccoliths, frequent diatoms, mainly ***Azpeitia***, broken valves, calcite grains
708.4	dark		Frequent coccoliths, frequent diatoms, mainly ***Azpeitia;*** broken valves
712.7	dark		Few coccoliths, frequent diatoms, mainly ***Azpeitia***, broken valves
719.8	light		Few coccoliths, frequent diatoms, mainly ***Azpeitia***, broken valves
726.2	dark		Few coccoliths, frequent diatoms, mainly ***Azpeitia;*** broken valves
728.4	dark		Frequent coccoliths, frequent diatoms, mainly ***Azpeitia;*** broken valves
737.6	light		Few coccoliths, frequent diatoms, mainly ***Azpeitia***
745	black		Few coccoliths, common diatoms, mainly ***Azpeitia***
753.8	dark		Few coccoliths, few diatoms, mainly ***Azpeitia***; broken valves
760.4	dark		Few coccoliths, few diatoms, mainly ***Azpeitia***; broken valves
761.8	black		Few coccoliths, frequent diatoms, mainly ***Azpeitia***
770.7	dark		Frequent coccoliths, frequent diatoms, mainly ***Azpeitia***
777	black		Few coccoliths, frequent diatoms, mainly ***Azpeitia***
780	dark		Few coccoliths, frequent diatoms, mainly ***Azpeitia***, broken valves
782.3	black		Few coccoliths, rare diatoms, broken valves
785	grey		Abundant coccoliths, few diatoms, broken valves
786	olive		Abundant coccoliths, **no diatoms**